CUKUROVA UNIVERSITY

INSTITUTE OF NATURAL AND APPLIED SCIENCES

MSc THESIS

Investigation of Mechanical and Corrosion Properties of Ni-B/ZrC Nanocomposite Coatings Produced by Electrodeposition Method

Ömer HÜKÜMDAR

Department of Automotive Engineering

December, 2024

CUKUROVA UNIVERSITY

INSTITUTE OF NATURAL AND APPLIED SCIENCES

MSc THESIS APPROVAL

Investigation of mechanical and corrosion properties of Ni-B/ZrC nanocomposite coatings produced by electrodeposition method

---

Ömer HÜKÜMDAR

Department of Automotive Engineering

This Master's Thesis was evaluated by the following Jury Members on 27/12/2024 and was approved by unanimity / majority of votes.

Jury : Prof. Dr. Ali KESKİN (Advisor) ……

: Prof. Dr. Mustafa Atakan AKAR ……

: Prof. Dr. Ahmet ÇALIK ……

This Thesis was written in the Department of Automotive Engineering, Institute of Natural and Applied Sciences.

Thesis Number:

Prof. Dr. Sadık DİNÇER
Director
Institute of Natural and Applied Sciences

This work was supported by the Çukurova University Scientific Research Projects Unit.
Project ID: FYL-2023-16325

CONTENTS

CUKUROVA UNIVERSITY
INSTITUTE OF NATURAL AND APPLIED SCIENCES

MSc THESIS

Investigation of mechanical and corrosion properties of Ni-B/ZrC nanocomposite coatings produced by electrodeposition method

Ömer HÜKÜMDAR

Advisor: Prof. Dr. Ali KESKİN

Department of Automotive Engineering

ABSTRACT

The electrodeposition method can be used to coat metallic or conductive non-metallic materials, providing enhanced properties suitable for various applications. Low-cost and low-conductivity metals such as copper or steel are often coated with harder, more corrosion- and wear-resistant materials like nickel and boron to meet specific performance requirements. This study focuses on Ni-B/ZrC nanocomposite coatings applied on copper substrates, examining the effects of Zirconium carbide (ZrC) and Trimethylamine borane complex (TMAB) content in the electroplating bath on the resulting coating's surface properties. The electrodeposited samples were evaluated in terms of mechanical characterization, surface morphology, and corrosion performance. The highest microhardness value, measured at 1020.4 HV, was received with bath concentrations of 6 g/L TMAB and 4 g/L ZrC. Morphological analysis revealed a decrease in ZrC content on the coating surface as TMAB concentration increased. Additionally, the composite coating with a ZrC concentration of 4 g/L exhibited the best corrosion resistance, reducing the corrosion current by 70% compared to the Ni-B alloy.

Keywords: Electroplating, ZrC, Nickel, TMAB, Electrodeposition

ÇUKUROVA ÜNİVERSİTESİ
FEN BİLİMLERİ ENSTİTÜSÜ

YÜKSEK LİSANS TEZİ

Elektrokaplama yöntemi ile üretilen Ni-B/ZrC nanokompozit kaplamaların mekanik ve korozyon özelliklerinin incelenmesi

Ömer HÜKÜMDAR

Danışman: Prof. Dr. Ali KESKİN

Otomotiv Mühendisliği Anabilim Dalı

ÖZ

Elektrokaplama yöntemi, çeşitli uygulamalar için uygun gelişmiş özellikler sağlayarak metalik veya iletken metalik olmayan malzemeleri kaplamak için kullanılabilir. Bakır veya çelik gibi düşük maliyetli ve düşük iletkenliğe sahip metaller, belirli performans gereksinimlerini karşılamak için genellikle nikel ve bor gibi daha sert, daha korozyon ve aşınmaya dayanıklı malzemelerle kaplanır. Bu çalışma, bakır alt tabakalara uygulanan Ni-B/ZrC nanokompozit kaplamalara odaklanarak, elektrokaplama banyosundaki Zirkonyum karbür (ZrC) ve Trimetilamin boran kompleksi (TMAB) içeriğinin ortaya çıkan kaplamanın yüzey özellikleri üzerindeki etkilerini incelemektedir. Elektrokaplama numuneleri, mekanik karakterizasyon, yüzey morfolojisi ve korozyon performansı açısından değerlendirildi. 1020,4 HV'de ölçülen en yüksek mikro sertlik değeri, 6 g/L TMAB ve 4 g/L ZrC banyo konsantrasyonlarıyla elde edildi. Morfolojik analiz, TMAB konsantrasyonu arttıkça kaplama yüzeyindeki ZrC içeriğinde bir azalma olduğunu ortaya koydu. Ayrıca, 4 g/L ZrC konsantrasyonuna sahip kompozit kaplama, Ni-B alaşımına kıyasla korozyon akımını %70 oranında azaltarak en iyi korozyon direncini göstermiştir.

Anahtar Kelimeler: Elektrokaplama, TMAB, ZrC, Nikel, Kaplama

GENİŞLETİLMİŞ ÖZET

Modern endüstriyel uygulamalar, malzemelerin yüzey özelliklerinin iyileştirilmesini gerekli kılmıştır. Malzemelerin yüzey özellikleri, otomotiv, havacılık, denizcilik ve enerji üretimi gibi kritik sektörlerde kullanılan bileşenlerin performansı için büyük önem taşımaktadır. Bu sektörlerde, kullanılan malzemelerin yüzey özellikleri genellikle en zorlu çevre koşullarına dayanıklılık gerektirir. Bu bağlamda, yüzey özellikleri arasında öne çıkan parametreler korozyon direnci, aşınma direnci, sertlik ve yüksek sıcaklıklara dayanıklılıktır. Bu özellikler, bileşenlerin ömrünü uzatmada ve güvenilirliklerini artırmada kritik bir rol oynar. Ekonomik açıdan değerlendirildiğinde, yalnızca korozyondan kaynaklanan mali kayıplar İngiltere'de yılda yaklaşık 17 milyar sterlin ve Türkiye'de 8 milyar ABD dolarıdır. Bu rakamlar yalnızca korozyondan kaynaklanan kayıpları temsil eder; sürtünme ve aşınma gibi diğer yüzey hasarlarından kaynaklanan kayıplar eklendiğinde bu maliyetler daha da artar. Örneğin, İngiltere'de sürtünme ve aşınmadan kaynaklanan ek kayıpların yılda 4 milyar sterlin olduğu tahmin edilmektedir.

Son yirmi yılda, korozyon ve aşınma gibi süreçleri anlamaya ve bu süreçleri önlemek için yöntemler geliştirmeye olan ilgi artmıştır. Bu bağlamda, yüzey teknolojileri üretim mühendisliği süreçlerinde temel bir teknoloji olarak kabul edilir. Uygun yüzey teknolojilerinin kullanımı, malzemelere gelebilecek hasarı önleyebilir veya en azından hasar sürecini geciktirebilir. Ancak, yüzeyde belirgin özellikler oluşturmak için uygun bir yöntemin seçilmesi, malzemenin çeşitli özelliklerini ve karakteristiklerini değiştirmeyi içeren karmaşık bir süreçtir.

Malzemelerin yüzey özelliklerinin sertliği, aşınma, yıpranma ve korozyon direnci termal püskürtme, kimyasal buhar biriktirme (CVD), dönüşüm kaplama, daldırma kaplama, hidrotermal kaplama, kimyasalsız kaplamalar, mikro ark oksidasyonu, fiziksel buhar biriktirme (PVD), elektrokaplama vb. ile iyileştirilebilir. Bu yüzey teknikleri arasında, elektrokaplama yöntemi en yaygın kullanılan tekniktir çünkü yüzeyin görünümünü ve diğer istenen özelliklerini homojen olarak iyileştirmek için ekonomik olarak tercih edilen yöntemdir.

Elektrokaplama, yüzey yapısı modifikasyonu için uygulanan bir elektrokimyasal işlemdir. Elektrokaplama işlemi, uzun bir geçmişe sahip eski bir yüzey mühendisliği işlemidir. Bu işlemde, elektrot/elektrolit arayüzünde meydana gelen elektrokimyasal reaksiyonlar ve elektrokaplama banyosundan gelen iyonların yüzey üzerine birikmesi nedeniyle tek katmanlı veya çok katmanlı kaplama oluşur. Kaplama, lehimlenebilirliği, yağlama özelliklerini, elektrik iletkenliğini, korozyon direncini ve alt tabaka malzemesinin aşınma ve termal direncini iyileştirmek için yüzeye biriktirilebilir. Araştırmacılar, geleneksel malzemelere alternatifler keşfetmek ve malzeme performansını iyileştirmek için sürekli çalışmaktadır; bu da kompozit sistemlerin geliştirilmesine olan ilgiyi artırmıştır. Nanokompozitler, en az biri nanometre ölçeğinde olmak üzere farklı arayüzlere sahip iki veya daha fazla farklı malzemeden oluşan gelişmiş malzemeler olarak tanımlanır. Bu sistemlerde, bir malzeme genellikle sürekli bir matris oluştururken diğeri takviye görevi görür. Bu

nanokompozitlerde, metal matris sürekli fazı oluştururken, ikinci faz metal oksitler, karbürler, nitrürler veya silisyum (Si), alüminyum (Al), titanyum (Ti), zirkonyum (Zr), Tungsten (W) ve Bor (B) gibi elementler gibi takviye malzemelerinden oluşabilir. Son yıllarda, bu kaplamalar iyileştirilmiş mekanik, manyetik, yüksek sıcaklık direnci, optik ve katalitik özellikleri nedeniyle büyük ilgi görmüştür.

Son yıllarda kompozit kaplamalar arasında yer alan Ni-B alaşımları özellikle sertlik, aşınma direnci ve korozyon direnci bakımından üstün özellikler göstermektedir. Elektrokaplama ve kimyasal kaplama yöntemleri kullanılarak elde edilen Ni-B kaplamalar yaygın olarak kullanılmaktadır. Bu kaplamalar sertlik ve aşınma direnci bakımından krom kaplamalardan daha iyi performans gösterirken, Ni-P kaplamalarla karşılaştırılabilir düzeyde korozyona karşı koruma sağlamaktadır. Ayrıca Ni-B kaplamalar düşük maliyet, kayganlık, iyi süneklik, kalınlık, homojenliği, iyi elektriksel özellikler, üstün bağlanma kabiliyeti, düşük gözeneklilik, mükemmel lehimlenebilirlik, antibakteriyel özellikleri ve olağanüstü elektromanyetik özellikler gibi birçok avantajlı özelliğe sahiptir.

Zirkonyum karbür (ZrC) seramikleri, düşük yoğunluk (yaklaşık 6,7 kg/m^3), yüksek sertlik (yaklaşık 2500 HV), yüksek yük taşıma kapasitesi, olağanüstü korozyon direnci, üstün aşınma direnci, üstün termal şok direnci ve termostabilite (ZrC'nin erime noktası yaklaşık 3500 ºC'dir) gibi mükemmel fiziksel ve kimyasal özellikleri nedeniyle kısıtlayıcı kuvvet parçacıkları için ideal bir adaydır. Bu çalışmada, bakır malzemelere göre üstün mekanik özellikler geliştirmek için Ni-B alaşımı ZrC nanopartikülleri ile takviye edilmiş ve elektrokaplama yöntemi ile bakır alt tabaka üzerine biriktirilmiştir. Elde edilen nanokompozit kaplamaların gelişen özellikleri çeşitli analiz yöntemleri ile incelenmiş ve ZrC nanopartikül ve bor kaynaklı trimetilamin boran kompleksi (TMAB) banyo konsantrasyonu değişiminin etkileri açısından detaylı incelemeler yapılmıştır. Ni-B/ZrC kompozit kaplamaların çalışma parametrelerini optimize etmek, mikro sertliği, yüzey morfolojisini ve elektrokimyasal korozyonu ölçmek için kapsamlı bir çalışma yürütülmüştür.

Elektrokimyasal olarak biriktirme banyosu olarak, Watts tipi nikel banyosu esas alınarak belirlenmiştir. Nikel yapısını bor ile alaşımlamak amacıyla, banyoya bor kaynağı olarak değişen banyo miktarlarında (3-6-9 g/L) trimetilamin boran bileşiği (TMAB) eklenmiştir. Nanokompozit kaplamada takviye fazı olarak kullanılan ZrC parçacıklarının etkilerini incelemek amacıyla elektrolit içerisine farklı banyo miktarları (2-4-6 g/L) eklenerek depolama işlemi gerçekleştirilmiştir. Banyo içerisine nano veya mikro parçacıkların eklenmesi, elektrolit içerisinde çözünmüş kimyasalların eklenmesinden çok farklı bir olaydır. Elektrolite tamamen çözünebilen bir kimyasal eklendiğinde, banyo içerisinde tamamen homojen bir şekilde dağılır ve iyonik olarak moleküllerine veya atomlarına ayrılır. Ancak ikinci faz parçacıkları için aynı şeyi söylemek mümkün değildir. Çünkü takviye parçacıkları çözünmeden aynı şekilde elektrolit içerisinde kalmaktadır. Takviye tipinin özelliklerine bağlı olarak ıslanmama, aglomerasyon, dibe çökme veya yüzeye çıkma gibi sorunlar ortaya çıkmaktadır. Çalışmamızda bu sorunları çözmek için iki farklı önlem alınmıştır. İlk olarak,

aglomerasyonu azaltan ve takviye parçacıklarının elektrolit içerisinde kalmasını sağlayan sodyum dodeasil sülfat (SDS) yüzey aktivatör katkı maddesi banyo içerisine eklenmiştir. Parçacıkların kümelenmesini önlemek için bir diğer çözüm yöntemi, depolamadan önce banyoya ultrasonik karıştırma uygulamaktır. Bu işlem, yoğun ultrasonik dalgalar vasıtasıyla parçacık kümelerini parçalar. Bu işlem sırasında banyonun sıcaklığı yükselir, bu nedenle depolama işlemine başlamadan önce uygun sıcaklığa ulaşana kadar bekler. Ultrasonik karıştırma için Vicra Cell VCX 750 marka ve model cihaz kullanıldı. Bu işlem sırasında, çevrim değeri 1'e ve genlik değeri %70'e (~20 kHz) ayarlandı. Kaplamaların üretimi iki elektrotlu elektrokaplama sisteminde gerçekleştirildi. Anot olarak bir nikel plaka ve katot (substrat) olarak bir bakır plaka kullanıldı. Kaplama işleminden önce, 4,5 cm^2'lik bir alanı maskeleyen katot bileşeni belirli işlemlere tabi tutuldu. Kaplama için belirlenen yüzeyden çeşitli kir, pas ve yağ katmanlarını ortadan kaldırmak için yüzey, pürüzsüz bir yüzey elde etmek için kaba taneliden ince taneliye doğru kademeli olarak zımparalandı. Daha sonra, asetonla temizlenen numune saf su ile durulandı. Daha sonra, bakır substrat, hidroklorik asitte (HCl) 1-2 dakikalık bir aktivasyon işlemi ile yüzeyin aşındırılmasıyla aktive edildi. Daha sonra, numune saf su ile durulandı ve elektroliz işlemi için hazırlandı. Elektrolit sıcaklığı, biriktirme işlemi boyunca sürekli olarak 50 ± 1 °C'de kontrol edildi. Watt banyosunun pH'ı dörde dengelendi. Daha sonra, çözelti 30 dakika boyunca çökmeye bırakıldı ve bu süre zarfında kaplama banyosu manyetik bir karıştırıcı kullanılarak sürekli olarak çalkalandı. Elektrokaplama işleminin ardından üretilen nanokompozit kaplamalar saf su ile yıkanarak ortam sıcaklığında kurumaya bırakıldı.

Ni-B/ZrC nanokompozit kaplamaların özelliklerine elektrodepolama açısından önemli üretim değişkenlerinden ZrC parçacık banyo miktarı (2-4-6 g/l), TMAB banyo miktarı (3-6-9 g/l) değişiminin etkileri araştırılmıştır. Ayrıca nanokompozit kaplamaların özellikleri, Ni-B alaşım karşılaştırılmış ve bu kaplamalar esas alınarak özelliklerindeki gelişmeler analiz edilmiştir. Elde edilen kaplamaların sertliklerini belirlemek amacıyla mikrosertlikleri ölçülerek analiz edilmiştir. Ayrıca kaplamaların kristal yapıları XRD örüntüleri elde edilerek incelenmiş, yüzey yapıları taramalı elektron mikroskobu (SEM) görüntüleri ile değerlendirilmiştir. Buna ek olarak SEM cihazı EDS aparatı ile kaplamaların içerik analizleri yüzey yapıları üzerinden yapılmıştır. 3 boyutlu profilometre cihazı ile kaplamaların yüzey pürüzlülük ölçümleri alınmıştır. Son olarak Kaplamaların korozyon davranışları açık devre potansiyeli (ADP), Tafel dış değer bulma yöntemleri ile incelenmiştir.

SEM ile yapılan analiz sonuçlarına göre ZrC parçacıklarının anayapıya başarı ile dahil olduğu ve ZrC parçacıklarının yüzey yapısının karnabaharımsı bir görünüme kavuşturduğu anlaşılmıştır. Ni-B alaşım yüzeyinin incelenmesi, yüzeyde belirgin dairesel çıkıntılarla karakterize edilen bir morfoloji ortaya koymuştur. Bu yapı, kaplama işlemi sırasında oluşan birim hücrelerin kaplama yüzeyinde düzenli olarak büyüdüğünü göstermektedir. TMAB ve ZrC konsantrasyonlarındaki artışla birlikte yüzeyde oluşan dairesel yapıların çaplarının hafifçe arttığı ve daha seyrek dağıldığı görülmüştür. Mikrosertlik ölçümlerine göre saf Ni-B matrisinin sertlik değeri yaklaşık 458,4 HV olarak ölçülmüştür. TMAB banyo konsantrasyonlarının karşılaştırmalı

analizinde, maksimum sertlik değerinin 6 g/L TMAB seviyesinde elde edildiği belirlenmiştir. Dolayısıyla, maksimum mikrosertliğin elde edilebileceği optimum TMAB konsantrasyonunun 6 g/L olduğu sonucuna varılabilir. ZrC nanopartikülleri açısından değerlendirildiğinde, 4 g/L ZrC banyo konsantrasyonu en uygun değer olarak öne çıkmaktadır. 1020,4 HV'lik maksimum sertlik değeri,4 g/L ZrC ve 6 g/L TMAB banyo konsantrasyonlarında elde edilmiştir. En düşük sertlik değeri ise 2 g/L ZrC ve 9 g/L TMAB içeren banyolardan hazırlanan numunelerde 644,4 HV ile gözlenmiştir. Kristal yapıları bakımından incelendiğinde, TMAB, nikelin çökelmesini hızlandırarak daha küçük kristal tanecikleri ve daha düzensiz bir yapı oluştururken, ZrC parçacıkları çekirdeklenme alanlarını artırarak daha büyük kristalitlerin büyümesini engeller ve daha ince tanecik boyutu ve iyileştirilmiş yüzey morfolojisi oluşturur. Elektrokimyasal korozyon analiz arasında yer alan açık devre potansiyel analiz sonuçlarına göre, farklı TMAB ve ZrC banyo konsantrasyonlarında üretilen Ni-B/ZrC nanokompozit kaplamalar, hem bakır alt tabaka hem de saf Ni-B alaşım kaplamalarla karşılaştırıldığında üstün korozyon direnci göstermektedir. Ni-B alaşım kaplamaların ortalama korozyon potansiyeli yaklaşık olarak -0,23 V'dur. Ancak, Ni-B/ZrC nanokompozit kaplamalar arasında en pozitif korozyon potansiyelini gösteren 6T4Z (6 g/L TMAB – 4 g/L ZrC) kaplamanın ortalama OCP değeri yaklaşık -0,15 V'dur. Potansiyodinamik polarizasyon analizi sonuçlarına göre ise, Kaplamaların değişen TMAB konsantrasyonlarında analizi, TMAB konsantrasyonundaki artışın korozyon direncini hafifçe azalttığını ortaya koymaktadır. Korozyon akımı açısından değerlendirmede, TMAB ve ZrC banyo konsantrasyonu 6T4Z (6 g/L TMAB – 4 g/L) ZrC kodlu numune en düşük değere sahipken, TMAB ve ZrC banyo konsantrasyonu 6T0Z (6 g/L TMAB – 0 g/L ZrC) kodlu numune en yüksek değere sahip olmuştur. AFM (Atomik Kuvvet Mikroskobu) analizi sonuçlarına göre, Ni-B matrisinin yüzeyi, yaklaşık 0 ile 30 nm arasında değişen nispeten düşük bir pürüzlülük gösterdi ve bu da Ni-B kaplamaların Ni-B/ZrC kompozit kaplamalara kıyasla pürüzsüz bir yüzeye sahip olduğunu gösterdi. Buna karşılık, Ni-B/ZrC kompozit kaplamalar, matrisin içine ZrC parçacıklarının dahil edilmesi nedeniyle daha pürüzlü bir yüzey sergiledi. Bu ZrC parçacıkları, çukurlar ve tepeler gibi yüzey özelliklerinin oluşmasına neden olarak artan pürüzlülüğe katkıda bulundu. Kaplamaların yüzey pürüzlülüğü ZrC parçacıklarının eklenmesiyle artmış, en yüksek ortalama yüzey pürüzlülüğü (Ra) değeri 6T4Z (6 g/L TMAB – 4 g/L) numunesi için 128,80 nm olarak kaydedilmiştir. En düşük Ra değeri ise 31,68 nm Ra değerine sahip 6T0Z (6 g/L TMAB – 0 g/L) numunesi için gözlenmiştir.

ACKNOWLEDGEMENTS

First of all, I would like to express my sincere gratitude to my valuable advisor Prof. Dr. Ali KESKİN for his unique support, patience, guidance, and motivation throughout my study. He has greatly contributed to my successful completion of this study by guiding me through the research and writing process of this thesis with his competence in mentoring and his shared knowledge.

I would like to express my deepest gratitude to Prof. Dr. Mustafa Atakan AKAR, who supported me like my second advisor throughout my work and who did not refrain from providing assistance at every stage. His valuable advice and guidance significantly contributed to my thesis's content.

I would like to thank our Head of the Automotive Engineering Department, Prof. Dr. Mustafa ÖZCANLI.

I would especially like to thank Res. Asst. Berkay KARAÇOR and Res. Asst. Umut KUMLU for their help and valuable advice throughout my education.

I would like to express my sincere gratitude to all my research assistant colleagues with whom I worked at Çukurova University Automotive Engineering and the valuable staff of Çukurova University Automotive Engineering Department for their continuous support and motivation throughout my work.

Last but not least, I would like to express my endless gratitude to my beloved mother and father, Fatma HÜKÜMDAR and İskender HÜKÜMDAR, and my valuable brother Uğur HÜKÜMDAR, for always being there for me and for being the greatest source of strength in completing this thesis with their support and encouragement.

And finally, I would like to express my sincere thanks to my dear students Eda Nur ÇAMCI, Yusuf AYBACI and Fatih YALYANÇ, who always supported me throughout my experiments, and express my deepest gratitude for their contributions and efforts.

I would like to thank Çukurova University Scientific Research Projects Coordination Office (FYL-2023-16325) for the financial support provided to this project.

LIST OF TABLES

LIST OF FIGURES

SYMBOLS AND ABBREVIATIONS

US	:	United States
USA	:	United States
PVD	:	Physical Vapor Deposition
MAO	:	Micro-Arc Oxidation
CVD	:	Chemical Vapor Deposition
Mg	:	Magnesium
UK	:	United Kingdom
ELP	:	Electroless Coating
Ti	:	Titanium
Al	:	Aluminum
$	:	Dollar
Si	:	Silicon
Zr	:	Zirconium
W	:	Tungsten
B	:	Boron
£	:	Pound Sterling
Ni	:	Nickel
P	:	Phosphorus
ZrC	:	Zirconium Carbide
kg/m^3	:	Kilogram Per Cubic Metre
HV	:	Vickers Hardness Number
UHTC	:	Ultra-High Temperature Ceramic
ºC	:	Celcius
TMAB	:	Trimethylamine Borane Complex
$NiSO_4.6H_2O$	:	Nickel Sulfate Hexahydrate
$NiCI.6H_2O$	:	Nickel Chloride Hexahydrate
NaBH4	:	Sodium Borohydride
DMAB	:	Dimethylamine Borane
$Na_2B_{12}H_{12}$	:	Sodium Decahydrochlorodecaborate
TiN	:	Titanium Nitride
PED	:	Pulsed Electrodeposition
%	:	Percentage
XRD	:	X-ray Diffraction
µm	:	Micrometer

mm^3/Nm	:	Cubic Metre Per Nanometer
i_{corr}	:	Corrosion Current
E_{corr}	:	Corrosion Potential
A/cm^2	:	Ampere Per Square Centimeter
V	:	Voltage
WC	:	Tungsten Carbide
g/L	:	Grams Per Liter
$mg.cm^{-2}$	:	Milligram Per Square Centimetre
hBN	:	Hexagonal Boron Nitride
TiO_2	:	Titanium Dioxide
mL/L	:	Liter Per Milliliter
$C_2H_3NaO_2$	:	Sodium Acetate
CH_4N_2S	:	Thiourea
$(CH_3)_2NBH_2$	:	Dimethylamine Borane
pH	:	Power of Hydrogen
rpm	:	Revolutions Per Minute
Ni_2B and Ni_3B	:	Nickel Borides
Al_2O_3	:	Aluminum Chloride
SEM	:	Scanning Electron Microscope
EDS	:	Energy-Dispersive Spectroscope
B_4C	:	Boron Carbide
COF	:	Coefficient of friction
µA	:	Microampere
SiC	:	Silicon Carbide
K	:	Kelvin
CeO_2	:	Cerium Oxide
GPa	:	Gigapascal
Si_3N_4	:	Silicon Nitride
AlN	:	Aluminum Nitride
V_2O_5	:	Vanadium Oxide
ZrO_2	:	Zirconium Oxide
Tl_2O_3	:	Thallium Oxide
TEM	:	Transmission Electron Microscope
La2O3	:	Lanthanum Oxide
YSZ	:	Yttrium Stabilized Zirconia
i_{peak}	:	Peak Current

$i_{average}$	:	Average Current Density
A/dm^2	:	Ampere Per Square Decimeter
Hz	:	Hertz
ms	:	Millisecond
nm	:	Nanometer
SWCNTs	:	Single-Walled Carbon Nanotubes
3D	:	Three-Dimensional
N	:	Newton
h	:	Hour
min	:	Minute
OCP	:	Open Circuit Potential
EIS	:	Electrochemical İmpedance
TiC	:	Titanium Carbide
CV	:	Cyclic Voltammogram
Co	:	Cobalt
XPS	:	X-ray Photoelectron Spectroscopy
AFM	:	Atomic Force Microscopy
mm/min	:	Millimetre Per Minute
VIII	:	Eighth
g/mol	:	Mass Per Mole
g/cm^3	:	Grams Per Cubic Centimetre
W/Mk	:	Watt Per Meter Kelvin
Cu	:	Copper
IACS	:	International Annealed Copper Standard
$m/\Omega\ mm^2$	:	Meter Per Ohm-Square Millimeter
N/mm^2	:	Newtons Per Square Millimeter
Cl_2	:	Chlorine Gas
$CuCl_2$	:	Copper (II) Chloride
NaCl	:	Sodium Chloride
n_e	:	Electrochemical Valence
coulomb	:	The Unit Of Electric Charge
Ag	:	Silver
M	:	Meter
H_2	:	Hydrogen
DC	:	Direct Current
PC	:	Pulse Current

PRC	:	Reverse Pulse Current
Ton	:	Current On Time
T_{off}	:	Current Off Time
I_f	:	Cathode Current Density
i_r	:	Anodic Current Density
t_c	:	When Intermittent Cathode Current is Applied
t_a	:	When Intermittent Anodic Current is Applied
γ	:	Duty Cycle
H^+	:	Hydrogen
$CuInS_2$	:	Copper Indium Sulfide
BaCO3	:	Barium Carbonate
$Mg(OH)_2$	:	Magnesium Hydroxide
MgO	:	Magnesium Oxide
ZnO	:	Zinc Oxide
SDS	:	Sodium Dodecyl Sulfate
H_3BO_3	:	Boric Acid
cm^2	:	Square Centimeter
kV	:	Kilovolt
WAXD	:	Wide-Angle X-ray Diffraction
Å	:	Ångström
Mg	:	Milligram
Gf	:	Gram Force
kgf/mm^2	:	Kilogram-Force Per Square Millimeter
kgf	:	Kilogram-Force
kp	:	Kilopound
Ra	:	Highest Average Surface Roughness
Rz	:	The Difference Between The Highest and Lowest Points
Rt	:	Total Height of The Roughness Profile
Rq	:	The Square Root of The Arithmetic Mean Deviations
mV	:	Millivolt
mV/s	:	Millivolt Per Second
AC	:	Alternating Current
kHz	:	Kilohertz
FWHM	:	Full Width at Half Maximum
Zr	:	Zirconium
C	:	Carbon

1. INTRODUCTION

Modern industrial applications have made it necessary to develop the surface characteristics of materials. The surface characteristics of materials are of great stature for the performance of components used in critical sectors such as automotive, aviation, marine, and energy generation. In these sectors, the surface properties of the materials used usually require resistance to the most difficult environmental conditions. In this context, the prominent parameters among the surface properties are corrosion performance, wear performance, hardness, and resistance to high temperatures. These characteristics play an essential role in extending the life of the components and increasing their reliability. However, in many cases, the surface properties of materials may be insufficient to meet certain functional demands. In particular, the difficulties caused by environmental conditions can seriously affect the performance of materials. These conditions can be caused by harsh environmental factors such as being in an extremely corrosive atmosphere or being subject to severe abrasion. Such conditions can threaten the materials' basic structural integrity, causing the components' failure or shortening their service life. Therefore, adapting materials to such difficult conditions offers great advantages in terms of both economic efficiency and reliability. When evaluated from an economic perspective, the financial losses caused by corrosion alone are approximately £17 billion per year in the UK and US $8 billion in Turkey. These figures represent losses from corrosion alone; these costs increase even further when losses from other surface damage such as friction and wear are added. For example, in the UK, additional losses from friction and wear are estimated at £4 billion per year. This data clearly demonstrates the importance and necessity of improving the surface properties of materials. Furthermore, using materials with improved surface properties can significantly improve manufacturing processes and operational performance (Ramezani et al., 2023).

Today, issues such as the conservation of raw materials and natural resources, environmental protection, and energy saving have become increasingly important areas of focus in industrial production and material selection processes. In this context, improving the surface properties of materials contributes both to sustainability goals and to the reduction of environmental impacts. For example, some losses from corrosion in the USA are summarized in Table 1.1, highlighting surface treatment technologies' potential economic benefits. As a result, improving the surface properties of materials in modern industrial applications not only develops the performance of components but also provides substantial economic and environmental advantages. Therefore, the development of surface engineering and coating technologies plays a critical role in overcoming the challenges that the industry will face in the future.

Table 1.1. Economic Lost Caused by Corrosion in the USA (Davis, 2001).

Corrosion in the fuel system of Automobiles	100 million $ / Year
Corrosion in the cooler system of Automobiles	52 million $ / Year
Corrosion in the exhaust system of Automobiles	500 million $ / Year

Therefore, if wear and corrosion events are not properly monitored, the damage cannot be compensated (Davis, 2001).

In the last two decades, there has been rising interest in understanding processes such as corrosion and wear and in developing methods to prevent these processes. In this context, surface technologies are considered a fundamental technology in manufacturing engineering processes. The use of appropriate surface technologies can obstruct damage to materials or at least delay the damage process. However, the selection of an appropriate method to create distinct features on the surface is a complex process that involves changing various properties and characteristics of the material. In addition, the selection of the appropriate process generally needs consideration of finance and ecological requirements. By meeting these requirements, the surfaces of various engineering materials can be successfully improved with a variety of techniques (Song et al., 2023).

In particular, the degradation processes occurring on material surfaces, such as corrosion and wear, not only shorten the life of the material, but also cause significant costs in industrial production processes. Therefore, surface engineering techniques play a critical role not only in improving material performance but also in ensuring sustainable production and long-term economic efficiency (Harsimran et al., 2021).

The wear, abrasion, corrosion performance, and hardness of the surface properties of materials can be improved by physical vapor deposition (PVD), conversion coating, micro-arc oxidation, dip coating, thermal spraying, hydrothermal coating, electroless coatings, chemical vapor deposition (CVD), electrodeposition, etc (Cui et al., 2015). The thermal spraying method involves a few various deposition methods, all of which use concentrated heat wellsprings to melt the raw materials and project the molten particles onto the surface to be coated at different kinetic energy levels (Younus and Arshad, 2019). Chemical vapor deposition (CVD) is a vacuum-based method used to apply slim coatings, often for fiber production. PVD (Physical Vapor Deposition) is another method within this category that is low-maintenance and environmentally friendly. PVD has gained attention as an effective process for metal coatings, particularly for improving wear resistance. By enhancing the durability and performance of products, it contributes to their extended lifespan and increased value. Chemical Vapor Deposition (CVD) is a method where gaseous or vaporized substances react on a solid surface, resulting in the deposition of material onto that surface. This reaction typically occurs at high temperatures, causing the precursor gases to decompose and form a thin layer of solid material, often used for coatings or creating thin films. CVD is widely used in

industries for producing high-quality, durable materials (Musbah et al., 2022). Conversion coatings are applied to enhance corrosion resistance and/or improve the adhesion of organic coatings. The strictest definition of a conversion coating refers to a process that transforms the surface oxide of a metal into a coating with different properties, while retaining metal cations from the base metal. A broader definition, however, does not necessarily require the coating to contain cations from the substrate metal. These coatings are commonly used to protect metals from corrosion and to facilitate better bonding with other layers, such as paints or adhesives (Chen et al., 2011). Dip coating is a widely used technique for producing Perovskite solar cells. In this process, the substrate is immersed in a solution, allowing the material to be deposited onto the surface. After immersion, the substrate is removed, and the deposited material is allowed to dry or evaporate, leaving behind a uniform layer with controlled thickness. The key forces involved in the dip coating process include inertia, viscous drag, gravitational force, and surface tension, which all contribute to the formation and uniformity of the coating. This method is known for its simplicity and effectiveness in producing thin, consistent layers. The hydrothermal method is commonly used for synthesizing crystals, zeolites, and ceramic powders. The process involves creating a high-temperature and high-pressure environment by heating the materials in a closed vessel. Water or organic solvents are typically used as the reaction medium, enabling the formation of nanomaterials. This method is particularly effective for the controlled growth of materials with specific properties, making it a popular choice for various advanced material synthesis applications (Singh et al., 2018). Electroless coating (ELP) is a method for coating metallic films on a substrate by reducing metal complex ions in solution with the help of a reducing agent, without applying an external electric field, but using the formed metal as a catalyst (Cheng and Yeung, 2001). Micro-arc oxidation (MAO) is a widely used surface modification technique for creating functional ceramic coatings on valve metals such as magnesium (Mg), titanium (Ti), and aluminum (Al). This method enhances properties like corrosion and wear resistance. During the MAO process, the electrolyte is applied above the breakdown voltage of the oxide layer, causing transient micro-discharges that generate local high temperatures on the substrate surface. These high temperatures promote physical and chemical reactions that result in the creation of a durable oxide surface. This process is effective in improving the surface performance of these metals in various applications. Among these surface techniques, the electrodeposition method is the most widely used technique because it is the economically preferred method to homogeneously improve the appearance and other desired properties of the surface (Zhang et al., 2023).

Electrodeposition is an electrochemical technique used for modifying surface structures. It has a long history, dating back over 2000 years. The process became more widely applied with the development of galvanic cells by Volta around 1800 and the advancements in electric motors from 1800 to 1900, making it a cost-effective method for producing coatings. In electrodeposition, single-layer or multi-layer coatings are formed through electrochemical reactions at the electrode/electrolyte interface, where ions from the electroplating bath are deposited onto the surface. This process

enhances various properties of the substrate, including solderability, lubrication, electrical conductivity, corrosion resistance, and wear and thermal resistance. Researchers are constantly working to discover alternatives to traditional materials and improve material performance, which has increased interest in the development of composite systems. Nanocomposites are defined as advanced materials composed of two or more different materials with distinct interfaces, at least one of which is at the nanoscale. In these systems, one material usually forms a continuous matrix, while the other acts as a reinforcement. Ideally, these two materials should be chemically inert to each other, meaning that no interaction occurs during heating until one of the components melts; however, a small degree of interdiffusion at the interface is acceptable for the purpose of increasing bonding (Dini, 1994).

By adding ceramic particles to a metallic matrix, it allows the creation of composite materials with diverse and unique properties. These composite materials combine the beneficial characteristics of both the metal and the added particles, resulting in enhanced performance in areas for example strength, wear resistance, thermal stability, and corrosion resistance. In these nanocomposites, the metal matrix forms the continuous phase, while the second phase can consist of reinforcement materials such as metal oxides, carbides, nitrides, or elements such as tungsten (W), aluminum (Al), zirconium (Zr), boron (B), titanium (Ti), and silicon (Si). In recent years, these coatings have attracted great attention due to their improved mechanical, magnetic, high-temperature resistance, optical, and catalytic properties. Metal matrix nanocomposites have wide applications in the aerospace, automotive, and military industries due to their superior physical behaviors such as lightweight, high mechanical properties, electrical and thermal conductivity. In addition, the corrosion performance and wear of components can be greatly increased with these coatings, representing a growing industry with significant economic value (Huang et al., 2023).

In recent years, Ni-B alloys, which are among the composite coatings, have shown superior properties, especially in terms of wear performance, corrosion performance, and hardness. Ni-B coatings obtained by using electroplating and chemical coating methods are widely used. These coatings perform better than chrome coatings in terms of wear performance and hardness while providing protection against corrosion at a level comparable to Ni-P matrix. Moreover, Ni-B matrix has many other advantageous properties such as low price, good electrical properties, lubricity, low porosity, good ductility, excellent solderability, thickness uniformity, extraordinary electromagnetic properties, antibacterial properties, and superior bonding ability. Thanks to these attractive properties, Ni-B coatings find wide applications in many areas such as electronics, automotive, aviation, food, optics, plastic, printing, textile, paper, and computer industries. These coatings are preferred especially in applications requiring high performance and show superiority in parameters such as thickness and uniformity of the coating, wear performance and corrosion performance. Ni-B coatings also attract attention with their antibacterial and electromagnetic properties. These coatings have a wide area of applications due to their advantages such as price activity and ease of application

(Ünal et al., 2023). In this research, the characterization of the Ni-B alloy coating was enhanced by supporting it with zirconium carbide (ZrC) ceramic particles.

Zirconium carbide (ZrC) ceramics are highly regarded as ceramic particles because of their exceptional physical and chemical features, including light density (approximately 6.7 kg/m^3), loud hardness (around 3000 HV), remarkable load-carrying capacity, excellent corrosion performance, superior wear performance, and excellent thermal shock performance. With a melting point of about 3500ºC, ZrC is classified as an ultra-high temperature ceramic (UHTC). Commercially available, ZrC is widely used as a protective coating material in diverse industrial applications. Several methods for fabricating ZrC-containing coatings exist, such as plasma sputtering, pulsed laser deposition, magnetron sputtering, pack cementation, and chemical vapor deposition. But the use of ZrC ceramics as reinforcement in electrodeposited composite coatings is limited, and studies on the corrosion performance and mechanical feature of ZrC nano-ceramics in alloy composite matrices are still incomplete and not fully understood (Li et al., 2021).

In this research, Ni-B alloy was strengthened with ZrC nanoparticles to improve the mechanical characterization of copper plates, with the composite coatings deposited onto a copper substrate using the electroplating method. The resulting nanocomposite coatings were thoroughly analyzed using various techniques to investigate the impact of ZrC nanoparticle addition and the bath concentration of the boron source, trimethylamine borane complex (TMAB). A comprehensive study was conducted to develop the operating conditions of the Ni-B/ZrC deposited, focusing on the measurement of microhardness, surface morphology, and electrochemical corrosion performance.

2. PRELIMINARY WORK

2.1. Ni-B Main Matrix Nanocomposite Coatings

Nickel–boron (Ni-B) matrix coatings have been the subject of relatively limited research, and most of the existing work has concentrated on the manufacture and characterization of these coatings. Typically, these studies employ a Watt-type nickel electrolyte, where nickel sulfate hexahydrate ($NiSO_4.6H_2O$) and nickel chloride hexahydrate ($NiCI.6H_2O$) serve as the primary nickel sources. The formation of the Ni–B coating by precipitation of boron into the nickel alloy is facilitated by the incorporation of various boron sources during the electroplating process. Commonly used boron sources include dimethylamine borane (DMAB), carborane ion, sodium borohydride ($NaBH_4$), trimethylamine borane (TMAB), and sodium decahydrochlorodecaborate ($Na_2B_{12}H_{12}$). These reagents play a critical role in the code position method, affecting both the composition and properties of the resulting Ni-B alloys (Bekish et al., 2010; Karabulut et al., 2017; Ünal and Karahan, 2018b).

Doğan et al., (2020) employed the pulsed electrodeposition (PED) method to deposit a Ni-B/TiN nanocomposite coating reinforced with titanium nitride nanoparticles. Trimethylamine borane (TMAB) was employed as the boron source in the Watt-type nickel bath. The pulsed electroplating method was employed at varying duty cycles of 20%, 40%, 60%, and 80%. In order to analyze the phase structures of the deposited layers, X-ray diffraction (XRD) was utilized. Nanoindentation hardness analysis were conducted on the cross-sections of the deposits, while back-and-forth ball-disc tests were performed for tribological results. A coating thickness of ~69.7 μm was obtained on the cathode surface depending on the duty cycle. Microhardness results showed that the coating hardness reached 1170 HV at 40% duty cycle. The results of the wear analysis demonstrated that the dispersion of TiN particles in the coating resulted in a reduction in the wear rate of the coating to 2.121 x 10^{-5} mm^3/Nm. In consideration of the duty cycle/reinforcement particle distribution relationship, the i_{corr} and E_{corr} results were determined to be 2.27 x 10^{-6} (A/cm^2) and -0.427 V, respectively.

Hosseini et al., (2019) investigated the impact of WC bath concentration on the characteristics of Ni-B/WC nanocomposites manufactured via the pulsed current process. It was observed that the grain size increased with the addition of 4 and 8 g/L WC nanoparticles to the bath concentration. As a result, it was determined that the mechanical and electrochemical properties deteriorated. With the addition of 12 g/L WC, great corrosion and wear resistance was obtained as a consequence of the generation of fine and compact structures. The corrosion performance of the Ni-B/WC coating obtained at 12 g/L bath concentration was 59.967, the wear weight loss was 2.1 $mg.cm^{-2}$, and the friction coefficient was 0.64.

Ünal and Karahan, (2018a) produced Ni-B/hBN composite coatings using electroplating method on St-37 low carbon steel plate. Trimethylamine borane (TMAB) was used as a boron source

in composite coatings and electroplating was carried out at different hBN bath concentrations. In addition, pure Ni and Ni-B alloy coatings were deposited in comparison with composite coatings. The study revealed the production of smooth, compact and fine-grained composite coatings. The microhardness of the composite coatings was observed to be 325% higher than that of the pure nickel coating and 10% lower than that of the Ni-B coating. Furthermore, it was determined that the corrosion rate of the composite coatings was 87.5%, 86%, and 30% lower than that of the mild steel substrate, the Ni-B alloy, and the pure nickel coating, respectively.

Wang et al., (2014) deposited Ni-B/TiO_2 nanocomposite coatings on mild steel using a novel sol-enriched method. Ni-B/TiO_2 nanocomposite coatings were improved by adding a small amount of TiO_2 sol solution and DMAB particles to the base solution. The mechanical properties of the improved Ni-B/TiO_2 nanocoating's were significantly improved compared to Ni and Ni-B alloy coatings. The microhardness of the Ni-B alloy matrix with 12.5 mL/L TiO_2 was received to be 1061 HV, that of the Ni-B alloy was 677 HV, and that of pure nickel was 350 HV. Considering the wear resistance, significant improvements were achieved. The Ni-B alloy coating strengthened with 12.5 mL/L TiO_2 decreased compared to pure nickel but improved compared to the Ni-B coating.

Duru et al., (2021) investigated the impact of varying the amount of reducing agent, stabiliser, coating bath temperature and stirring speed on the optimization of Ni-B coatings. The resulting effects on coating hardness and wear were also examined. Nickel chloride ($NiCI_2.6H_2O$) was used as the nickel source of Ni-B coatings, sodium acetate ($C_2H_3NaO_2$) as the complexing agent, thiourea (CH_4N_2S) as the stabilizer and DMAB ($(CH_3)_2NBH_2$) as the reducing agent. The bath coating deposition was set to 1 hour and the pH was set to 6. Bath parameters and concentrations are as follows, reducing agent amount (2 g/L, 3 g/L, and 4 g/L), coating bath temperature (65ºC, 70ºC and 75ºC), stabilizer amount (0.5 mg/L, 1 mg/L, and 2 mg/L) and stirring speed (250, 300 and 350 rpm). As a result of the coatings, the surface morphology is seen to be in the form of cauliflower. The XRD analysis revealed that the coatings produced in different reducing agent (DMAB) bath concentrations were amorphous after annealing at 400°C for 2 hour. Furthermore, the formation of nickel borides (Ni_2B and Ni_3B) phases was observed, accompanied by an increase in the preferential orientation of the nickel crystal plane (111). The impact of DMAB bath concentration on the coating was subjected to comprehensive investigation in both the precipitated state and following annealing. It was observed that the formation of nickel borides subsequent to annealing resulted in enhanced hardness. As a result, the free-crack and compact properties of the B2 sample with hardness (850 HV), wear rate (2.92 x 10^{-7} mm^3/Nm), and friction coefficient (0.37) were obtained. Accordingly, the results show that a high-strength B2 sample received with 3 g/L DMAB bath concentration and 70ºC electrolyte temperature can be used in a harsh environment.

Aslan and Duru, (2022) investigated the high-temperature wear characteristics of Ni-B/Al_2O_3 nanocomposite coating produced on low-carbon steel using the electroplating method. The surface morphology of the coating was analysed by scanning electron microscope (SEM), while the

dispersion of chemical elements within the coating was evaluated through the use of an energy-dispersive spectroscope (EDS) connected to SEM. Following the application of a heat treatment to the resulting coatings at 400°C for a period of two hours, the asset of Ni_2B and Ni_3B phases was confirmed by XRD analysis. The friction-wear characteristics of the Ni-B/Al_2O_3 nanocomposite coating were examined under diverse sliding velocities and loads at elevated temperatures (100, 200, 400 and 600°C), and the surface topography of the worn surfaces was analysed. It was demonstrated that the deposition of Al_2O_3 on the surface of the samples led to a notable enhancement in the wear resistance of the coating. Upon increasing the temperature to 400°C, the friction coefficient of the coating exhibited a notable decline, reaching a value of 0.42.

Zhang et al., (2021) deposited Ni-B/B_4C nanocomposite coatings on N80 steel by pulsed electrodeposition (PED) method. To obtain the optimum parameters of the composite coating, the effects of B_4C content at different bath concentrations on the surface morphology, microstructure, hardness, and electrochemical characterization were investigated. The findings indicated that B_4C particles were consistently distributed across the surface of N80 steel, and no evidence of pinholes or microcracks was discerned. In terms of hardness and wear analysis, Ni-B/B_4C had the highest hardness of 1030.61 HV and the average coefficient of friction (COF) was 0.22 (the average COF of Ni-B was 0.49). Electrochemical corrosion analysis was carried out in 3.5 w% NaCl solution. As a result of this analysis, Ni-B/B_4C (2 g/L) exhibited great corrosion performance at bath concentration, with a corrosion voltage of -0.30 V and a corrosion current of -1.15 μA.

Ogihara et al., (2014) deposited Ni-B/SiC composite coatings containing bath concentrations of trimethylamine borane and SiC nanoparticles by electrodeposition method. The overarching objective of the study was to examine the influence of key parameters, namely the size of SiC nanoparticles, the concentration of SiC nanoparticles in the bath, the application of heat treatment, and the current density, on the formation of Ni-B/SiC composite coatings. When the results were examined, it was seen that the microhardness value increased with the increase in SiC bath concent. While the hardness value in the solution containing 1 g/L SiC reinforcement was 760 HV, the hardness value in the solution containing 8 g/L SiC particles was 858 HV. Similarly, there were changes in the hardness of the composite coatings with current density. The application of heat treatment at 573 K in air also had a notable impact on the hardness of the material. The hardness of the Ni-B/SiC composite coating increased from 845 HV before heat treatment to 1499 HV after heat treatment. XRD analysis patterns showed that heat treatment caused structural change from the amorphous structure of the Ni-B matrix to crystalline Ni metal and Ni_3B alloy. Finally, according to the wear analysis results, Ni-B/SiC composite coatings showed higher wear resistance performance than Ni/SiC and Ni-P/SiC.

Shakoor et al., (2014a) deposited Ni-B/CeO_2 composite coating on low carbon steel substrate using Watt type electrolyte. Boron source was 3 g/L DMAB, reinforcing particle was 15 g/L CeO_2, bath temperature was 43°C and pH was set as 4. The elemental weights of the composite coatings

obtained were found to be Ni 88.66%, B 6.54%, and CeO_2 4.79%. Surface morphology analysis revealed that smooth, intense and fine-grained deposits were formed in both Ni-B and Ni-B/CeO_2 composite coatings. However, with the addition of CeO_2 grain to the Ni-B matrix, the composite coatings exhibited higher surface roughness. The durability value of Ni-B coatings was devised to be 11 GPa and that of Ni-B/CeO_2 composite coatings was found to be 37 GPa. When the elastic modulus was compared, it was measured as 120 GPa while it was measured as 180 GPa for Ni-B/CeO_2. The results of electrochemical polarization tests demonstrated that the incorporation of CeO_2 enhanced the corrosion resistance of Ni-B coatings. This enhancement in corrosion resistance can be ascribed to the reduction in the active surface of Ni-B coatings in the asset of CeO_2 grain that are inactive within the Ni-B matrix.

Krishnaveni et al., (2009) produced Ni-B and Ni-B/Si_3N_4 composite coatings using the electrodeposition method. The effect of incorporating Si_3N_4 nanoparticles into the Ni-B main matrix on surface morphology, structural characteristics, microhardness, and wear resistance properties was evaluated. The addition of Si_3N_4 nanoparticles to the Ni-B main matrix resulted in a reduction in the metallic luster of the coating, an increase in surface roughness, and a change in the coating's chemical composition. While the chemical composition of the Ni-B main matrix was 97 wt% Ni and 3 wt% B, with the addition of Si_3N_4 to the Ni-B main matrix, 89.6 wt% Ni, 2.4 wt% B and 8 wt% Si_3N_4 were formed. While the surface morphology of Ni-B alloy coatings showed homogeneous and fine-grained structure formation, Ni-B/Si_3N_4 composite coatings showed a homogeneous fine structure formation with Si_3N_4 particles evenly distributed throughout the matrix. As a result of heat treatment (400 ºC for 1 hour), the crystallinity of the coatings increased and the formation of the Ni_3B phase occurred. When the hardness results of the coatings were compared, the hardness value of the Ni-B alloy coating with 8 wt% Si_3N_4 nanoparticles was 640 ± $HV_{0.1}$, while the hardness value of the Ni-B alloy was 609 ± 15 $HV_{0.1}$. After heat treatment, the hardness value of the Ni-B alloy was measured as 817 ± 22 $HV_{0.1}$, while the hardness value of the Ni-B/Si_3N_4 composite coatings was measured as 955 ± 24 $HV_{0.1}$. Heat treatment (400 ºC for 1 hour) increased the hardness of the electrodeposition Ni-B and Ni-B-Si_3N_4 composite coatings to 817 ± 22 and 955 ± 24 $HV_{0.1}$, respectively. The increase in the hardness of these coatings after heat treatment was thought to be due to the precipitation of nickel boride (Ni_3B). The wear resistance of Ni-B/Si_3N_4 nanocomposite coatings was received to be higher than Ni-B alloys both before and after heat treatment.

Arai et al., (2010) Ni-B alloy composite coatings produced by electrodeposition method of Ni-B alloys containing boron particles were heat treated and as a result, their microstructures and microhardness results were investigated. The boron content of the alloy composite coatings increased with increasing boron particle concentration in the bath concentration and reached a maximum value of 34.3 atom%. When the microstructure of the coatings was examined, boron particles were distributed evenly in the Ni-B alloy composite coatings. When the 34.3 atom% B alloy composite coatings were heat treated above 500°C, the microstructure became homogeneous due to the

diffusion between the boron particles and the Ni-B alloy matrix. After heat treatment, the hardness of the Ni 34.3 atom% B alloy composite coating was found to be higher than the Ni 6.4 atom% B alloy coating.

Ogihara et al., (2011) obtained Ni-B/diamond composite coatings by electrodeposition method. Ni-B main matrix and diamond particles added to the bath solution have very high hardness, so the obtained Ni-B/diamond composite coatings also showed very high hardness. The hardness of Ni-B/diamond composite coating was about 3000 HV at most, which is about the same hardness among previously reported superhard coatings. Among the parameters affecting the coating hardness, it was found to be dependent on the diamond content and the size of the diamond particles deposited therewith. Among the things affecting the diamond content, it can be controlled by electrodeposition conditions such as diamond concentration in the baths and current density. The highest hardness values were observed in composite coatings with high diamond content and larger diamond particles. Also, after heat treatment (573 K in air) the hardness of the composite coatings increased.

Waware et al., (2018) investigated the structure, hardness, and corrosion resistance of Ni-B/AIN composite coatings formed by the deposition of AIN nanoparticles on the Ni-B main matrix. DMAB was used as a B source in Ni-B main matrix coating and DMAB and iron sulfate were used as B and AIN sources in Ni-B/AIN composite coating, respectively. As a result of the studies, both Ni-B and Ni-B/AIN composite coatings were successfully performed. The addition of AIN particles to the Ni-B main matrix caused a 52% increase in hardness value. Similarly, the addition of AIN particles to the Ni-B main matrix caused a 46% increase in elastic modulus. The thermal stability of the Ni-B/AIN nanocomposite was found to be lower compared to Ni-B due to the crystallization of the Ni_3Al intermetallic phase at low temperatures. In terms of corrosion resistance, Ni-B/AIN composite coatings are higher than Ni-B alloys. By adding AIN particles to the Ni-B main matrix, the protection efficiency was increased by 3 times.

Waware et al., (2018) deposited Ni-B-V_2O_5/ZrO_2 hybrid composite coating by electrodeposition method using the direct current method. To investigate the properties of hybrid composites, Ni-B coating was obtained by adding two different V_2O_5 and ZrO_2 nanoparticles to the main matrix. To compare it with hybrid composite coatings, it was compared with Ni-B coating. It was observed that the addition of nanoparticles significantly affected the structure, mechanical, and electrochemical properties of the coating. When the surface morphology of Ni-B-V_2O_5/ZrO_2 composite coatings was examined, it was seen that they showed similar properties to Ni-B matrixes. But smaller structures in terms of protrusion and size were observed on the surface of Ni-B-V_2O_5/ZrO_2 composite coatings. Therefore, it was observed that the general surface roughness of Ni-B-V_2O_5/ZrO_2 was greater than Ni-B coatings. It was observed that the hardness and elastic modulus of the Ni-B-V_2O_5/ZrO_2 hybrid composite were almost 170% and 70% higher than those of Ni-B nanocomposite coating.

Waware et al., (2018) used the electroplating technique to produce composite coatings formed by adding Tl_2O_3 reinforcement to Ni-B matrix coatings. The impact of incorporating Tl_2O_3 particles on the morphology, structure, and electrochemical characteristics of Ni-B/Tl_2O_3 coatings was examined and contrasted with that of Ni-B alloy coatings. The addition of Tl_2O_3 particles to Ni-B alloy coatings resulted in notable alterations in surface roughness, thermal properties, crystal structure, mechanical properties, and corrosion resistance. The Ni-B alloy coatings were found to be amorphous in nature; however, the addition of Tl_2O_3 particles resulted in a notable enhancement in the curly height of the composite coatings. The surface analysis revealed an increase in surface roughness due to the addition of Tl_2O_3 particles, thereby confirming the formation of fine and dense structures in both the Ni-B and Ni-B/Tl_2O_3 composite coatings. The elastic modulus and microhardness of the composite coatings obtained by adding Tl_2O_3 particles to Ni-B alloy coatings were observed to have improved by approximately 80% and 60%, respectively. Following the incorporation of Tl_2O_3 into the Ni-B matrix, a notable enhancement in corrosion resistance was observed, which can be attributed to the reduction in the active area of the Ni-B matrix.

Zhang et al., (2018) employed the electro brush coating technique to create Ni-B/La_2O_3 amorphous/nanocrystalline composite coatings on an AISI 1045 steel substrate. The surface morphology, composition and phase structure of the coatings were investigated in detail using a scanning electron microscope (SEM), energy-dispersive X-ray spectroscopy (EDS) and X-ray diffraction (XRD). Furthermore, analysis was conducted using a transmission electron microscope (TEM). The thermal stability of the coatings obtained in different La_2O_3 bath concentrations was analysed at varying heat treatment temperatures. While metastable structures were obtained when the heat treatment temperature was above 355°C with the addition of La_2O_3, the thermal stability of the Ni-B alloy coating was improved. In terms of surface morphology, typical cauliflower heads were observed in Ni-B/La_2O_3 composite coatings. In addition, the size of cauliflower heads decreased with the increase of La_2O_3 content. According to these results, the most optimum La_2O_3 content was found to be <10 g/L. Finally, according to XRD and TEM analysis, Ni-B alloy coatings were found to have an amorphous/nano crystalline structure, while the addition of La_2O_3 could prevent the growth of the (111) lattice plane.

Li et al., (2019) a new metal-ceramic composite coating of Ni-B/YSZ was deposited by electrodeposition process at different current densities. The applied current densities were comparatively investigated as i_{peak} 4, 6, 8, and 10 A/dm^2 while $i_{average}$ was 2, 3, 4, and 5 A/dm^2, respectively. The frequency value was set as 1100 Hz and the duty cycle was set as 50%. In contrast, T_{on} and T_{off} values were both 0.455 ms. The size of YSZ nanoparticles used as reinforcement was smaller than 50 nm. The effect of current density on the structure, composition, hardness and corrosion resistance properties was analyzed. The crystallite sizes of the obtained coatings varied between approximately 9-11 nm. It was understood that the surface morphology consisted of cauliflower-like structures and was crack-free and compact. Hardness and corrosion resistance

properties were significantly affected by current density, YSZ bath concentration in the coating and particle size. The maximum microhardness value was determined as 920.5 HV in the coatings obtained at 5 A/dm^2. In terms of surface roughness, it varied between 67-71 nm depending on the current density. However, low current density slightly reduced the surface roughness. Electrochemical impedance spectroscopy results showed that the most optimum corrosion resistance properties were obtained at a current density of 4 A/dm^2. In line with all these results, the addition of YSZ particles to Ni-B alloy coatings has great potential advantages in the field of corrosion and wear resistance.

Doğan et al., (2022) examined the wear resistance performance of single-walled carbon nanotube (SWCNT) reinforced Ni-B composite coatings produced by electrodeposition using pulsed current on a mild steel substrate. Single-walled carbon nanotubes (SWCNTs) with a purity of 95%, a length of 10–20 μm, and an outer diameter of 10–30 nm was selected as the reinforcement particles. Single-walled carbon nanotubes (SWCNTs) were introduced to the electrolyte solution in varying concentrations, specifically 0.2 g/L, 0.4 g/L, 0.6 g/L, and 1.0 g/L. Subsequent to electrodeposition, all samples underwent characterization via X-ray diffraction (XRD) algorithms, scanning electron microscopy (SEM), and other measurements. Furthermore, the mechanical performance of the coatings was investigated through nanoindentation and wear testing analyses. Following the wear analysis, the surfaces were subjected to further examination using scanning electron microscopy (SEM), energy dispersive spectroscopy (EDS), and three-dimensional (3D) profilometry. Wear analyses were conducted using Al_2O_3 beads at room temperature with a 2 N load. The coating deposited with a bath concentration of 0.6 g/L SWCNT was observed to exhibit the most optimal result, namely a decrease in the friction coefficient from 0.51 to 0.28. The findings demonstrated that the incorporation of SWCNT reinforcement particles resulted in enhanced tribological performance for Ni-B alloy composite coatings.

Ahmadiyeh et al., (2019) optimized the addition of SiC particles to Ni-B solution to obtain Ni-B/SiC composite coatings with superior corrosion resistance and wear properties. A Watt-type nickel bath was prepared using Trimethylamine borane (TMAB) as boron source and SiC nanoparticles as reinforcement particles. To prevent agglomeration of the prepared solution, sodium dodecyl sulfate (SDS) was added to the bath. SiC bath concentration was added to the bath solution as 0, 4, 8, and 12 g/L. After addition, it was stirred on a magnetic stirrer at 400 rpm for 24 h. Finally, it was dispersed on an ultrasonic stirrer for 20 min before electroplating. The electrodeposition process was carried out with a pulsed current form. The current density was set as 50 mA/cm^2, the duty cycle was set as 20% and the frequency as 10 Hz. The main objective was to investigate the effect of SiC bath concentrations on the obtained nanocomposite coatings. Field Emission Scanning Electron Microscopy (FE-SEM), Energy Dispersive Spectroscopy (EDS) and X-ray diffraction (XRD) were used to analyze the characterization of the coatings. Open circuit potential (OCP), electrochemical impedance (EIS) and potentiodynamic polarization (Tafel) tests were applied in

3.5% NaCl solution to evaluate the corrosion behavior of the coatings. In addition, wear analysis was performed to evaluate the wear character of the coatings. Increasing the bath concentration of SiC nanoparticles up to 12 g/L had a positive effect on the coating microstructure. This provided the production of a coating containing 11% SiC particles. The corrosion resistance of the coatings increased by including 4-12 g/L SiC. The wear resistance of the composite coatings obtained by adding 12 g/L SiC exhibited better performance than the other coatings. The friction coefficient value in this coating was measured as 0.57.

Shakoor et al., (2015) synthesized new Ni-B/ZrO_2 nanocomposite coatings using electrodeposition method. The effect of ZrO_2 addition to Ni-B alloy coatings on the structural, surface, thermal and electrochemical properties of the coating was investigated. In addition, Ni-B alloy coatings were deposited for comparison. Dimethylamine borane complex (DMAB) was used as a boron source. Two bath solutions were prepared with ZrO_2 particles of 0 and 15 g/L. Mild steel samples were used as base samples (cathode). Crystal structure, surface roughness, and thermal properties of Ni-B/ZrO_2 composite coatings obtained by adding ZrO_2 particles showed superior properties compared to Ni-B alloy coatings. When the surface morphology was examined, it was found that Ni-B and Ni-B/ZrO_2 coatings had fine and dense structures. In addition, it was observed that surface roughness increased with the addition of ZrO_2 particles to the main matrix. Electrochemical corrosion analysis showed that the corrosion resistance was significantly improved by adding ZrO_2 particles to the Ni-B main matrix. This may be due to the decrease in the active surface area of the Ni-B matrix.

Ünal et al., (2023) obtained Ni-B/TiC composite coatings by reinforcing TiC particles with Ni-B main matrix on stainless steel substrate using electrochemical deposition method. Trimethylamine borane (TMAB) was used as boron source. The properties of Ni–B/TiC nanocomposite coatings produced by electrodeposition method and the effect of TMAB content were investigated. TMAB content was added as 3, 6 and 9 g/L bath concentrates. Pure nickel and Ni-B alloy coatings were also produced for comparison. In all composite coatings, 50 mA/cm^2 current density was used and the pH of the bath was fixed to 4. The electrodeposition bath was stirred with a magnetic stirrer at 200-300 rpm throughout the storage. The storage time was limited to 60 minutes. According to the cyclic voltammogram (CV) analysis, it was observed that TMAB added to the bath contributed to the increase in the deposition rate. In the crystal structure analysis, it was revealed that TiC became dominant as the bath content increased, while the effect of TMAB weakened when the TiC content decreased. The crystal grain sizes of the composite coatings varied between 5.8 and 16.8 nm. These values were 86% lower than pure nickel. When the microhardness results were compared, it first increased with the increase in TMAB content and then decreased. The highest hardness value was obtained as 817 HV in Ni-B/TiC composite coatings produced in 5 g/l TiC and 6 g/l TMAB bath contents. This value is approximately 2.81 times higher than pure nickel. TMAB did not have a significant effect on the surface morphology, but it caused the B content of the nanocomposite

coating to increase and the TiC content to decrease with the increase in TMAB. TMAB has a significant effect in terms of corrosion resistance. When evaluated in terms of corrosion current, a reduction of approximately 44% was obtained in the coating obtained at 9 g/l TMAB content compared to the coating obtained at 3 g/l TMAB content.

2.2. ZrC Nanoparticle Reinforced Nanocomposite Coatings

Li et al., (2020) Ni-Co and Ni-Co/ZrC coatings were deposited using electrodeposition method. Cobalt sulfate bath concentration added to the main matrix was used as 0, 20, 40, and 80 g/L respectively. Zirconium carbide bath concentration used as reinforcement particle was used as 0 and 20 g/L. The prepared solution was stirred in an ultrasonic mixer for 30 minutes to avoid agglomeration. When the results were examined, ZrC particle content decreased when Co bath content was increased. The phase structure of the obtained coatings changed from face-centered cubic lattice (fcc) to hcp with increasing Co content. Coatings with smaller grain sizes were obtained by adding ZrC reinforcement particles to the Ni-Co main matrix. In addition, greater microhardness, best wear performance, and lower friction coefficient were obtained. Ni–43Co/ZrC coating exhibited the highest hardness (547 HV) and lowest average friction coefficient among the electrocoating's, while Ni–75Co/ZrC coating exhibited the best wear resistance among the electrocoating's.

Zhang et al., (2021) to investigate the effect of ZrC particles on the structure and properties of Ni-ZrC nanocomposite coatings, nickel baths prepared with ZrC particles at different bath concentrations were coated by electrodeposition process. X-ray diffraction and Scanning electron microscope analyses were performed on the obtained Ni-ZrC composite coatings. In addition to these analyses, microhardness and electrochemical corrosion tests were also performed. According to the surface morphology results, a significant change occurred in the structure by adding ZrC particles to the main matrix. By increasing the bath content of the ZrC particle added to the bath solution, the crystal face (200) was suppressed and as a result, the grain size of the coatings decreased. Microhardness results, whereas the microhardness of pure nickel was 221 HV, the highest hardness value was found to be 428 HV at 10 g/L ZrC bath concentration. According to these results, the coating obtained is 1.93 times higher than pure nickel. When the corrosion current values are compared, the coating obtained is lower than pure nickel. According to these results, the microhardness and corrosion performance of Ni-ZrC nanocomposite coatings obtained by electrodeposition were found to be better than pure Ni coating.

Li et al., (2021) zirconium carbide (ZrC) nanoparticle reinforced Ni-W nanocomposite coatings were produced by electrodeposition method using pulsed current form at 5 A/dm^2 current density. The effect of ZrC particles on the coating was investigated at different bath concentrations. They were produced in 0, 0.4, 1, 2, 4, and 6 g/L ZrC particle bath solution, respectively. The duty cycle was set as 50%, frequency as 800 Hz. The chemical composition, crystal properties, microstructure and micromorphology of the electrocoating were subjected to comprehensive

evaluation through the utilization of XRD, XPS, SEM and EDS tests. Furthermore, mechanical properties, including hardness, wear resistance, surface wettability and surface roughness, were evaluated using a Vickers hardness tester, a piston friction test, a water contact angle test and an atomic force microscope (AFM), respectively. The corrosion resistance was investigated through the use of potentiometric polarization, electrochemical impedance spectroscopy, and scanning electrochemical microscopy. The incorporation of ZrC nanoparticles into the Ni-W primary matrix resulted in notable enhancements in the surface morphology, mechanical properties, and corrosion resistance. The most optimum values among the composite coatings obtained were received at 2 g/L ZrC bath concentration. Microhardness results were obtained as 723.36 HV, average friction coefficient as 0.235, and corrosion potential as 0.200 V.

Fayyaz et al., (2021) focused on the production and characterization of novel Ni-P/ZrC nanocomposite coatings with ZrC reinforcement particles using electrodeposition technique. ZrC particles were successfully deposited on the substrate, and bath solution and parameters were optimized. ZrC particles were used with an average size of <80 nm and 99% purity. Structural, surface, mechanical, and electrochemical corrosion tests of Ni-P and 0.75 g/L ZrC reinforced Ni-P/ZrC composite coatings were performed and compared between them. Storage time was 30 minutes, and current density was selected as 48 mA/cm^2. The addition of ZrC particles to Ni-P alloy created a significant effect. According to the microhardness, nanoindentation, wear, and erosion results, the addition of ZrC particles caused the composite coatings to become stronger. In addition, the corrosion protection was improved from 71% to 85.4% by adding ZrC particles to Ni-P alloy coatings.

Song et al., (2022) reported the successful deposition of ZrC particle-reinforced Ni-B/ZrC nanocomposite coatings by the pulsed electrodeposition method. The magnetic stirring speed was selected as 400 rpm, and the bath temperature was set to 50°C. The current density was set at 5 A/dm^2, the frequency at 600 Hz, and the duty cycle at 40%. The micromorphology and microstructure of the metal composite coatings were investigated. The mechanical and corrosion resistance properties of the coatings were subjected to analysis and characterization. The micromorphological test results demonstrate that ZrC was successfully embedded into the pristine Ni-B alloy, which led to a notable enhancement in the coating's micromorphology and crystalline properties, a reduction in the number of pores and cracks on the coating's surface, and an increase in its overall integrity. The surface morphology and roughness of the coating were analysed using scanning electron microscopy (SEM), X-ray photoelectron spectroscopy (XPS) and atomic force microscopy (AFM). The mechanical properties were evaluated through the measurement of Vickers hardness and reciprocating friction, with the resulting scratches analysed by scanning electron microscopy (SEM) and energy-dispersive X-ray spectroscopy (EDS). Furthermore, electrochemical corrosion tests were conducted using electrochemical impedance and polarization techniques. The results demonstrated that the properties of the Ni-B alloy coatings were markedly enhanced by the uniform deposition of

ZrC nanoparticles on the substrate surface. The most optimal result was observed when the concentration of the ZrC bath was 4 g/L. The microhardness of the Ni-B/ZrC composite coatings (1073 HV) was found to be superior to that of the Ni-B alloy coatings (523 HV). Wear analyses were conducted using a 10 mm linear reciprocating sliding method at a speed of 50 mm/min for 20 minutes under a load of 20 N. The friction coefficient exhibited a notable decrease, from 0.462 to 0.218. The electrochemical corrosion results indicated a notable increase in impedance and a reduction in corrosion potential.

3. MATERIAL AND METHOD

3.1. Material

3.1.1. Nickel

Nickel is one of the elements in Group VIII of the periodic table and has an essential place in chemistry. Nickel, with an atomic number of 28, is a complex, heavy, silvery metal. Nickel is an element with ferromagnetic properties, which a magnetic field can attract. This property allows it to form alloys with iron. The atomic weight of nickel is 58.69 g/mol, its melting point is 1455°C, and its boiling point is 2913°C. Nickel oxidizes when in contact with water and air, making it corrosion-resistant. The most common use of nickel is in the production of stainless steel. Stainless steel is obtained by alloying nickel with iron, and this alloy increases the stainless and durable properties of steel. Stainless steel is used in many areas, such as aircraft, trains, automobiles, and household goods. In addition, nickel is resistant to high temperatures and is used in applications requiring high heat, such as gas turbines and jet engines. The catalytic properties of nickel also play an important role in hydrogenation and other chemical reactions in the chemical industry.

Advantages;

- Nickel has a high resistance to oxidation and corrosion, making it ideal for stainless steel and other alloys.
- Nickel has a very high melting point (1455°C), making it suitable for high-temperature applications.
- It has ferromagnetic properties that allow it to be used in magnetic fields.
- It can be used as a catalyst in chemical reactions, especially effective in hydrogenation processes.
- It does not become brittle even at low temperatures, which is why it is used in cryogenic applications.
- It is resistant to wear, which makes it ideal for producing long-lasting parts.
- When alloyed with other metals, it can give materials hardness and durability.
- It is malleable and easily amenable to various forming processes.
- Nickel is an important ingredient in stainless steel production and increases the steel's resistance to corrosion.

Disadvantages;

- Nickels are more expensive than many other metals, which can increase the cost of use.
- Some people are allergic to nickel, which can cause skin irritation and other health problems.

- Mining and processing nickel can harm the environment, causing soil and water pollution.
- When processed at high temperatures, nickel can sometimes become more difficult to process.
- At high temperatures, nickel can begin to oxidize, which can cause an undesirable layer to form on the surface.
- Nickel resources are limited, which can cause supply shortages in the long term.
- Nickel has a lower electrical conductivity compared to metals such as copper (Genchi et al., 2020).

3.1.2. Boron

Boron is an element in group 13 of the periodic table that exhibits semi-metallic properties. Its chemical symbol is B, and its atomic number is 5. Boron has many vital uses in industry and technology. It is a complex and brittle element in the crystal structure. While amorphous boron is powdered in black, crystalline boron is gray-black. It is a semiconductor element that exhibits both conductive and insulating properties. This feature is especially important in the field of electronics. Its melting point is relatively high (about 2076°C), making it useful in producing heat-resistant materials. It has a low density, which makes it preferred in applications that require lightness. It can react with oxygen and other elements at high temperatures but has a stable structure under normal conditions.

Advantages;

- Its low density and high strength provide significant advantages, especially in applications requiring lightness and durability. This feature allows boron to be preferred in composite materials, vehicle bodies and armor plates used in the space and aviation industry. Its lightweight structure also contributes to energy saving by increasing fuel efficiency.
- Boron and boron compounds are highly resistant to high temperatures. For example, boron carbide is a compound with a very high melting point (approximately 2763°C). Thanks to this feature, boron is used in ceramics, heat-resistant glass and refractory materials. It prevents wear and melting by maintaining its structural integrity at high temperatures.
- Boron is resistant to most chemicals and can remain stable even in corrosive environments. Boric acid and boron compounds are used in detergents and cleaning products to increase the water softening and cleaning effects of these products. The chemical resistance properties of boron are especially advantageous in materials used in aggressive chemical environments.

- Boron is an important semiconductor material in the electronics industry. Particularly boron-doped semiconductors ensure efficient operation of electronic devices. Boron is used as a doping agent in silicon-based electronic components, increasing the material's electrical conductivity. This property is preferred to be born in the production of microchips and transistors.
- When alloyed with steel and other metals, boron provides hardness, durability, and wear resistance to materials. For example, boron steel is widely used in the construction, automotive, and defense industries. These alloys are preferred to produce more durable and wear-resistant parts.

Disadvantages;

- High amounts of boron and boron compounds can have harmful effects on human health. Boric acid and borate salts in particular can cause skin, eye, and respiratory tract irritation. In addition, excessive intake of boron can damage the digestive system and have adverse effects on the kidneys. Therefore, safety precautions and restrictions should be taken into account in products that use boron.
- Processing and purifying boron can be costly. Energy-intensive processes are required to produce boron compounds, especially those of high purity. Additionally, some boron-based materials can be more expensive than alternatives. This is one factor limiting the widespread adoption of boron-based technologies.
- Boron mining and processing can harm the environment. Soil and water pollution from mining sites can have negative effects on ecosystems. In addition, boron waste poses environmental risks and can pollute the environment if not disposed of properly. Therefore, environmental protection measures must be taken during boron mining.
- Large reserves of boron are concentrated in certain regions, with Turkey and the United States leading the world in boron production. However, the limited nature of these reserves could lead to supply problems in the long term. In addition, geopolitical tensions between countries with boron reserves could affect boron trade and supply chains.
- Boron can be a difficult element to process at high temperatures. Crystalline boron can be difficult to machine and shape because it is extremely hard and brittle. This can complicate the manufacturing process for boron-based materials and increase costs (Uluisik et al., 2018).

3.1.3. Ni-B Alloy

Nickel-boron (Ni-B) alloy coatings are coating types that stand out with their high hardness, wear, and corrosion resistance and are preferred especially in industrial applications. These coatings are applied to the surface by chemical precipitation or electrodeposition method and are obtained by homogeneously dispersing boron into the nickel matrix. The addition of boron to the nickel coating significantly increases the hardness of the coating and after heat treatment, the hardness can reach 1000-1100 HV levels. This hardness level increases the durability of Ni-B coatings in corrosive environments and high friction conditions. Hardness is a critical property for producing parts that are particularly resistant to wear, so it is widely used in components exposed to wear such as gears, shafts, bearings, and other moving parts. Ni-B alloys offer high corrosion resistance thanks to the natural passive layer of nickel. This property protects the coating against corrosion-causing agents such as seawater, chemicals, and harsh environmental conditions. Therefore, Ni-B coatings are also preferred in applications in sectors such as marine, chemical, and petrochemical. The low coefficient of friction of the coating minimizes friction and wear, providing high performance even in mechanical systems operating without lubrication. Ni-B coatings, whose amorphous structure is transformed into a crystal structure by heat treatment, can thus be optimized for hardness and durability. The application of heat treatment, generally in the temperature range of 300-400°C, increases the wear resistance of the coating while also improving the adhesion performance of the coating to the metal surface. In addition, Ni-B coatings can be turned into a hybrid coating with ceramic particles that can be added to the surface, thus increasing wear and corrosion resistance even further. These hybrid structures are used in environments requiring extreme wear resistance (Doğan et al., 2020; Shakoor et al., 2014a; Waware et al., 2018).

3.1.4. Zirconium Carbide (ZrC) Reinforcement Particles

Zirconium Carbide (ZrC) is an important ceramic material in engineering and industrial applications due to its superior properties such as high melting point, hardness, and chemical stability.

- Approximately 3500 °C, making ZrC suitable for high-temperature applications. It is a very dense ceramic material at approximately 6.73 g/cm^3.
- The hardness of ZrC is in the range of 9-10 on the Mohs hardness scale, making it suitable for use as an abrasive and cutting material. It has good thermal conductivity even at high temperatures.
- Its thermal conductivity at room temperature is around 20 W/m.K.
- ZrC is an inert material. It does not react with most acid and alkaline solutions and is resistant to oxidation.
- It is a good conductor, and its electrical conductivity is comparable to metals.

- It generally contains 11.6% carbon, and its carbide structure increases the strength of the material.
- Zirconium carbide has high mechanical strength and a hard and impact-resistant structure.
- Thanks to its high hardness, it shows superior performance in corrosive environments.
- It offers lower density compared to other carbides, which allows its use in lightweight yet high-strength materials (Fayyaz et al., 2021; Li et al., 2021).

3.1.5. Copper

Copper is an important metal that has a wide range of uses in engineering and industry due to its superior properties such as high electrical and thermal conductivity, mechanical strength, corrosion resistance and easy workability. Copper, which is located in the d-block of the periodic table, has an atomic number of 29 and the symbol Cu, and has remarkable physical properties such as a density of 8.96 g/cm^3, a melting point of 1083 °C and a boiling point of 2567 °C. Its electrical conductivity is defined as 100% based on the International Annealed Copper Standard (IACS), and with this feature, it has become a preferred material in electrical and electronic applications, especially in cable and conductor production. Copper, which also has a thermal conductivity of ~401 W/m.K, is used in applications where heat must be transmitted quickly and efficiently, such as heat exchangers and cooling systems. These physical properties of copper are given in Table 3.1.

Table 3.1. Some physical properties of copper (Mao et al., 2024).

Properties	**Values**
Symbol	Cu
Melting Temperature	1083°C
Thermal Expansion Coefficient	17.7 x 10^{-6} K
Thermal Conductivity	401 W/(m.K)
Electrical Conductivity	40-59 m/Ω mm^2
Module Of Elasticity	125000-128500 N/mm^2
Molar Mass	63.546 g/mol
Boiling Point	2567°C
Longitudinal Expansion Coefficient	0.0000166 cm/°C (0°C)
Density	8.96 g/cm^3
Color	Orange

The mechanical properties of copper are supported by its easy formability and ductility. Thanks to its high deformation capacity, it can be easily processed with different production methods such as rolling, forging, and extrusion. Corrosion resistance, especially due to its low tendency to oxidation and the formation of a passive oxide layer on its surface, shows long-term durability in open-air and humid environments. Chemically, copper is relatively sensitive to acids but is quite resistant to atmospheric conditions. For this reason, it is also used in the marine industry, roofing, and decorative applications. Copper is also extremely suitable for alloying and its mechanical and chemical properties can be further optimized when combined with different components such as bronze (copper-tin alloy), and brass (copper-zinc alloy). Thanks to its high biocompatibility, it is widely used in the production of medical devices in the healthcare sector, in the design of antibacterial surfaces, and in drinking water installations. The combination of these properties allows copper to play a critical role in modern engineering applications and innovative material designs (Mao et al., 2024).

3.2. Method

3.2.1. Electrolysis and Basic Principles

Electrolysis is derived from Greek words meaning to separate electrons. When a current is applied to any electrolyte, the ions formed move towards the electrodes. The ions reaching the electrodes either receive or give electrons. As a result, a chemical change occurs. In short, the chemical change that occurs when an electric current is applied to an electrolyte at low voltage is called electrolysis. For electrolysis to occur, an external current greater than the sum of the anode and cathode equilibrium potentials must be applied to the cell.

Some reduction-oxidation reactions may not occur in the desired direction. Electrical energy is used to make such reactions proceed in the desired direction. The realization of a reaction in the desired direction using electrical energy is also done by electrolysis. Cells in which chemical transformations are carried out using electrical energy are called electrolysis cells. The synthesis of many substances in the industry is carried out by electrolysis. For example, chlorine gas (Cl_2), Al metal, and the nylon raw material adiponitrile. Processes such as purification of copper, metal coating of various surfaces, and recharging of batteries are also carried out by electrolysis. Many metals are also obtained by electrolysis of their compounds, e.g. copper (II) chloride ($CuCl_2$), sodium chloride (NaCl), aluminum oxide (Al_2O_3), etc.

Looking at the historical background of the electrolysis phenomenon, after Volta discovered the battery for the first time in 1800, Carlisle and Nicholson first separated water into its elements. A short time later, Johann Ritter measured the amounts of hydrogen and oxygen, which he detected by separating water into its elements. At the same time, Ritter was a scientist who showed that electroplating could be done with this method. In 1805, the Italian Brugnatelli succeeded in plating gold with the help of an accumulator. In 1807, Humpry Davy decomposed potassium by electrolysis

for the first time. In 1834, Michael Faraday explained the results of his electrochemical research as Faraday's laws of electrolysis. In 1840, the British scientist Wright discovered cyanide electrolytes for gold and silver plating and offered the possibility of coating oxidized metals with nobler metals. Today, the electrolysis method is also used in other areas, especially in processes such as the separation of elements, the recovery and coating of metals, etc (Güney, 2020).

The basic components of the system are an electrolyte containing free ions and an insulation container containing them, a power source that produces the energy required for the formation of ions in the bath, and the anode connected to the positive (+) pole and the cathode connected to the negative (-) pole immersed in the electrolyte and other connection elements. The electrolysis cell is given in Figure 3.1.

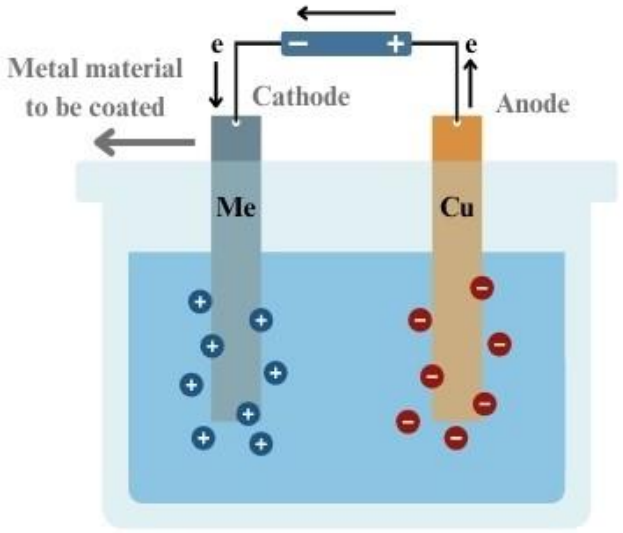

Figure 3.1. Electrolysis cell (Dong et al., 2022)

While electrons move from the anode to the cathode outside the system, they move in the opposite direction, from the cathode to the anode, inside the system (in the electrolyte). When a low voltage current is applied to the system, the positively charged cations (Me^{n+}) in the electrolyte move to the cathode because of ionization, while the negatively charged anions (Me^{n-}) move to the anode. Metal coating is done in this context under different experimental conditions. The coating thickness, coating duration, and other issues required in the coating process can be calculated with Faraday's laws. The thickness obtained in the coating varies in direct proportion to the applied current intensity and coating duration. The strength of the coated material directly determines the strength of the part, and the coating applied to it determines its surface appearance and hardness. The basic philosophy of obtaining metals by electrolysis is always a result of these reduction and purification processes. During the process, the ions that are dissolved because of oxidation from the anode are reduced at the cathode. If an insoluble anode is used (such as noble metals, graphite, or lead), the anode reaction

is due to the oxidation of an anion in the electrolyte. This reaction, expressed in aqueous solutions, is the oxidation of water and as a result, gas will be released at the anode.

When an electric current is applied to the system, positively charged ions (cations) in the solution accumulate at the cathode because of the following reaction.

$$Me^{n+} + ne^- \rightarrow Me^0 \quad (3.1)$$

In the case of using an insoluble anode, the electrons collected at the anode during electrolysis continuously increase and when it reaches the oxidation potential of the water, oxygen starts to be released from the anode.

$$2H_2O \rightarrow O_2 + 4H^+ + 4e^- \quad (3.2)$$

If an insoluble anode is used in the system, the reaction that will occur is as follows:

$$Me^0 \rightarrow Me^{n+} + ne^- \quad (3.3)$$

The electrons that emerge as a result of the anodic reaction are transmitted to the cathode through first-class conductors, and thus the anodic and cathodic reactions occur reciprocally towards each other.

Michael Faraday explained the electrolysis phenomenon, which is basically among the electrochemical subjects, with the following two laws:

First Faraday Law of Electrolysis: When an electric current is passed through any electrolyte, the amount of substance reduced (accumulated) or oxidized (released/dissolved) at the electrodes is directly proportional to the electric charge (amount) passing through the solution.

Second Faraday Law of Electrolysis: As a result of the amount of electric charge passing through the system, the amount of element accumulated or released at the electrodes can be expressed as being proportional to the chemical equivalent weight of that element (Bakan, 2011).

The chemical equivalent is obtained by dividing the ionic weights by their electrochemical valence (n_e). If an electrode dissociates and gives a, v_+ cation with a valence of z_+ and a v_- anion with a valence of z_-, then the electrochemical equivalence of this electrolyte is:

$$v_+ \text{ x } z_+ = v_- \text{ x } z_- = n_e \text{ becomes.} \quad (3.4)$$

To explain this situation, Faraday proposed that uncharged molecules dissolved in solution were composed of equal and oppositely charged particles called ions. When current was applied to the system, the (+) charged ions (cations) moved towards the cathode and the (-) charged ions

(anions) moved towards the anode. Based on this, Faraday introduced the concept of dissociation. The ratio of the number of molecules separated into ions in a solution to the total number of molecules is called the degree of dissociation or ionization.

The amount of a substance that is released or dissolved because of the passage of 1 coulomb of electric charge through an electrolyte is called the electrochemical equivalent of this substance. The electrochemical equivalent of the silver element is 0.001118 grams. If we divide the chemical equivalent of silver by its electrochemical equivalent; 107.88 / 0.001118=96494 coulomb is obtained. This amount of electricity is called 1 Faraday and is indicated by the letter F. 1F = 96500 coulomb is taken as a round figure. Thus, when 1F current is passed through any electrolyte, 1 equivalent gram of the substance is released at the electrode. If 1F current is passed through a solution containing more than one electrolyte, the total of the equivalent weights of the products formed will be in the unit amount.

If the number of ions of the element that becomes free is taken as A, its electrochemical equivalence as n, the amount of electricity passing through the solution as Q = I x t (coulomb), and the amount of substance accumulated at the cathode as m;

$$m = \frac{A \times Q}{n \times F} \text{ or} \tag{3.5}$$

Since Q = I x t, if the formula is rearranged by taking I x t instead of Q,

$$m = \frac{A \times I \times t}{n \times F}, \tag{3.6}$$

it is possible to write Faraday's law as follows (Ehl and Ihde, 1954).

If the values in the formula are taken with their units, they can be written as follows;

m = Amount of product obtained (accumulated in the cathode) (g),

A = Atomic weight of the substance deposited in the cathode, Ag=107.88 (g/mol),

I = Current intensity passing through the system (A),

t = Time (s),

n = Valence of the substance deposited at the cathode in the compound, for Ag=1

F = Faraday constant (96.500 A.s/mol)

Electrode reactions play an important role in the surface treatment of metals. The areas where these reactions are used are;

- Controlling the structure of a metal's surface,
- Repairing or cleaning metals to prepare them for reuse,
- Helping maintains the undissolved metal level in the electrodeposition bath by providing a suitable and controlled source.

- Used in creating copper-plated paths by selectively removing metal from workpieces by open circuit solution or anodic means.
- Allows the regeneration of worn or oxidized parts.
- Environmentally friendly.

The basic components of an electrochemical storage cell are the anode and cathode, which can make contact with an electrolyte. At the cathode, the reduction of the reacting substance occurs by gaining electrons. In other words, electrons are transferred from the cathode to the substance in the electrolyte. At the anode, the oxidation of the reacting substance occurs by losing electrons. Electrons are transferred from the electrolyte to the anode. Both electrodes must be effective electron conductors, and generally metal. (It can be special ceramics, carbon, conductive polymers, and semiconductors) The general points to be considered during electrode storage are as follows:

- Current flow is in the same direction as electron flow.
- Charge transfer in the interface regions is very small (=10^{-9} m) (Özdemir, 2010).

3.2.2. Electrodeposition Method

Developing technology has brought with it the need to improve the performance of materials. In this direction, the method of alloying materials has come to the fore. However, it was realized that alloying the entire material would increase the cost and it was thought that it would be more appropriate to protect only the surface. Coating is a widely used method for protecting materials from the external environment and providing the necessary properties. One of the coating techniques uses the electrodeposition method to coat metals. Electrodeposition can serve many different purposes such as protecting materials, decorative purposes, corrosion resistance, magnetic properties, heat resistance, wear resistance, lubricity, electrical conductivity, and jewelry coatings. Electrodeposition is the process of forming a thin film on a substrate surface by electrochemical reduction of metal ions. This process is carried out in a solution (electrolyte). Electrolyte baths contain metal salts and additives and chemicals that provide pH balance. These chemicals are used to increase the conductivity of the coating process and to optimize the desired properties of the coating. The electrodeposition system includes the surface to be coated, the electrolyte solution, and a counter electrode. To provide current, two electrodes are connected to an external power source. The material to be coated is connected to the negative electrode, and the metal ions are reduced to metal atoms on the surface, and the coating is formed.

There are three basic electrodes in an electrochemical cell: the reference electrode, the counter electrode, and the working electrode. The reference electrode measures the potential of the working electrode without participating in the reaction and stabilizes the solution resistance. The counter electrode completes the circuit by providing the electric field. The 3-electrode electrodeposition system is given in Figure 3.2. While the metal ions are reduced on the working electrode, oxidation occurs on the counter electrode. If it is not desired for the counter electrode to

release metal ions in the solution, a suitable electrode must be selected. The working electrode forms the surface on which the coating process takes place and is also called the substrate (Mao et al., 2024).

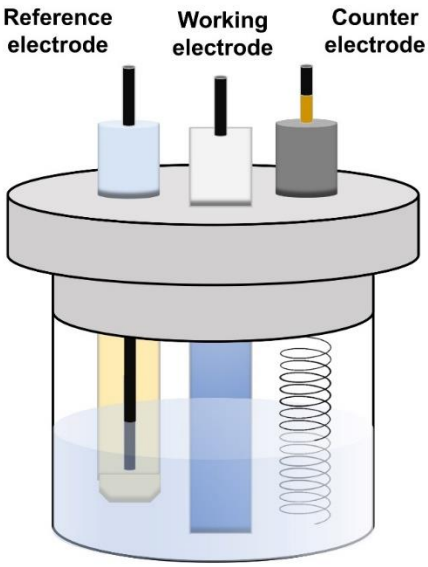

Figure 3.2. Electrodeposition system (Eom et al., 2022)

In the electrodeposition process, when an electric field is applied between two electrodes, ions move from one electrode to the other under the influence of electric current. The passage of electric current in the solution is provided by the movement of these ions. During the electrodeposition process, positively charged ions (cations) move towards the negatively charged electrode called the cathode, while negatively charged ions (anions) move towards the positively charged electrode called the anode. While oxidation reactions occur on the anode electrode connected to the positive end of the power supply, metal ions are reduced on the cathode surface and metal deposits form on the surface.

In this process, the formation of hydrogen (H_2) around the cathode is because hydrogen has a more positive standard potential than metal ions. The formation of hydrogen bubbles can affect the coating structure and have negative effects on corrosion resistance and mechanical properties. Hydrogen bubbles formed in the electrodeposition process can also reduce current efficiency and coating rate. However, this problem can be minimized by keeping the pH of the electrolyte solution under control (Nasirpouri, 2017).

3.2.3. Electrodeposition Method for Coating Nickel Main Matrix Materials

Electrolytic plating of nickel is a surface treatment process that provides nickel deposition on the substrate material in industrial and decorative applications. Electrolytic deposition of nano-crystalline nickel is preferred for various industrial uses due to its advantages such as hardness, wear and corrosion resistance. This plating method of nickel has been developed for many years and is

widely applied in the industrial field today. The electrolytic bath composition used during plating, together with the electrical plating parameters, is a very suitable method in terms of surface engineering due to its low cost, simple installation advantages and the ability to produce dense nickel metal matrix composites in a single process. Nickel coatings produced by electrolytic plating are distributed homogeneously over the entire surface and thus the coatings exhibit superior mechanical properties and corrosion resistance. Today, nickel plating technology is widely used in different industrial applications due to these advantages. The plating process is carried out by suspending the anode and cathode electrodes in a solution (Watts bath) containing nickel salts and reducing the nickel ions to the metal surface with the help of an external electrical source.

The electrical potential applied between the anode and cathode using a power source causes the nickel to dissolve in the solution as positively charged nickel ions from the anode surface. This process is one of the basic steps of the electroplating process and allows the nickel metal in the anode to mix with the electrolyte medium in the solution. These nickel ions, which become free in the solution, move towards the cathode under the influence of the electric field. When they reach the cathode surface, these ions gain electrons and return to the metallic nickel form and accumulate on the substrate surface to be coated. In this way, the desired coating is obtained by depositing metallic nickel on the cathode surface. However, this process does not only involve the precipitation of nickel ions as metal on the surface; at the same time, a side reaction occurs that negatively affects the coating efficiency. This side reaction is the formation of hydrogen ions on the cathode surface as hydrogen gas by taking electrons. This hydrogen formation reaction can reduce the energy and material efficiency of the coating process and affect the quality of the coating. There are three basic reactions that occur during the coating process. The anodic reaction is the electrochemical process that causes the dissolution of nickel, and this process is expressed in Equation 3.7. The cathodic reaction represents the accumulation of nickel ions in the solution as metallic nickel on the cathode surface and is shown in Equation 3.2. In addition, the hydrogen evolution reaction, which is related to the formation of hydrogen gas that occurs during the coating and reduces the efficiency of the process, is defined in Equation 3.3. These three reactions constitute the basic dynamics of the electrolytic coating process and are the factors that determine the success rate of the process and the final coating quality (Gezerman, 2007; Oriňáková et al., 2006).

$$Ni \rightarrow Ni^{2+} + 2e^{-} \quad (3.7)$$

$$Ni^{2+} + 2e^{-} \rightarrow Ni \quad (3.8)$$

$$2H^{+} + 2e^{-} \rightarrow H_2 \quad (3.9)$$

3.2.4. Formation of Composite Coatings by Electrodeposition of Reinforcement Particles with Metal or Alloy Materials

Composite electrodeposition is a complex and technical electrochemical coating method used to produce metal-based composites in a solution containing reinforcement ceramic particles of micro or nano size. This process involves the aggregation of metal ions and ceramic particles in solution to form a solid coating. A schematic description of this process is given in Figure 3.3. The Guglielmi model describes the simultaneous deposition of reinforcement particles with metal or alloys in this process. According to this model, the second-phase particles in the electrolyte solution are surrounded by a cloud of reducible metal ions. In simple terms, metal ions are adsorbed onto the reinforcement particles. The particles surrounded by these ionic clouds are attracted towards the coated substrate (cathode) upon the application of electric current. At this stage, the reinforcement particles are initially weakly adsorbed on the cathode surface. Later, when the metal ions discharge their electric charges, these particles are trapped between the metal atoms that accumulate on the cathode surface and grow over time. In this way, the simultaneous deposition of the metal-based structure and the reinforcing particles, i.e., the co-deposition process, takes place. The Guglielmi model explains this process step by step. In the first stage, the reinforcing particles are surrounded by the ionic cloud formed by the metal ions. When an electric current is applied, these particles are attracted to the cathode surface and are weakly adsorbed there. Then, when the metal ions discharge their electric charges, these particles are trapped between the metal atoms and accumulate on the cathode surface. This process continues with the step-by-step deposition of reinforcing particles and metal atoms on the cathode surface. As a result, metal-based composite structures are obtained. This process is detailed in the model proposed by Guglielmi in 1972 and reveals the dynamic interactions of metal ions and reinforcing particles (García-Lecina et al., 2009).

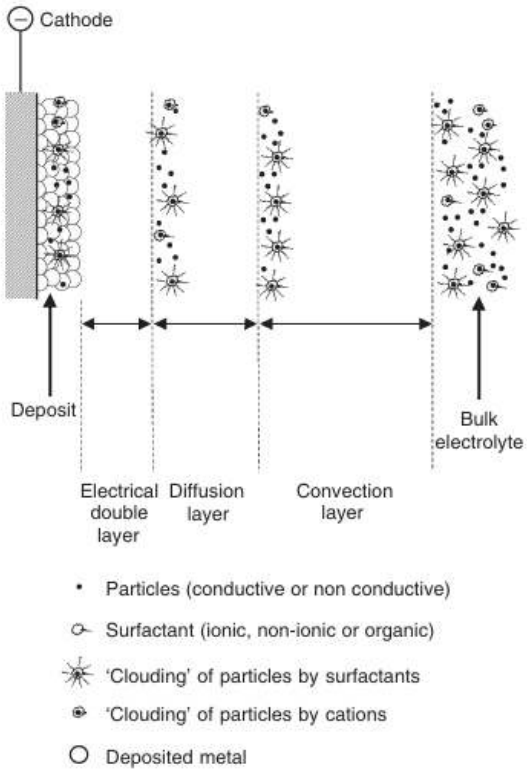

Figure 3.3. Schematic view of the electro-co-deposition process (Lelevic and Walsh, 2019)

The electrodeposition process is a complex surface coating method that develops under the influence of many parameters that determine the coating properties. In addition to the main parameters such as bath content, pH, temperature, current density, and electrolyte mixing, surface activators and additives directly affect the quality of the process. Especially in the case of composite coatings, additional variables such as the type, shape, concentration and particle size of the second phase come into play. Each of these factors plays a decisive role in the thickness, homogeneity, hardness and general durability of the coating to be obtained. The fact that the electrodeposition process is largely based on experimental knowledge requires experience and knowledge accumulation on the part of the operators. In addition, this process often involves aggressive chemicals and solutions, and therefore requires special safety precautions. In this context, each parameter should be examined in detail and the effect of these variables on the coating properties formed during electrodeposition should be evaluated. The effects of these parameters and their contributions to the coating quality are detailed in the following headings (Lapinski et al., 2011; Low et al., 2006; Lu et al., 2014; Saini et al., 2023).

Current Type, Current Density, and Duty Cycle

In the electrodeposition process, current type, current density and duty cycle are the key parameters that directly affect properties such as coating microstructure, mechanical strength, homogeneity and coating thickness. The current type can be in the form of continuous direct current

(DC), pulse current, (PC) or reverse pulse current (PRC) depending on the current profile applied during electrodeposition. Continuous direct current provides continuous coating at a constant current density and is often preferred for homogeneous coating. However, in this case, the coating layers tend to contain larger crystal grains, which can limit the hardness and wear resistance of the coating. In contrast, the use of pulse current and reverse pulse current promotes the formation of fine-grained crystal structures in the coating layer, thus providing a significant increase in coating hardness and wear resistance (Buelens et al., 1983; Zech et al., 1999; Torabinejad et al., 2017). DC, PC, and PRC current methods are coating techniques in which some metals, metal alloys and metal matrix composites are reinforced with ceramic particles. In coatings made with the DC current method, the current is applied directly without interruption. In the PC current method, a constant current is not applied and the current is applied intermittently by giving a certain period to the system. In the PRC current method, the anode and cathode current pulses are applied by mixing. In the discontinuous current display, T_{on} is the time when the current is applied during pulse generation, and T_{off} is the time when the current is cut off. In the reverse intermittent current diagram, i_f represents the cathode current density, i_r represents the anodic current density, t_c represents the time when the intermittent cathode current is applied and t_a represents the time when the intermittent anodic current is applied (Das et al., 2018; Kamnerdkhag et al., 2017; Karslioglu and Akbulut, 2015). Current types are given in Figure 3.4.

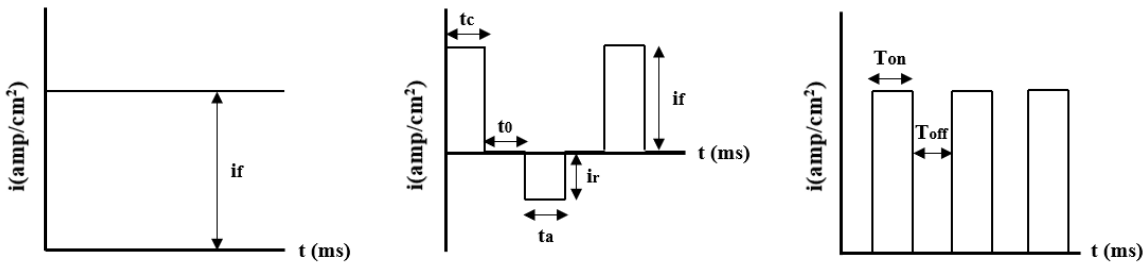

Figure 3.4. Current types (Wang et al., 2022)

DC Current Deposition

DC coating process is generally preferred for thick coatings with short coating times. However, due to the decrease in concentration and potential in the double layer, grain boundary shifts, irregular composition, and structural damage may occur in the coating. For metal ions to be reduced on the substrate surface, they must diffuse from the ion layer formed on the cathode surface during coating. The increase in double-layer thickness and the decrease in metal ions reaching the surface increase the amount of hydrogen entering the coating and cause the coating to clog. The current density waveform in the DC coating process is linear. Since the current cycle time is 100%

in DC coating, the average current density is equal to the peak current density. Two electrodes in a DC electrolyte solution are connected to the output of the DC current source. The cathode is placed on a metal or alloy, where the metal can be a semiconductor or a non-metallic conductor such as graphite. In order for the system to work, the electrical circuit is first completed and then one or more stabilization processes are created at the anode to separate the anions while the metal cations are separated from the solution. Therefore, the total charge in the solution is kept neutral. Here the anode is divided into two layers, the first of which is made of metals such as copper, allowing copper ions to dissolve at the anode and collect the solution at the cathode. The second method is achieved by reducing metal ions in solutions such as copper sulfate metal salts on the cathode surface using a titanium-coated platinum anode (Torabinejad et al., 2017).

PC Current Deposition

In pulse electrodeposition, the potential or current is rapidly changed between two different values. This results in a series of pulses of equal amplitude and duration. Each pulse is an on-time (T_{on}) when a potential or current is applied and an off-time (T_{off}) when zero current is applied. By regulating the composition of the deposited film and the pulse amplitude, it is possible to control the thickness and width of the atomic order. They promote the initiation of grain nuclei and greatly increase the number of grains per unit area, resulting in a finer-grained coating with better properties than traditionally deposited coatings. The pulsed current deposition is a modern electrochemical method that improves the quality of the deposits better than direct current. In the case of pulse deposition, as in any electrodeposition process, the microstructure of the layer depends on crystallization and growth. During crystallization, the atomic population on the surface is higher than in the case of direct current deposition due to the high current density applied, resulting in a smaller grain size in the coating. On the other hand, the adsorption and desorption of various species originating from the electrolyte determine the surface diffusion of new atoms, which influence their incorporation into new crystallites. This results in a change in the microstructure and properties of the deposit. The pulsed electrodeposition process has an advantage over the continuous process, namely, pulsed current electrodeposition induces a higher rate of grain nucleation and results in a more refined grain structure, which benefits the deposit properties of the coatings. In pulsed electrochemical deposition, ions pass through the electrical interface where charge transfer takes place, then they become incorporated into the crystal lattice of the cathode material. However, atoms are usually adsorbed far from the growth stages, so incorporation into a crystal lattice requires surface diffusion. On the other hand, surface segregation may occur during surface diffusion, which may affect the structure, physical and chemical properties of nanostructured thin films. Pulsed coatings form more compact layers and impose less stress on the surface coating than direct current coatings, therefore, the oxide film developed on pulsed current coatings exhibits a more stable form than direct current coatings. Pulsed currents include non-stationary current waves and intermittent currents. Current applications

include unipolar wave (PC) where all current flows in one direction and bipolar wave (PRC) where anodic and cathodic pulses are mixed. Three different parameters change during intermittent current coating. These parameters are independent of each other and are peak current density (I_p), pulse start time (t_{on}), and pulse stop time (t_{off}). ton and toff can be expressed as the time during which the coating current is applied and stopped. I_P is the peak current density or maximum current density, while t_{on} and I_A are the average current density. Pulsed current type is given in Figure 3.5. In pulsed current (PC), the duty cycle (γ) corresponds to the percentage of total time elapsed for one cycle and is as in equation 3.10 (Beattie and Dahn, 2003; Chandrasekar and Pushpavanam, 2008; Karami and Babaei, 2012; Kollia et al., 1990).

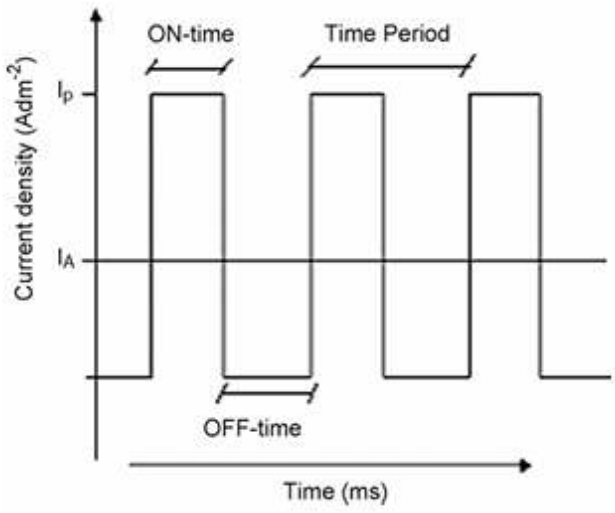

Figure 3.5. Pulse waveform (Chandrasekar and Pushpavanam, 2008)

$$Duty\ Cycle = \frac{T_{on}}{T_{on} + T_{off}} \tag{3.10}$$

Concepts of PC Techniques

In electroplating, a negatively charged layer forms around the cathode as the process proceeds. When DC is used, this layer is charged to a certain thickness and prevents ions from reaching the part. In pulsed current plating, the output is periodically turned off to cause some discharge of this layer. This allows ions to pass through the layer and into the part more easily. High current density areas in the bath cause more depletion of ions than low current density areas. During the t_{off}, ions migrated to depleted areas in the bath. When the pulse tone is formed, more evenly distributed ions are available for deposition onto the part. Advantages of PC techniques;

- Pulsed current significantly increases the limiting current density during T_{off} by simply replenishing the metal ions in the diffusion layer.
- By varying the pulse parameters with a pulsed current, deposits with the desired composition, structure, porosity, and hydrogen content can be obtained.

- Pulsed current coating reduces the need for additives.

Disadvantages of PC techniques;

- In most cases, the cost of a pulse rectifier is much higher than a direct current unit.
- This technology requires a person to think and plan and there are a series of procedures that must be followed to obtain the best results.
- The need for additives is reduced for chemical manufacturers (Chandrasekar and Pushpavanam, 2008).

PRC Current Deposition

The PRC technique is a waveform consisting of cathode and anode pulses over a certain period of time. The PRC technique produces the same diffuse filling effect as the PC technique and can form a uniform coating. The parameters used in the high PRC process require greater attention during the process. In the PRC technique, structural features such as particle size distribution and particle size can be adjusted by adding an anodic pulse to the cathode pulse current and the average current ($-I_A$) and time equations. The PRC technique is given in Figure 3.6. Here, T_{AA} is the anode time, T_C is the cathode time, I_{AA} is the anode current density, I_C is the cathode current density, $\bar{I}_A$ is the average current density, and T is the cycle time (Beattie and Dahn, 2003; Chandrasekar and Pushpavanam, 2008; Karami and Babaei, 2012).

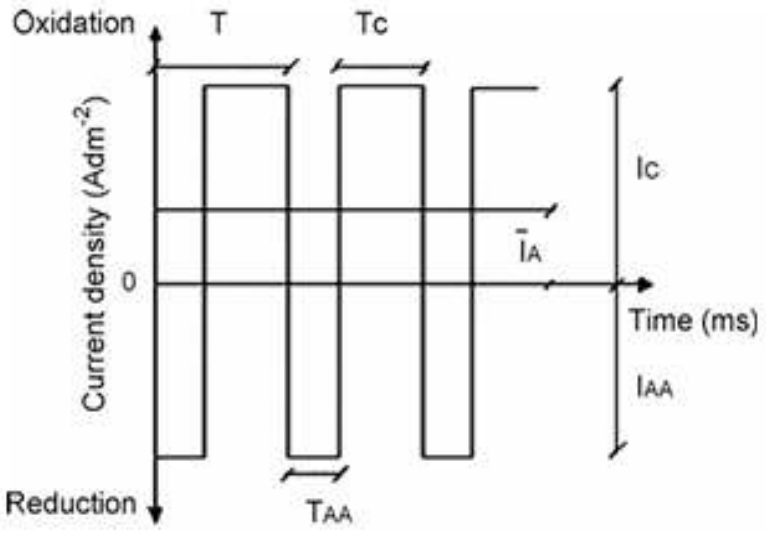

Figure 3.6. Pulse reverse waveform (Chandrasekar & Pushpavanam, 2008b)

Pulse and Pulse Reverse Current Parameters

In the conventional DC plating, there is only one parameter, namely current density (I), which can be varied. But in PC (Figure 3.5.), we have three independent variables, (i) on-time (T_{on}), (ii) off-time (T_{off}), and (iii) peak current density (I_P). In PC, the duty cycle (γ) corresponds to the percentage of the total time of a cycle and is given in equation 3.11.

$$Duty\ Cycle = \frac{T_{on}}{T_{on} + T_{off}} = T_{on} \times f \quad (3.11)$$

where f is frequency, defined as the reciprocal of the cycle time (T).

$$Frequency = \frac{1}{T_{on} + T_{off}} = \frac{1}{T} \quad (3.12)$$

In practice, pulse plating usually involves a duty cycle of 5% or greater and T_{on} from s to ms. PC will deposit metal at the same rate as DC provided the average pulse current density equals the latter. The average current density (I_A), in pulse plating is defined as:

$$I_A = peak\ current\ (I_P) \times duty\ cycle\ (\gamma) \quad (3.13)$$

In the case of the PRC technique, the average current ($\bar{I}_A$) is as given below:

$$\bar{I}_A = \frac{(I_C \times T_C) - (I_{AA} \times T_{AA})}{T_{AA} + T_C} \quad (3.14)$$

In PRC, the duty cycle (γ) is given as below,

$$\gamma = \frac{T_C}{T_{AA} + T_C} \quad \text{with } T_{AA} = T_C \quad (3.15)$$

The current efficiency of PRC is always less than that of PC (Chandrasekar and Pushpavanam, 2008; Colli et al., 2024).

Bath Additives and Ph

In electroplating processes, bath additives, and pH are important parameters that determine the coating quality. Studies on the effects of additives on properties such as surface structure, grain size, and surface roughness show how these components improve or limit the coating quality. Bath additives are chemical components that provide various functions to the coating bath. For example, polishing additives helps to obtain a smooth, shiny, and decorative coating on the surface. Similarly, grain refiners increase the hardness and strength of the coating by reducing the size of the grains formed during metal coating. This feature is quite advantageous in applications where wear resistance is important. Dendrite and roughness inhibitors are important for keeping the coating surface smooth. These additives prevent cracks or pores by covering the surface with a thin film layer. Thus, irregular formations that may occur during deposition are prevented and a more

homogeneous surface is provided (Dini, 1993). For example, Morana (2006) showed in his study that dendrite inhibitor additives provide a great improvement in the coating structure. Wetting additives reduce the surface tension during the coating process and allow metal ions to interact better with the surface. This is important for a homogeneous coating structure, especially in composite coatings with added particles. It prevents agglomeration and ensures that particles are distributed evenly throughout the coating.

Ünal (2016) states that surfactants contribute to homogeneous coating quality by increasing the rate of particle adhesion to the surface. However, there is a possibility that additives in the solution may integrate into the coating during deposition. This may cause the formation of undesirable components in the coating and therefore decrease the coating quality.

Brenner (1963) states that the use of controlled amounts of additives, especially those that create internal stress, reduces this risk. The pH value determines the hydrogen ion (H^+) concentration in the coating bath and has a direct effect on the speed of electrochemical reactions. Low pH provides high ion mobility, which allows the coating to occur rapidly. However, excessively low pH can cause porous structures to form on the coating surface and negatively affect the coating quality. Mohamed and Golden (2016) stated that pH is generally kept below 5 to manage internal stress, and that low pH reduces coating stress and provides homogeneous coating. pH also plays an important role in hydrogen gas formation and hydroxide precipitation during the coating process. Adjusting the solution pH value is critical for the homogeneity of the coating and the conductivity of the solution.

Schlesinger and Paunovic (2010) state that the pH level affects the mass balances and the density of electroactive species in the solution, and therefore different pH levels lead to different coating thicknesses and hardnesses. Inorganic acids or bases can be added to the solution to provide high conductivity. This is especially preferred to save energy and to obtain equal thickness in every area of the coating layer. If the bath pH is not kept stable, fluctuations in coating quality may occur. Buffer substances are added to keep the pH level constant. These substances provide homogeneous coating by minimizing pH fluctuations in areas close to the electrode surface. Brenner (1963) stated that buffer substances prevent undesirable reactions by regulating pH changes on the electrode surface.

Mixing the Electrolyte

During electroplating, mixing the electrolyte is a critical process for the homogeneity and quality of the coating. Mixing ensures that the ions and particles in the electrolyte are evenly distributed on the surface, while also improving the thickness and structural properties of the coating. During the mixing process, the temperature in the solution is balanced, thus increasing the mobility of the ions, and the ions are transported to the coating surface in a balanced manner. In this way, unwanted accumulation and roughness on the surface during the electroplating process are prevented. The correct adjustment of the mixing speed is of great importance for the quality of the coating.

Excessively fast mixing can cause the particles to hit the cathode at high speed; this can lead to the particles not being able to adhere sufficiently to the cathode surface. On the other hand, slow mixing can cause the particles to coalesce and agglomerate, which disrupts the homogeneity of the coating. It is recommended to keep the mixing speed higher for nano-sized particles, as such particles tend to aggregate and cluster easily in solution.

Although magnetic stirrers are traditionally used, pre-mixing the coating bath with ultrasonic homogenizers provides significant benefits for composite coatings. Ultrasonic mixing is an effective method to increase the homogeneity of the bath and to distribute the particles in the solution evenly. In addition to reducing the amount of agglomeration in the solution, this process also increases the co-deposition of the particles during the coating, thus achieving a more uniform and homogeneous structure on the coating surface. In addition, the particles in the solution are reduced in size by ultrasonic mixing, which improves the properties of composite coatings. Ultrasonic mixing has a direct effect on the particle structure of the solution. In particular, this process prevents particle agglomeration, i.e., prevents the particles from sticking together and forming large clusters. Thus, smaller and homogeneous particles are obtained, which reduces the roughness on the coating surface. During ultrasonic mixing, high-frequency vibrations of sound waves shake the particles in the solution, distributing them more uniformly. This type of process ensures that especially nano-sized particles are mixed in the coating baths and guarantees that these particles are evenly distributed in the solution. In the literature, many studies have addressed how ultrasonic mixing is effective on different types of materials (Mohamed and Golden 2016; Buelens et al., 1983; García-Lecina et al., 2012).

For example, Bahrami Mousavi et al., (2012) stated that semiconductor materials such as $CuInS_2$ provide more homogeneous distributions with ultrasonic mixing. Alavi and Morsali, 2010) showed that $BaCO_3$ and SiC materials obtain a finer and more homogeneous structure with ultrasonic mixing. In addition, Ünal and Karahan (2018a, 2018b) stated in their study on $Mg(OH)_2$ and MgO materials that ultrasonic mixing provides better distribution by reducing the size of the particles and thus increases the coating quality. Studies on ZnO (Lu et al., 2014) and hBN (Ünal and Karahan, 2018a, 2018b) materials have also shown that materials obtained by ultrasonic mixing have a more uniform crystal structure and a more balanced distribution in the coating matrix. Coating obtained by ultrasonic mixing can exhibit higher mechanical and aesthetic performance since they contain more uniform crystal structures, homogeneous distribution, and fine, nano-sized particles compared to the materials used. This method provides a significant advantage especially in the coating processes of nanostructured and composite materials. As a result, ultrasonic mixing allows more durable, smooth, and uniform coatings to be obtained by homogeneously distributing the particles in the solution.

Temperature

The solution temperature has a significant effect on the efficiency of the electroplating process and the quality of the coating. This effect can manifest itself in two opposite ways, depending on how the temperature directs the chemical and physical reactions in the electrolyte solution. On the one hand, increasing the temperature increases the mobility of the ions in the solution and accelerates the rate of diffusion between the ions. This allows the crystals to grow faster, allowing small crystalline structures. Small crystals form more uniform and smooth coating surfaces, which can improve the aesthetic quality and mechanical properties of the coating. However, as the temperature increases, an effect such as a decrease in polarization on the cathode can also be observed. This can lead to the formation of larger crystals, since the growth of large crystals is a slower but less energy-intensive process. Thus, when the temperature is high, the crystal structures can generally be larger and rougher, which can lead to poor coating quality. An increase in the temperature of the solution also affects the viscosity of the electrolyte and its tendency to sediment. As the temperature increases, the viscosity of the electrolyte solution decreases, which makes the movement of the ions more free and thus can increase the speed of the coating process. However, high temperatures can also increase the rate of hydrolysis of some components in the solution, which can trigger undesirable reactions. Increasing the temperature can also increase the evaporation rate, leading to the loss of components of the electrolyte solution and thus to the imbalance of the electrolyte components. This can negatively affect the coating quality. In addition, the deposition rate of additives in the solution can increase due to high temperatures. In this case, the homogeneous distribution of particles used in the production of composite coatings in the solution can be disrupted, especially because as the temperature increases, the tendency of additives to stick together increases. All these mutual effects make it difficult to determine the correct temperature value in the electroplating process. Therefore, temperature values in electroplating processes are usually determined experimentally. Keeping the temperature in a narrow range of ±2 °C is necessary to obtain the best results (Rezende et al., 2016; Ünal, 2016). In the literature, it is seen that composite coatings obtained by electrodeposition are mostly obtained in electrolytes in the range of 40-60°C. This temperature range ensures that the coating has a homogeneous and smooth structure, while at the same time preventing the formation of undesirable large crystals. In this temperature range, the particles in the electrolyte are distributed more stably and the performance properties of the composite coatings (hardness, durability, corrosion resistance, etc.) are optimized (Sheu et al., 2019; Ünal and Karahan, 2018a; Ünal, 2016).

3.2.5. Electrodeposition of Ni-B/ZrC Nanocomposite Coatings

Electrochemically deposited coating with nickel boron alloy (Ni-B) structure was reinforced with zirconium carbide (ZrC) second phase ceramic particles and Ni-B/ZrC nanocomposite coating was obtained on copper substrate. For comparison, Ni-B alloy was also produced by electrochemical

deposition method. Basic components of electrolytes in which coatings were produced were determined based on Watts type nickel bath. Trimethylamine borane compound (TMAB) was added to bath as boron source in varying bath amounts to alloy nickel structure with boron. Although there are other options that can be used as boron source other than TMAB in order to alloy nickel with boron in electrical or electroless coating method, TMAB is generally preferred in literature. In addition, Sheu et al., (2019) stated in their studies on Ni-B that dimethylamine borane (DMAB), which can be used as a boron source in electrochemical storage, dissolves at higher temperatures (> 75 °C) than trimethylamine borane compound (TMAB) and that the plating bath with TMAB is more stable than the other. In the light of this information, it can be suggested that TMAB is a suitable boron source for electrochemical baths.

In order to examine the effects of ZrC particles used as reinforcement phase on nanocomposite coating, storage process was carried out by adding different bath amounts to electrolyte. Adding nano or micro particles to the bath is a very different event from chemicals dissolved in electrolyte. When a completely soluble chemical is added to the electrolyte, it is completely uniformly distributed throughout the bath and ionically separated into its molecules or atoms. However, it is not possible to say the same thing for second phase particles. Because reinforcement particles remain in the electrolyte in the same way without dissolving. Problems such as non-wetting, agglomeration, settling to the bottom or rising to the surface occur depending on the characteristics of the reinforcement type. Two different precautions were taken to solve these problems in our study. First, sodium dodecyl sulfate (SDS) surface activator additive, which reduces agglomeration and ensures that the reinforcement particles remain in the electrolyte, was added to the bath. The main medium of the electrolyte we used in our study is pure water. Surface activators reduce the surface tension of water as well as ensure that the particles remain suspended in the liquid. A surfactant molecule consists of two sides: hydrophilic and hydrophobic. The hydrophilic side attaches to water molecules, while the hydrophobic side attaches to the surface of the particles. This prevents the particles from sinking to the bottom or rising to the surface, thus increasing the probability of the particles being stored with metal or alloy during co-storage. Another solution method to prevent the particles from clumping is to apply ultrasonic mixing to the bath before storage. This process breaks up the particle clumps by means of intense ultrasonic waves. During this process, the temperature of the bath rises, so it waits until it reaches the appropriate temperature before starting the storage process. The Vicra Cell VCX 750 brand and model device was used for ultrasonic mixing. During this process, the cycle value was set to 1 and the amplitude value was set to 70% (~20 kHz). Ünal and Karahan (2018) investigated the effect of ultrasonic mixing before storage and reported that this process was very effective both in terms of preventing particle agglomeration and in terms of uniform distribution of particles.

Table 3.2 gives the operating parameters and bath contents used to prepare the coatings. In the bath concentration, nickel sulfate ($NiSO_4.6H_2O$), which stands out with its economic feasibility

and high purity, was determined as the predominant nickel source. Additionally, nickel chloride ($NiCl_2.6H_2O$) served as another nickel source in the Watt-type nickel bath, recognized for its high purity and cost-effectiveness. To mitigate the corrosive impact on the equipment, the concentration of nickel chloride was decreased relative to nickel sulfate within the bath, due to the latter inducing lesser internal stress in the plating bath compared to nickel chloride. Furthermore, varying quantities of trimethylamine borane complex (TMAB), utilized as a boron source, were introduced into the Watt bath.

Table 3.2. Operating parameters and bath contents for electrodeposited coating

Bath Components (Chemicals)	**Parameters**
Nickel Sulfate Hexahydrate ($NiSO_4.6H_2O$)	250 $g \cdot L^{-1}$
Nickel Chloride Hexahydrate ($NiCl_2.6H_2O$)	40 $g \cdot L^{-1}$
Boric Acid (H_3BO_3)	30 $g \cdot L^{-1}$
Trimethylamine Borane Complex (TMAB)	3-9 $g \cdot L^{-1}$
Zirconium Carbide (ZrC)	0-6 $g \cdot L^{-1}$
Sodium Dodecyl Sulfate (SDS)	0.1 $g \cdot L^{-1}$
Operating Conditions	
pH	4 ± 0.1
Temperature	50 ± 1ºC
Deposition Time	30 min
Current Density	50 $mA \cdot cm^{-2}$
Stirring Rate	300 rpm
Ultrasonic Mixing Before Coating	30 min

The production of the coatings was carried out in a two-electrode electrodeposition system. A nickel plate was used as the anode, and a copper plate was used as the cathode (substrate). Before the coating process, the cathode component, which masked an area of 4.5 cm^2, was subjected to certain processes. To eliminate assorted layers of dirt, rust, and oil from the surface designated for coating, the surface was progressively sanded from coarse to fine grit to achieve a smooth finish. Subsequently, the specimen, which was cleaned with acetone, was rinsed with pure water. Thereafter, the copper substrate was activated by etching the surface with an activation process of 1-2 minutes in hydrochloric acid (HCl). Afterward, the specimen was rinsed out with pure water and prepared for the electrolysis process. The mechanism that performs the coating process as electrodeposition and the electrodeposition process diagram are given in Figure 3.7.

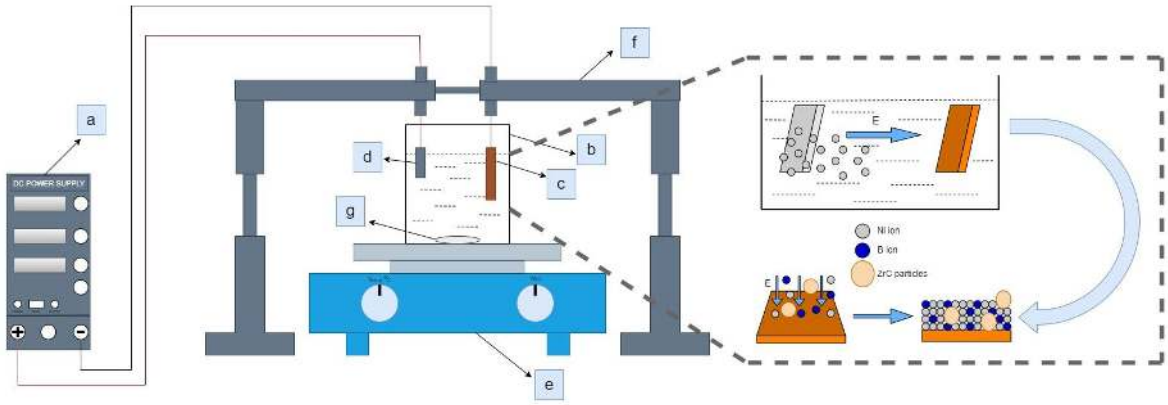

Figure 3.7. Equipment required for electrodeposition experiment and electrodeposition process diagram (a: DC source, b: Breaker, c: Copper substrate, d: Nickel plate, e: Magnetic stirrer, f: Handle, g: Magnetic fish)

Furthermore, the incorporation of SDS, a surfactant, into the electrolyte resulted in a reduction in particle agglomeration and ensured the stability of the particles within the solution. The substrate material's surface was positioned vertically within the bath. The electrolyte temperature was consistently controlled at 50 ± 1 °C during the deposition process. The pH of the Watt bath was balanced to four. Subsequently, the solution was allowed to settle for 30 minutes, during which the plating bath was continuously agitated using a magnetic stirrer. After preparing the plating bath, the color of the bath appears utterly black due to the presence of ZrC particles. Following the completion of the coating process, the surface was cleansed with 95% ethanol, rinsed with distilled water, and produced the Ni-B/ZrC nanocomposite coating. For clarity, Table 3.3 assigns code names to the bath concentrations of the nanocomposite coatings. Following the electrodeposition process, the manufactured nanocomposite coatings which were washed with naive water, allowed to dry at ambient temperature.

Table 3.3. Code names according to bath concentration

Bath Concentration		Codes of Samples
TMAB ($g \cdot L^{-1}$)	**ZrC ($g \cdot L^{-1}$)**	
3	0	3T0Z
3	2	3T2Z
3	4	3T4Z
3	6	3T6Z
6	0	6T0Z
6	2	6T2Z
6	4	6T4Z
6	6	6T6Z
9	0	9T0Z
9	2	9T2Z
9	4	9T4Z
9	6	9T6Z

3.2.6. Potentiostat / Galvanostat

Today, rapidly advancing technology also leads to significant developments in electrochemical devices. New generation devices stand out with their superior features compared to their predecessors. These devices provide advantages such as being able to measure with higher precision, offering a wide range of control and analysis parameters, low electromagnetic noise levels, and being able to accurately detect even very small currents. In addition, these devices make electrochemical analysis processes more efficient and reliable with both their user-friendly software and innovative technologies. Basically, electrochemical analysis devices can be defined as analog or digital power sources that can precisely control the potential and current applied to the working electrode; allow the possibility of changing the current types when necessary and measure the potential of the solution instantly. These devices increase the accuracy of the data obtained by continuously and decisively controlling the potential and current values in electrochemical experiments and minimizing systematic errors.

In this thesis, the Gamry Interface 1010E brand and model Potentiostat/Galvanostat device located in the Automotive Engineering Coating Laboratory of Çukurova University, shown in Figure 3.8, was used in coating experiments.

Figure 3.8. Potentiostat / Galvanostat device

In addition to providing the high sensitivity required for electrochemical analysis, the device is equipped with advanced software specific to Gamry. This software offers users a wide range of functionality in the design of experiments, data collection, and analysis stages. The device used not only provides stable data in experiments, but also stands out with its precise results and high measurement reliability.

3.2.7. Scanning Electron Microscope (SEM)

Electron microscopy is an advanced imaging technique that is basically based on the imaging of electrons scattered from the material. This method offers the opportunity of imaging in nanometric dimensions thanks to the very small wavelength of electrons. Electron microscopes are divided into different types depending on the energy levels of electrons interacting with the material and the operating modes of the device. The most common of these types are scanning electron microscope (SEM), transmission electron microscope (TEM) and low energy electron microscope (LEEM). The SEM device allows detailed analysis of the morphological and topographic features of the surface by sending a high energy electron beam focused on the material surface. Low energy Auger electrons are formed because of inelastic interactions between the electron beam and the outer orbital electrons of the material atoms. These electrons provide information about the surface chemistry and elemental composition of the material. In addition, some of the beam electrons interacting with the orbital electrons lose their energy or are torn from their orbits and move towards the surface. In this process, electrons emitted from a depth of approximately 10 nm below the surface, called "secondary electrons", are released. Secondary electrons play a critical role in obtaining high-resolution images of the material's surface.

As a result of elastic interactions between the electron beam and the material atoms, specific X-rays and continuous radiation occur. In addition, backscattered electrons are produced from the material surface as a result of the beam electrons changing direction due to the gravitational force of the atomic nucleus. Backscattered electrons create lower-resolution images compared to secondary electrons because they originate from deeper regions of the surface. However, these electrons allow information to be obtained about the atomic number and density of the material, which offers significant advantages in terms of elemental contrast and phase separation. In the SEM device, detectors play a critical role in the process of analyzing the obtained data and converting it into an image. In particular, three silicon detectors positioned under the objective lens collect the backscattered and secondary electrons, and a detailed surface image is created using this data. The working principles of SEM and the detailed analysis capacity it offers make it an indispensable tool in various disciplines such as materials science, nanotechnology, biology and engineering (Ali et al., 2023; Huang et al., 2023).

As a result, SEM analysis plays an important role in both research and industrial applications by providing detailed information about the surface morphology, chemical composition and internal structure of materials. Advanced detector systems and sensitive imaging capabilities have made SEM a prominent technology in surface science research. For SEM and EDS analyses, the FEI brand Quanta 650 Field Emission model device located in the Çukurova University Central Research Laboratory was used. The device is given in Figure 3.9.

Figure 3.9. Scanning Electron Microscope (SEM) device

3.2.8. Energy Dispersive X-Ray Spectroscopy (EDS)

Energy Dispersive X-Ray Spectroscopy (EDS) is an effective method used to analyze the chemical composition of materials qualitatively and quantitatively. This technique is based on the principle that X-ray beams sent to the material surface interact with the atomic structure of the material. High-energy electrons hitting the material cause the electrons in the inner orbits of the atoms to break away. The void created by the loss of electrons is filled by the transition of electrons from a higher energy orbit to ensure the balance between the energy levels of the atom. The energy released during this transition leads to the emission of a characteristic X-ray photon.

This emitted characteristic X-ray has a unique energy and wavelength for each element in the analyzed material. Therefore, the energy and intensity of the emitted X-rays can be used to identify the chemical composition of the material. An EDS system detects these characteristic X-rays by means of a specially designed detector and creates an energy spectrum. Each peak in the spectrum corresponds to a specific element in the material, and the height or area of this peak provides quantitative information about the amount of the relevant element. Thus, EDS analysis stands out as an effective tool for both determining the elements present in the material and measuring the concentrations of these elements (Girão et al., 2017).

The advantages offered by EDS include rapid data collection, a wide range of elements (boron and heavier elements), low level of destruction, and the ability to work in integration with other analysis methods. EDS, which is usually used in conjunction with scanning electron microscopy (SEM), is widely used especially in fields such as materials science, engineering, geology, and biotechnology. For EDS analyses, the FEI brand Quanta 650 Field Emission model device equipped with EDS 30 kV accelerating voltage located at the Çukurova University Central Research Laboratory was used.

3.2.9. X-Ray Diffraction (XRD) Analysis

Often, X-ray diffraction (XRD) is considered a subset of X-ray scattering, where X-rays are scattered by the electrons in atoms, and diffraction can occur for a periodic array of scattering centers, and finally analyzed by X-ray crystallography. Generally, wide-angle X-ray diffraction (WAXD), or typically established as X-ray diffraction (XRD), is elegantly exploited by researchers to determine the structure of the molecule, particularly for bulk polycrystalline particles with a diameter of > 10 nm. In-depth, XRD provides information about the arrangement of atoms within a crystalline material as well as lattice dimensions, non-bulk, and bulk material structures. X-rays have a wavelength λ in the range of 1–100 Å, the same order of magnitude as the interplanar spacing d (around 2–6 Å) between planes in the crystal. Diffraction occurs as a result of the interference of rays reflected from different layers of a periodic structure of matter. This is explained in Figure 3.10.

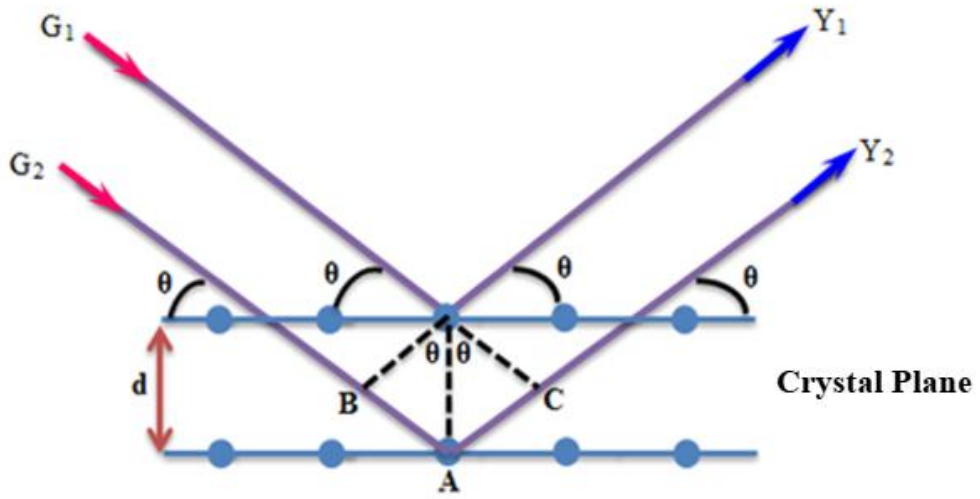

Figure 3.10. Rays incident on and reflected from crystal planes (Shah et al., 2021)

A concept of the XRD technique is that constructive interference occurs when the intensities of the waves add to each other while the waves cancel each other in most directions through destructive interference, determined by Bragg's law.

$$2d \times sin\theta = n \times \lambda \qquad n= 1,2,3,\ldots \tag{3.16}$$

where d is the spacing between the diffraction planes, θ is the angle of incidence, n is an integer, and λ is the wavelength of the beam. The resulting diffraction patterns can provide information about the size and symmetry of the unit cell, the crystal phase present, the position of atoms, and other crystal defects. XRD experiments are routinely performed with single crystal or powder samples. Both powder and single crystal have similar instrumentation setups for sample preparation. In principle, XRD requires very little material, but a complete structure determination can be made with 0.01 mg or less of crystal without destroying the sample. First, both a polycrystalline sample (fine powder) and a crystal are mounted, and then irradiated with X-rays. Typically, for metals, Cu-Kα or Mo-Kα are used as X-ray sources, depending on the molecular size and d-spacing. In a metal oxide colloidal, powder XRD is a useful technique for defining unit cell dimensions as well as phase identification, since colloidals are always formed as bulk material of a crystalline solid at the atomic scale. Often, all possible Bragg diffraction patterns can be observed in the powder pattern. The distinct Bragg peaks are labeled as diffraction indexed using numbers (hkl) under powder XRD. This technique is to identify unknown crystals in the synthesized material by matching the positions and intensities of the peaks observed in the diffraction pattern with a standard diffraction pattern or from calculation.

Bragg's law is used to find the distance d between crystal planes by measuring the angle θ by sending a beam of known wavelength to the sample. The setup used for this is shown

schematically in Figure 3.11. Single wavelength (monochromatic) X-rays coming out of the T tube are sent in a way that they make an angle θ with the planes of the sample, and the intensity of the diffracted rays is measured by the detector (D) that can move on the circle at the 2θ position. This is why the 2θ value is expressed as the diffraction angle in experimental measurements. These measurements are made for different θ angles, and the x-ray diffraction pattern is obtained for the sample.

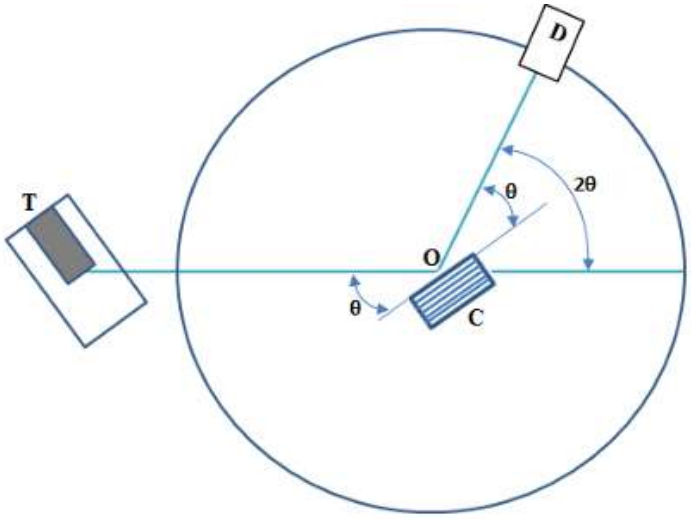

Figure 3.11. Schematic representation of X-Ray diffractometer (Wahab, M.A., 2024).

From the obtained diffraction pattern, the crystal planes of the sample and the distances between these planes are found using the Bragg law (Equation 3.17). The grain sizes of the crystal planes in the sample are determined by the Debye Scherrer formula:

$$d = \frac{K \times \lambda}{\beta \times \cos\theta} \tag{3.17}$$

In the equation; d; grain size, K; Scherrer constant (0.89), λ is the wavelength of the X-ray used in diffraction, β is the value of the width at half maximum (FWHM) of the peak of the examined plane in radians and θ is the Bragg reflection angle of the evaluated peak (Dilsizoğlu et al., 2023; Öztekin, 2014; Özdemir, 2019). In obtaining the XIK patterns of the samples we obtained, a PANalytical brand, Empyrean model XRD device (Figure 3.12) located in the Çukurova University Central Research Laboratory, which produces CuKα radiation at 40 kV and 30 mA in the range of 2θ=0-100°, was used (λ=1.5418 Å).

Figure 3.12. X-Ray diffraction (XRD) analysis device

3.2.10. Microhardness Analysis

Hardness is defined as the resistance of materials to plastic deformation and is usually measured by inserting a standard hard tip into the surface of the material. This resistance provides important information about the structural integrity and mechanical performance of the material. The tip used in hardness measurement usually has a conical, pyramidal or spherical geometry and is made of high-hardness materials (e.g. diamond or hardened steel). The applied force is applied to the surface of the material for a certain period of time, and as a result of this process, a mark formed by plastic deformation is left on the surface.

The hardness of the material depends on the geometrical features of this mark. A smaller mark indicates that the material has a higher hardness. The hardness value is calculated as the inverse proportion of the applied load and the size of the mark, and the formulas used in different test methods vary depending on the tip used and the test procedure.

Microhardness testing can be defined as a miniature version of traditional hardness tests and allows precise measurements to be made on small or thin samples. This method was developed to evaluate the resistance of micro and nanoscale materials to plastic deformation. The test is frequently applied to small-volume or heterogeneous materials such as thin films, coatings, microstructure materials and composites.

The load used during the test usually varies between 1 gram force (gf) and 1000 gf, and thanks to these low loads, the test creates minimal damage to the sample. Therefore, microhardness tests can be considered among non-destructive testing methods and allow measurements to be made while preserving the functionality of the surface.

There are two most commonly used test methods for micro-hardness testing under high loads. These are;

1. Vickers hardness test (HV = Hardness of Vickers)
2. Knoop hardness test (HK = Hardness of Knoop) tests.

In these tests, the microhardness value is determined by measuring the indentation formed by the effect of the load applied to the material surface, and the results are usually expressed in kgf/mm² (kilogram-force/square millimeter). Kilogram-force represents the force exerted by an object with a mass of 1 kg under standard gravity and is also commonly called kg, kgf or kilopound (kp). Despite the many advantages it provides in practice, microhardness tests also bring with them some limitations, such as the lack of standardization of measurements. One of the main reasons for this situation is that the operator performing the measurement is open to small amounts of measurement errors. Especially at low loads, small errors made in the measurement of the diagonal lengths of the trace (Vickers method) or the long axis of the trace (Knoop method) formed during the test can cause significant deviations in the results. Such errors can negatively affect the sensitivity of the test and cause superficial measurement errors to lead to larger results. In order to prevent such problems, it is recommended to select the highest possible loads in each test. High loads minimize measurement errors by ensuring that the trace is formed more clearly. However, it should also be taken into account that the values obtained in microhardness tests are generally higher than the macrohardness values of the material (e.g. uniaxial compressive strength). This difference is due to the fact that the local deformation hardening of the material is more pronounced in microhardness measurements. It should also be noted that microhardness values may vary depending on the load. The applied load can directly affect the microhardness results by affecting the deformation hardening of the material. Therefore, it is of great importance to carefully select the measurement conditions and follow standardized protocols in order to make a correct assessment. Considering these factors contributes to more reliable results in microhardness tests.

Microhardness measurement is used to determine the hardness value of the material, to analyze microstructures, material characteristics and mechanical properties. This measurement expresses the resistance of the material according to the microhardness scale. Microhardness provides information about the surface hardness, strength and wear resistance of the material.

The Vickers hardness measurement method was used to obtain the microhardness values of the coatings we obtained. A diamond pyramid tip with a square base and a 136° apex angle is used in the Vickers hardness measurement method. The hardness obtained in the Vickers test is shown as

VS and is found by measuring the diagonals of the trace. After the indenter actuation, the material sample presents an indentation region with the approximate shape of a regular lozenge (Figure 3.13).

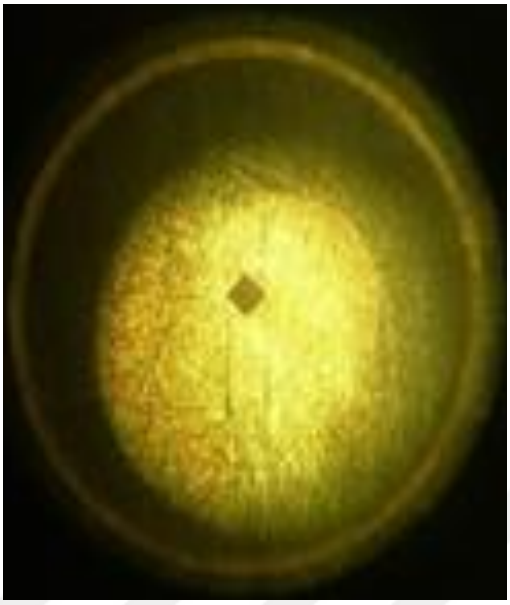

Figure 3.13. Image obtained after microhardness test

When we look at the basis of the experiment and the starting point of the calculation formula, the Vickers hardness (HV) value depends on the F/A ratio, where F= force and A= area. Here the A value;

$$A = \frac{d^2}{2\sin\left(\frac{136°}{2}\right)} \tag{3.18}$$

derived from the formula, approximately,

$$A \approx \frac{d^2}{1.8544} \tag{3.19}$$

It can be simplified as follows. Here d represents the average value of the diagonals of the resulting shape. Thus, the formula, which is further simplified, is finally,

$$HV = \frac{F}{A} \approx \frac{1.8544 \times F}{d^2} \tag{3.20}$$

takes the form. The F value here is kgf and d^2 has unit mm^2 (Ünal and Karahan, 2018b).

While measuring the microhardness values, a 500 g load was applied to the sample for 10 s. Measurements were taken from at least 10 different regions in each sample and the average of these

measurements was accepted as the microhardness value. As a result of the microhardness measurements, hardness values that deviated excessively from the average were not included in the general average of the sample. In microhardness measurements, AOB Lab brand microhardness measuring device (Figure 3.14) located in Çukurova University Automotive Engineering Laboratories was used. The load range of the device is 10-1000 g. Technical specifications of the test device are given in Table 3.4.

Table 3.4. Technical specifications of the test device

Specification	**Property**
Brand-model	Jiashan THV 1 MD
Test forces	0.01 kgf, 0.025 kgf, 0.05 kgf, 0.1 kgf, 0.2 kgf, 0.3 kgf, 0.5 kgf, 1 kgf
Hardness range	8HV-2900HV
Microscope	100X for observation 400X for measurement
Dwell time	0-60 s

Figure 3.14. Microhardness measuring device

3.2.11. Atomic Force Microscopy (AFM) analysis

Atomic force microscopy (AFM) is one of the microscopy techniques used to analyze any solid surface at high resolution and provide information about morphology and surface properties. This technique has advantages over other surface examination techniques in terms of ease of use,

sensitivity and versatility. Atomic force microscopy is the force-distance measurement between the tip and the sample. AFM records the surface topography by scanning the sample surface with the help of a small tip probe. The probe has a thin tip at the nanometer level to provide resolution of surface features. The movement of the probe is powered by a laser beam reflected from a mirror on the tip lever arm. Piezoelectric scanners scan the probe laterally in two dimensions. When the probe is scanned over the sample, the potential energy difference between the tip and the sample surface causes the probe to be displaced vertically. AFM uses this tip as a signal to image the sample force. A feedback loop is used to maintain a constant force on the tip by adjusting the sample height. A three-dimensional image of the sample surface is created (Marrese et al., 2017). A simple schematic of Atomic Force Microscopy is given in Figure 3.15.

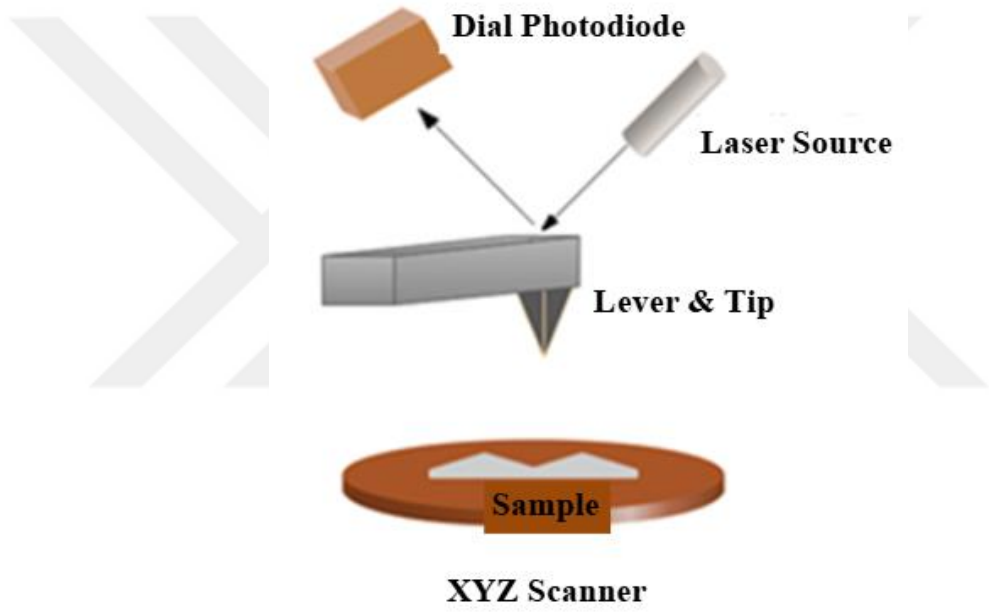

Figure 3.15. Schematic of a classical atomic force microscope (Omar et al., 2021)

There are two methods in AFM: contact and non-contact. The contact method is used to obtain images at the atomic scale. When this mode is used, it provides better lateral resolution. The contact mode is suitable for flat and hard surfaces. The non-contact method, on the other hand, creates vibration between the tip and the sample surface. There are different vibration modes in this method. Thanks to the advantages of the method, it is suitable for use for many samples.

Surface roughness measurement devices draw the surface profile graphically. The long wavelengths of the surface also affect the surface roughness measurement parameters, and therefore the effect of very long wavelengths is of great importance. Ra represents the arithmetic mean of all measurements, Rz represents the difference between the highest and lowest points, Rt represents the sum of the maximum height and maximum depth for the entire measurement length, and Rq

represents the square root of the arithmetic mean deviations. The two most important parameters explained in the standards are Ra and Rz (Joshua et al., 2023).

The Park Systems brand Park NX10 model device shown in Figure 3.16 was used in surface roughness measurements. The properties of the gauge used to determine the surface roughness class are given in Table 3.5.

Figure 3.16. Atomic Force Microscopy (AFM) analysis device

Table 3.5. Surface Roughness Classes (Demir, 2021)

Class	Ra (µm)	Class	Ra (µm)	Class	Ra (µm)
N1	0.025	N5	0.4	N9	6.3
N2	0.05	N6	0.8	N10	12.5
N3	0.1	N7	1.6	N11	25
N4	0.2	N8	3.2	N12	50

3.2.12. Corrosion Analysis

All corrosion analyses were conducted in Çukurova University, Faculty of Arts and Sciences Laboratories with a CH Instrument electrochemical analyzer (Figure 3.17). All corrosion experiments were carried out in 3.5% sodium chloride (NaCl) aqueous solution.

Figure 3.17. CH Instrument electrochemical analyzer

Open Circuit Potential (OCP)

Open circuit potential (OCP) is known as a passive corrosion analysis method and is expressed in literature with various terms such as corrosion potential, equilibrium potential, open circuit voltage, zero current potential, or resting potential. This technique is used to measure thermodynamic equilibrium in electrochemical systems and is based on the direct measurement of the potential difference between the electrodes. OCP analysis is performed by making the circuit passive. This passivity is provided by disabling the counter electrode used to pass current.

In the OCP method, the potential difference between the working electrode and the reference electrode is recorded. This technique differs from other corrosion analysis methods by being an electrolytic measurement method based entirely on thermodynamic principles. However, it should not be forgotten that electrochemical systems are not always in thermodynamic equilibrium. In some systems, the equilibrium state may not have been achieved before the measurement and these systems may reach equilibrium over time. For this reason, a sufficient waiting period may be required for equilibrium to be achieved during OCP analyses. Despite the simplicity of the OCP method, the information it provides is extremely valuable. By following the potential changes of systems over time, important data on the kinetics and equilibrium of electrochemical events can be obtained. These data are widely used in corrosion studies and material performance evaluation. Therefore, OCP analysis stands out as a basic electrochemical characterization method in both scientific and industrial applications (Erbil, 2012).

With OCP, it is possible to determine whether electrochemical systems are stable or not. In terms of corrosion analysis, although the most accurate results cannot always be obtained with OCP, it is generally used to determine the resting potential of a system, which forms the basis of other experiments. Especially in experiments such as electrochemical impedance spectroscopy (EIS), the working potential is set according to OCP instead of the reference. In this study, OCP experiments were carried out in a 3.5 wt% NaCl solution, the potential values were recorded as a function of time for 3600 seconds, and these data were plotted.

Tafel Extrapolation Method

The corrosion event occurring at the metal/solution interface is essentially a charge transfer mechanism. Charge transfer involves the processes of metal atoms dissolving into ionic form or ions in solution taking electrons to the metal surface and transforming into metallic form. However, reducing the kinetics of the corrosion process to charge transfer alone is insufficient to fully cover all the mechanisms that are actually present. However, a charge transfer-focused approach can provide a valuable basis for a better understanding of other kinetic processes affecting the corrosion rate.

In this context, current-potential relationships play an important role in corrosion kinetic analysis. As shown in Figure 3.18, these relationships differ in regions close to the corrosion potential and in regions far from the corrosion potential. Corrosion reactions on the metal surface are generally defined by two basic electrochemical reactions: anodic (oxidation of the metal) and cathodic (a reduction reaction, usually oxygen reduction or hydrogen evolution). The current-potential curves for these two reactions are mathematically expressed as exponential functions and give the algebraic sum of the currents for the anodic and cathodic reactions in the vicinity of the corrosion potential.

As the corrosion potential is moved away, one of the anodic and cathodic curves becomes dominant over the other. When the potential increases in the anodic direction, the anodic reaction (e.g., more oxidation of the metal) becomes dominant, while when the potential decreases in the cathodic direction, the cathodic reaction (e.g., reduction of ions in solution) becomes dominant. Therefore, in systems far from the corrosion potential, the total current can be described by a single exponential function representing either the anodic reaction alone or the cathodic reaction alone. This approach can be used to understand the electrochemical behavior of systems that are particularly highly polarized (over potentially applied). By writing this exponential function in linear form, the Tafel equation is obtained,

$$\eta = \pm a \pm b \log I \tag{3.21}$$

The Tafel equation was generally developed for use in over-polarized states of electrochemical systems. However, when the overpotential is brought close to zero, the system reaches corrosion potential conditions. Under these conditions, the current value obtained by means of the Tafel equation is called the corrosion current in the system. In order to express the kinetics of the electrochemical reaction more concretely, this current value is usually expressed in units of current density (the amount of current per unit area). Using the current density allows the corrosion rate to be determined both theoretically and experimentally. Experimental drawing of Tafel curves allows the behavior in the vicinity of the corrosion potential to be analyzed. Experimental data reveal that the current potential relationship in the vicinity of the corrosion potential is not strictly linear. However, as the corrosion potential is moved away, a certain region begins to exhibit linear behavior.

The data obtained from this linear region can be extrapolated along the potential axis to the corrosion potential and the corrosion current can be determined. Depending on the corrosion current value obtained, it becomes possible to calculate the corrosion rate in the system. This method is called "Tafel Extrapolation Method" in literature (Erbil, 2012). During the studies, a wide potential range was scanned starting from 250 mV negative of the free corrosion potential to 250 mV positive. During this scanning process, 0.166 mV/s was preferred as the potential application rate. As a result of these systematic polarization studies, Tafel curves were obtained. The linear regions obtained from the Tafel curves, and the corrosion current values were calculated by extrapolation to the corrosion potential, and the corrosion rate was determined quantitatively based on these values.

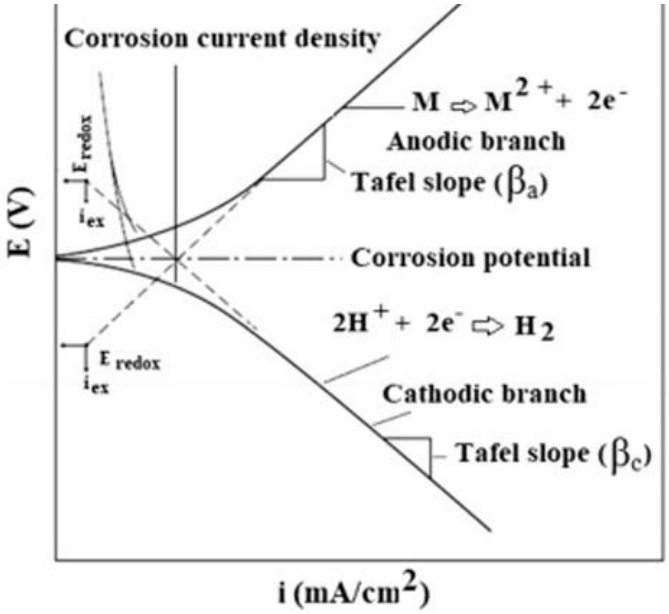

Figure 3.18. Potentiodynamic polarization curve and Tafel constants (Stoljarova et al., 2021)

Electrochemical Impedance Spectroscopy (EIS)

Electrochemical Impedance Spectroscopy (EIS) is a powerful technique that evaluates the electrical properties of electrochemical systems and measures the impedance of the system using various alternating current (AC) frequencies. In this method, a small amplitude sinusoidal potential, usually 5-10 mV, is applied to the electrode surface to provide stimulation to the electrode. The EIS technique makes it possible to determine the resistance (especially polarization resistance, Rp) and capacitance properties of the electrochemical system by examining the dynamic response of the electrode. In this way, detailed information can be obtained about the corrosion rates and electrochemical reaction mechanisms on the electrode surface. EIS analysis is performed by equivalent circuit modeling consisting of the electrical resistance and double layer capacitance between the metal surface and the solution. This model reflects the electrokinetic properties of the electrode and allows the calculation of the polarization resistance. This technique, which specifies the potential-current relationship, provides a very important parameter for understanding the

behavior of the electrode and the interactions of the material in the solution. Polarization resistance is considered as an indicator of the resistance of the electrode surface to corrosion and is a critical parameter in understanding the mechanism of electrochemical processes. This process measures the degree of obstruction of the electrical flow between the metal surface and the solution and provides important data on the corrosion properties of the material. Measurements made with EIS allow for a more detailed analysis of the electrical conductivity properties of the material by applying an alternating current signal to the electrode surface. This technique is widely used, especially in materials science, for understanding corrosion processes and characterizing surface properties. The metal/solution interface and equivalent circuit design, usually represented in a schematic form, help in determining the polarization resistance.

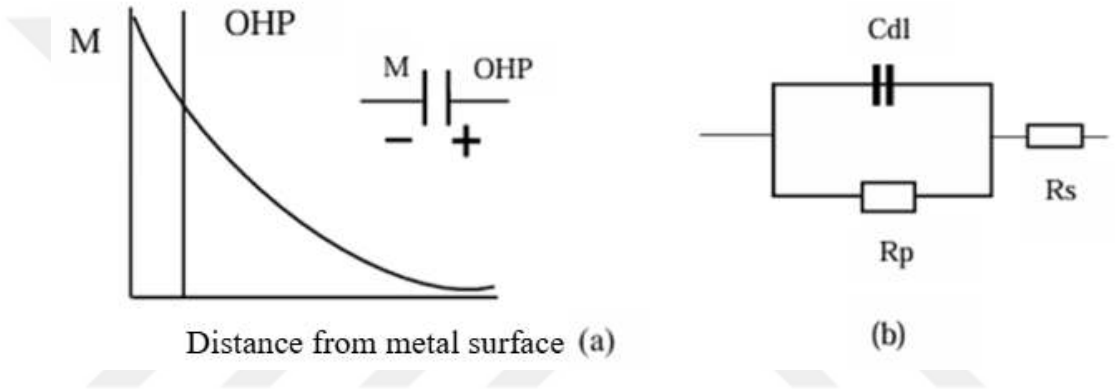

Figure 3.19.Double layer structure representing the capacitor structure at the metal/solution interface (a) and the electrical equivalent circuit diagram modeled for this interface (b) (Erbil, 2012)

In an electrical equivalent circuit where alternating current passes, resistance is called "impedance" (Z), while resistance in a circuit where direct current passes is defined as "ohmic resistance" (R). In order to apply this method, it is assumed that the double-layer region where charge accumulation occurs shows capacity in the electrical equivalent circuit representing the designed metal/solution interface, and this capacity is accepted as the double-layer capacity (Cdl). Considering that resistance must also be present in an electrical equivalent circuit where current passes, solution resistance (Rs) should also be taken into account. To calculate the impedance of the electrical equivalent circuit, resistance values for each circuit element should be defined. Polarization resistance (Rp) and solution resistance should show the path through which current passes and should be considered as connected in series with each other. These resistances are accepted as real resistances. While the capacitor does not allow direct current to pass, it acts as if current is passing due to the constant change of direction of the alternating current and creates virtual resistance. This virtual resistance is defined as $Rc = 1 / (j\omega \times Cdl)$. Here $j = \sqrt{-1}$ and ω represents the angular frequency ($\omega = 2\pi f$). In this relation, which gives the definition of the resistance of the capacitor,

when $\omega = 0$, the resistance will take an infinite value, and the current will not be allowed to pass. The impedance graph expressed as $Z = Z' + jZ''$ is known as the Nyquist diagram (Erbil, 2012). A typical configuration is obtained using a frequency range between 100 kHz and 0.1 mHz (Choudhary et al., 2016; Trentin et al., 2022).

4. RESULTS AND DISCUSSIONS

4.1. Properties of ZrC Particles

4.1.1. XRD Analysis of Reinforcement Particle ZrC Powders

The XRD graph presented in Figure 4.1 facilitates a detailed analysis of ZrC particles used as nanoparticles in composite coatings. The most prominent (111) main peak appeared at 32.9º. In addition to these peaks, peaks at 38.2° (200), 55.2° (220), 65.8° (311) and 69.186° (22) are also seen. Similar XRD patterns of ZrC powders reflecting these peaks are also found in the literature.

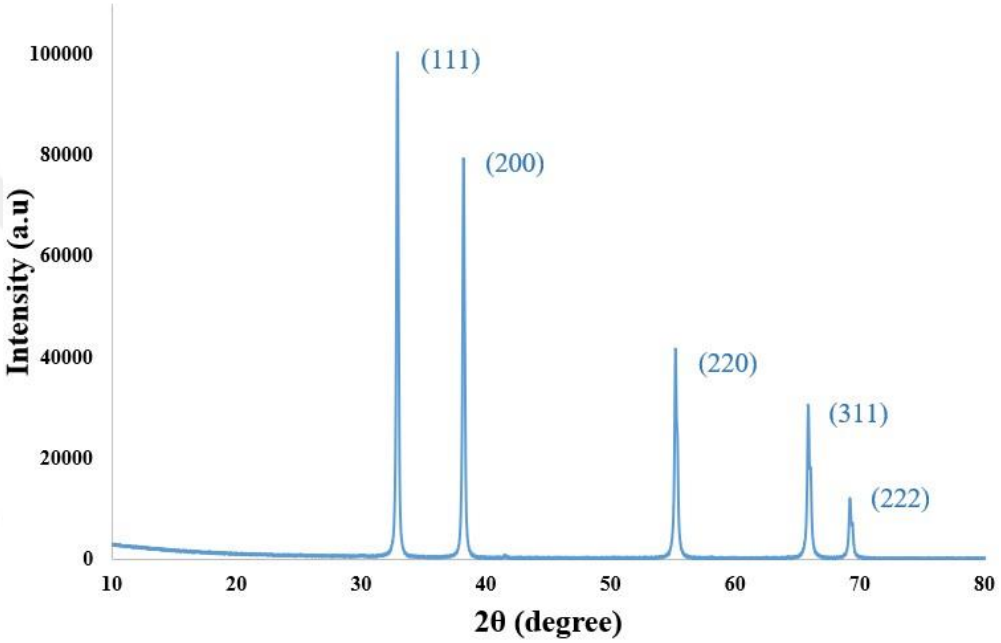

Figure 4.1. XRD graph of ZrC nanoparticle

The (111) and (200) peaks observed in the XRD patterns of the electrochemically coated Ni-B/ZrC nanocomposite coatings are strong evidence that the ZrC reinforcement particles were successfully deposited together with the Ni-B main structure in the coating. This situation was revealed by carefully interpreting the XRD analysis results. In the XRD pattern shown in Figure 4.1, these distinct peaks belonging to ZrC indicate that the ZrC particles were homogeneously distributed in the Ni-B matrix and effectively combined during coating. These peaks are associated with the (111) and (200) planes specific to the crystal structure of ZrC and were determined as one of the peaks with the highest intensity during XRD analysis.

In addition, the variables obtained from the XRD patterns of ZrC powders are given in detail in Table 4.1. In the calculation of these variables, the highest intensity peak in the ZrC pattern was taken as a basis and detailed mathematical analyses were performed accordingly. As a result of these calculations, the average crystal grain size of ZrC powders was found to be 54.2 nm. This value

reveals that ZrC has a grain size at the nanostructure scale and the reinforcement particles are in a very fine structure.

Table 4.1. Variables obtained from the XRD pattern of ZrC reinforcement particles

Sample	**2θ (degree)**	**FWHM-β (radian)**	**Average crystal grain size, D (nm)**	**Microstrain, ε**	**Dislocation density, δ (nm^{-2})**
ZrC particle	32.9	0.00279	54.2	2.36×10^{-3}	3.4×10^{-4}

4.2. Microhardness Analysis of Ni-B/ZrC Nanocomposite Coatings

Coating using different TMAB and ZrC concentrations in electrolyte baths was investigated to determine the effect on the microhardness values of all obtained samples. In this context, the hardness value of the pure Ni-B matrix was measured as approximately 458.4 HV. This basic hardness value was taken as a reference to evaluating the mechanical properties of the Ni-B matrix. In the coating process, the addition of TMAB (tetramethylammonium borohydride) to the pure Ni structure and the inclusion of ZrC (zirconium carbide) particles as reinforcement material significantly changed the microhardness value of the composite coating. It was observed that TMAB caused a significant increase in hardness by improving the structural properties of the coating. Similarly, a harder and more durable composite structure was obtained by integrating ZrC particles into the Ni-B matrix as reinforcement material. In this study, the effects of coating solutions prepared with different combinations of TMAB and ZrC bath concentrations on the coating microhardness were analyzed in detail. Figure 4.2-4.4 visually presents the effects of these different bath contents on the microhardness values of the coatings. These analyses clearly reveal how increasing the TMAB and ZrC contents changes the hardness properties of the coatings.

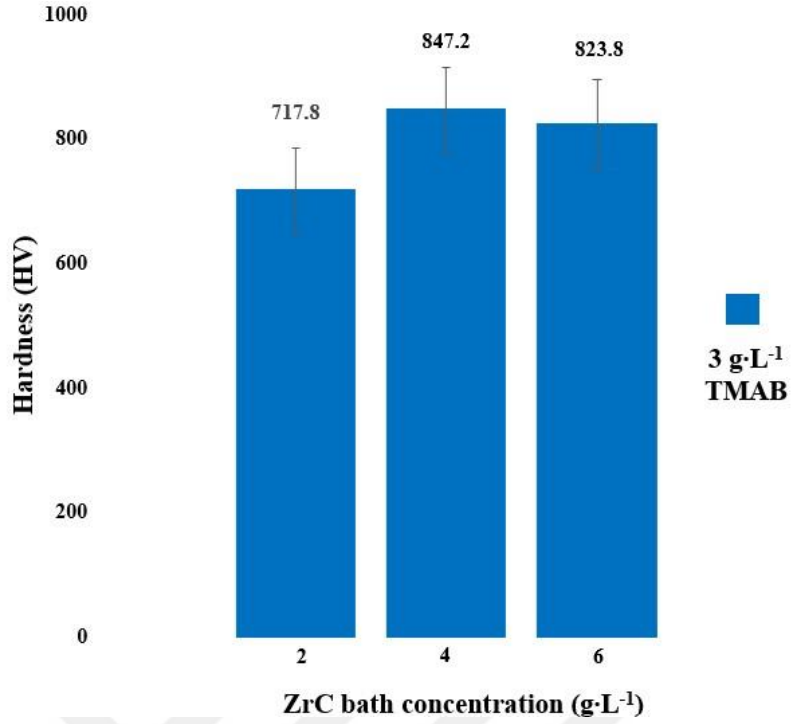

Figure 4.2. Microhardness values of coatings obtained at 3 g/L TMAB bath concentration

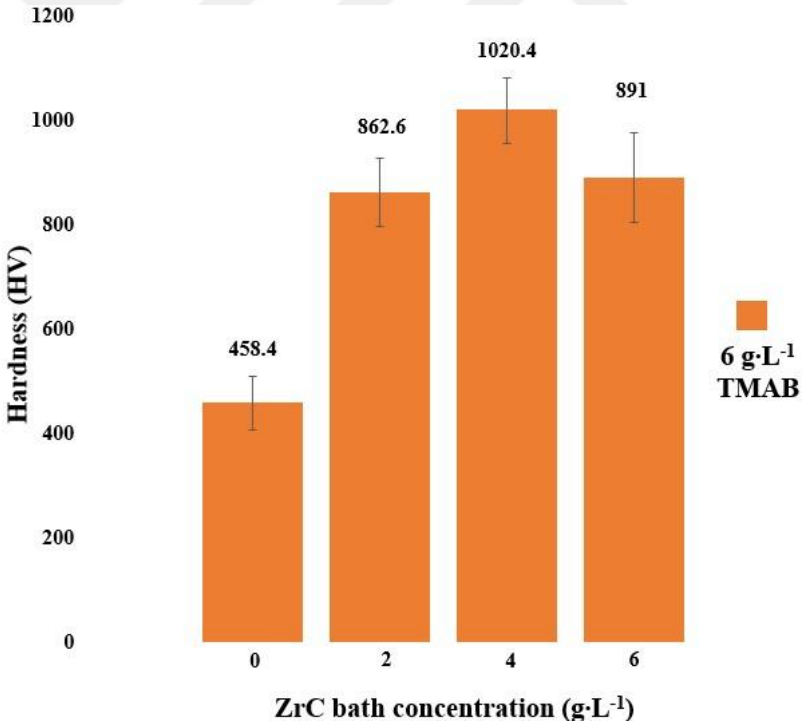

Figure 4.3. Microhardness values of coatings obtained at 6 g/L TMAB bath concentration

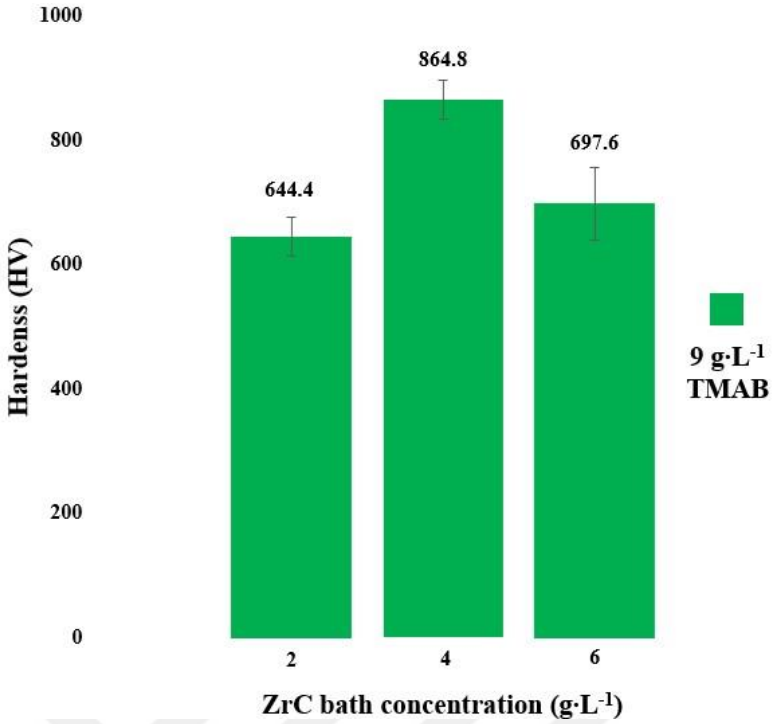

Figure 4.4. Microhardness values of coatings obtained at 9 g/L TMAB bath concentration

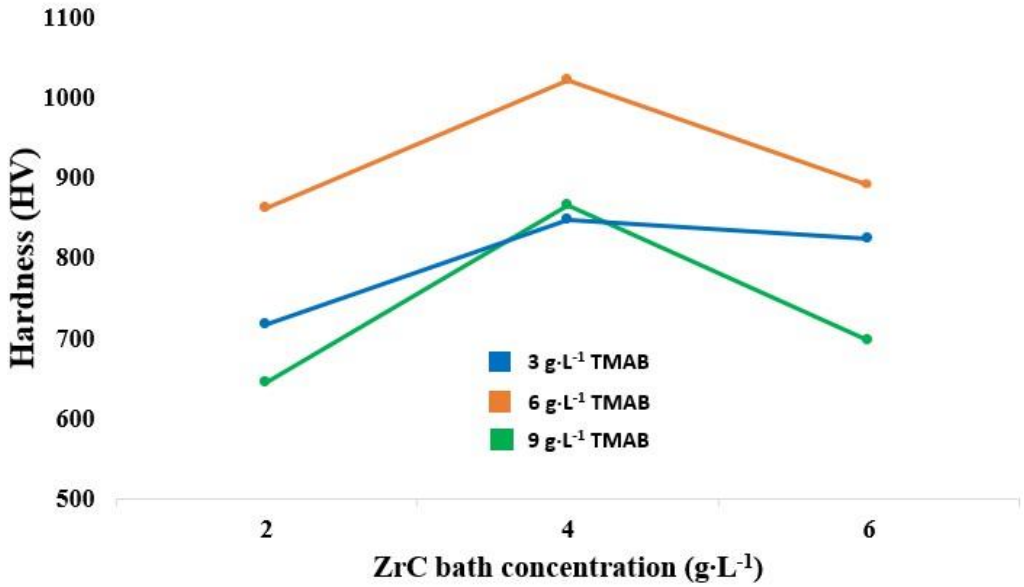

Figure 4.5. Microhardness results in different bath concentrations

As can be seen from the figure, when the TMAB concentration in the electrolyte was kept constant, a fluctuating change in microhardness values was observed. Microhardness values initially increased but decreased with the increase in TMAB concentration. This is due to the excessive increase in TMAB levels, especially the ZrC particles condensing in the electrolyte and forming agglomeration, and the decrease in particles adhering to the surface. When the ZrC concentration in the electrolyte bath was increased to 4 g·L⁻¹, the microhardness values exhibited an initial increase, indicating an improvement in the mechanical properties of the coatings. This enhancement can be

attributed to the uniform dispersion of ZrC nanoparticles within the coating matrix, which effectively contributed to the reinforcement of the structure. However, as the TMAB concentration in the bath was progressively increased to 3, 6, and 9 $g \cdot L^{-1}$, a noticeable decline in the microhardness values was observed. This reduction in hardness, particularly pronounced at 9 $g \cdot L^{-1}$ TMAB concentration, highlights the negative impact of excessive TMAB levels on the coating quality. The decrease is likely due to the agglomeration of particles caused by the high TMAB and ZrC concentrations, which disrupts the homogeneity of the coating and reduces particle adhesion to the surface. Specifically, it was determined that the coatings prepared using 9 $g \cdot L^{-1}$ TMAB exhibited lower hardness values compared to those prepared with 3 $g \cdot L^{-1}$ TMAB, emphasizing the critical importance of maintaining an optimal balance in the bath composition to achieve desirable mechanical properties. These findings underline the role of controlled TMAB and ZrC concentrations in optimizing the coating's microstructure and performance.

The incorporation of boron atoms into the pure nickel structure through TMAB typically leads to an increase in hardness due to the strengthening effect of boron on the nickel matrix. However, contrary to expectations, it was observed that increasing the TMAB concentration beyond a certain threshold resulted in a decline in hardness. This situation clearly reveals the effect of ZrC nanoparticles in the bath. Through comparative analysis of TMAB concentrations, it was identified that the maximum hardness value was achieved at a TMAB concentration of 6 $g \cdot L^{-1}$. According to this result, it was seen that the highest microhardness value was in the coatings produced at 6 g/L TMAB concentration. In terms of ZrC content, the analysis indicated that a bath concentration of 4 $g \cdot L^{-1}$ ZrC was the most effective in enhancing the coating’s hardness. The combined optimum bath conditions of 6 $g \cdot L^{-1}$ TMAB and 4 $g \cdot L^{-1}$ ZrC produced the maximum hardness value of 1020.4 HV. On the other hand, the lowest hardness value, 644.4 HV, was observed in samples prepared with bath concentrations of 9 $g \cdot L^{-1}$ TMAB and 2 $g \cdot L^{-1}$ ZrC. This demonstrates the adverse effects of excessively high TMAB levels and suboptimal ZrC concentrations, which lead to agglomeration and reduced particle adhesion, ultimately compromising the mechanical properties of the coatings. These findings underscore the importance of balancing TMAB and ZrC concentrations to optimize the coating's hardness and overall performance. Ogihara et al., (2012) investigated the impact of varying boron content on the hardness of Ni-B matrix coatings. Their findings revealed that hardness increased as the TMAB concentration in the bath rose to 6 $g \cdot L^{-1}$ but experienced a slight decline when the concentration exceeded this level. Similarly, Lee et al., (2005) studied the properties of Ni-B coatings produced through the electroplating process with different boron contents. They observed that as the boron content rised, the grain size of the coating reduced, leading to an enhancement in hardness, which peaked at 750 HV at a boron concentration of 2 at.%. However, beyond this threshold, a decline in boron content was noted, suggesting the limitations of excessive boron in maintaining enhanced mechanical properties.

The hardness values of the Ni-based composite coatings obtained in this study, incorporating ZrC and TMAB, align well with those reported in the literature (Liu et al., 2021; Shahzad et al., 2021; Wang et al., 2014). These results demonstrate the effectiveness of combining ZrC nanoparticles with TMAB to achieve improved mechanical properties in electroplated coatings. The concordance between the experimental findings and existing data underlines the potential of Ni-B/ZrC composite coatings to deliver superior performance in applications demanding high hardness and durability. The hardness results of all coatings are given in Table 4.2.

Table 4.2. Microhardness numerical values

Samples		**Microhardness (HV)**		
		TMAB bath concentrations		
		3 g/L TMAB	**6 g/L TMAB**	**9 g/L TMAB**
ZrC bath concentrations	**0 g/L**	422.5	458.4	416.7
	2 g/L	717.8	862.6	644.4
	4 g/L	847.2	1020.4	864.8
	6 g/L	823.8	891	697.6

4.3. Surface and Content Analyses of Ni-B/ZrC Nanocomposite Coatings

The effect of boron source TMAB and ZrC additives in the electrolyte was evaluated by surface morphology and composition analysis of Ni-B/ZrC composite coatings produced at different bath concentrations. These analyses were carried out using a scanning electron microscope (SEM). For comparison purposes, SEM images of the Ni-B matrix surface are presented in Figure 4.6. Examination of the Ni-B alloy surface revealed a morphology characterized by distinct circular protrusions on the surface. This structure indicates that the unit cells formed during the coating process grow regularly on the coating surface. This unit cell growth on the coating surface continues until the TMAB and ZrC concentration in the electrolyte bath reaches a certain level. This shows that the amount of TMAB and ZrC in the bath directly affects the morphological structure and growth process of the coating. Figure 4.7 - Figure 4.15 clearly shows the effects of TMAB and ZrC concentrations on the growth dynamics on the coating surface.

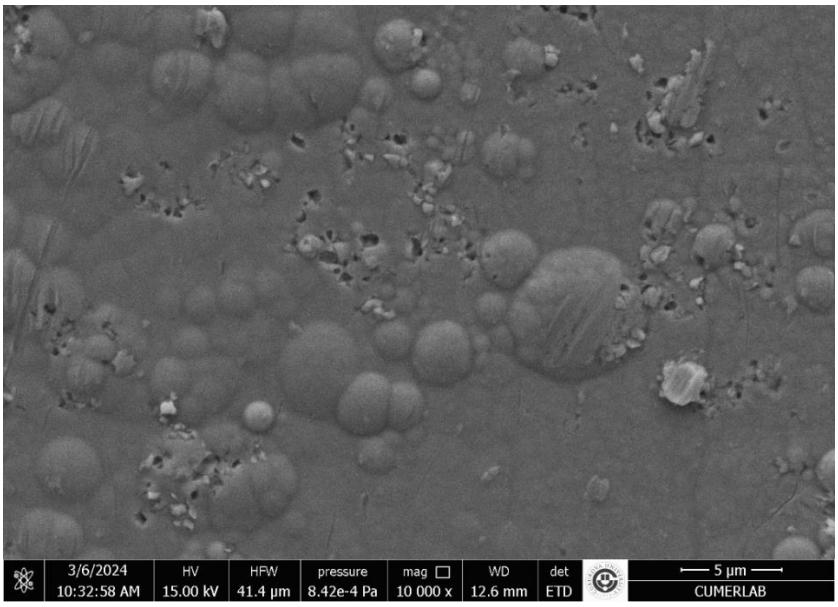

Figure 4.6. Surface morphology of the Ni-B alloy coating

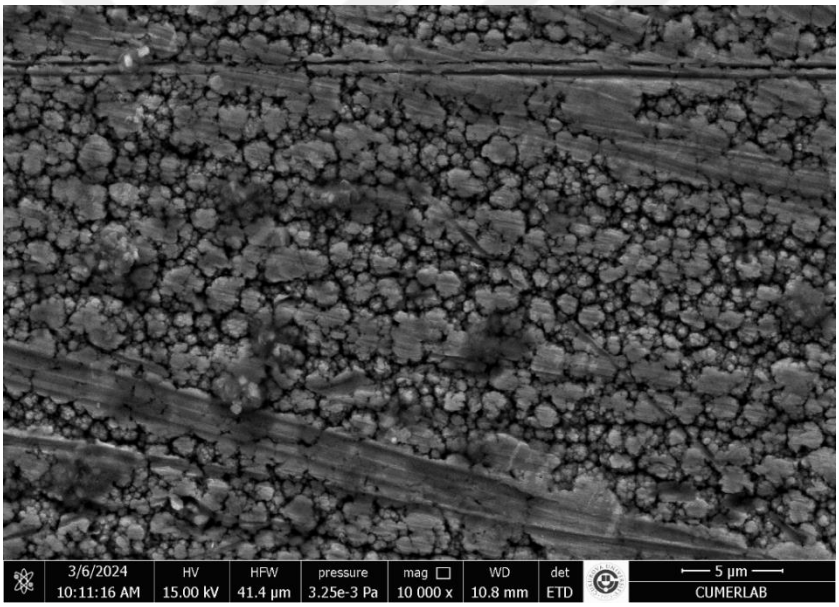

Figure 4.7. Surface morphology of Ni-B/ZrC composite coatings received with 3 g/L TMAB and 2 g/L ZrC bath concentration (3T2Z)

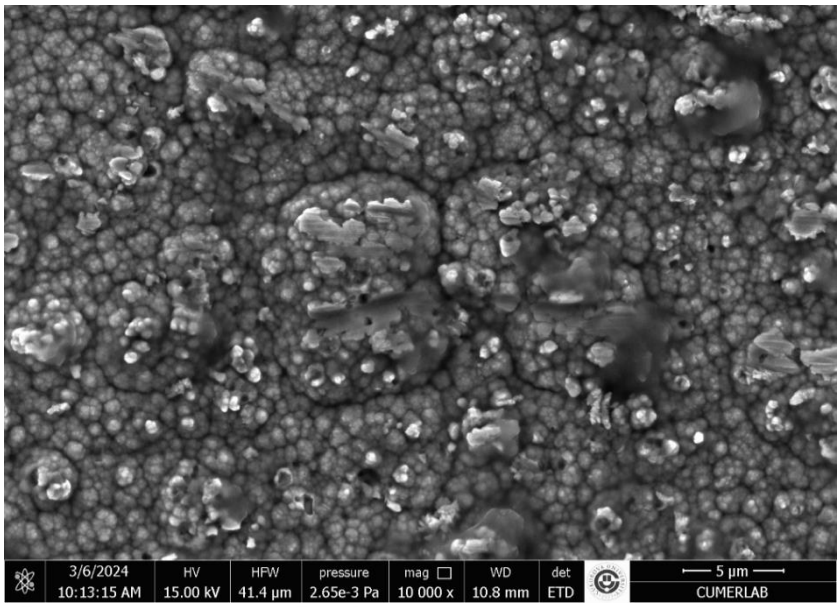

Figure 4.8. Surface morphology of Ni-B/ZrC composite coatings received with 3 g/L TMAB and 4 g/L ZrC bath concentration (3T4Z)

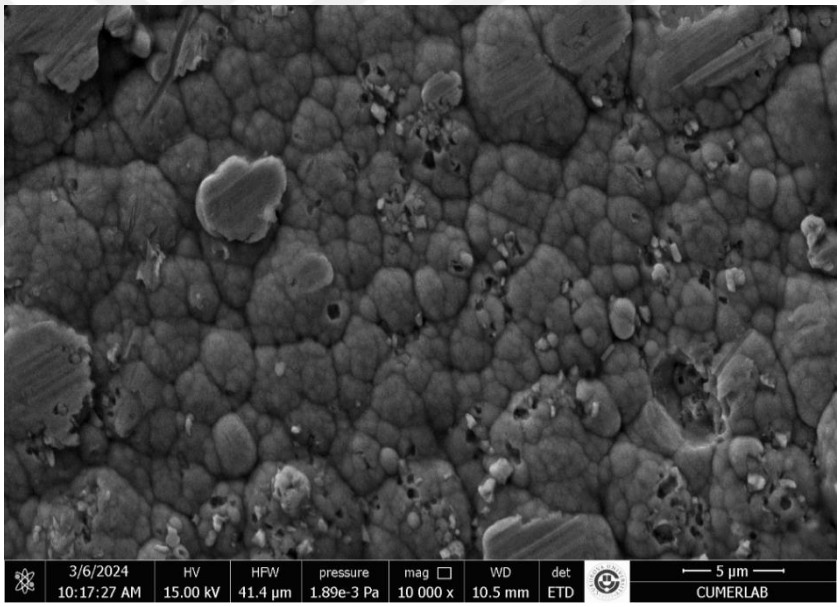

Figure 4.9. Surface morphology of Ni-B/ZrC composite coatings received with 3 g/L TMAB and 6 g/L ZrC bath concentration (3T6Z)

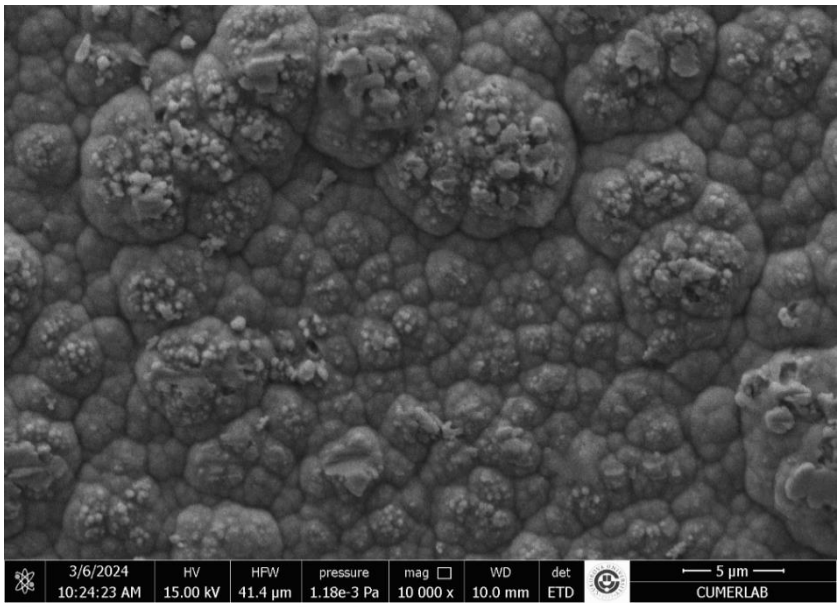

Figure 4.10. Surface morphology of Ni-B/ZrC composite coatings received with 6 g/L TMAB and 2 g/L ZrC bath concentration (6T2Z)

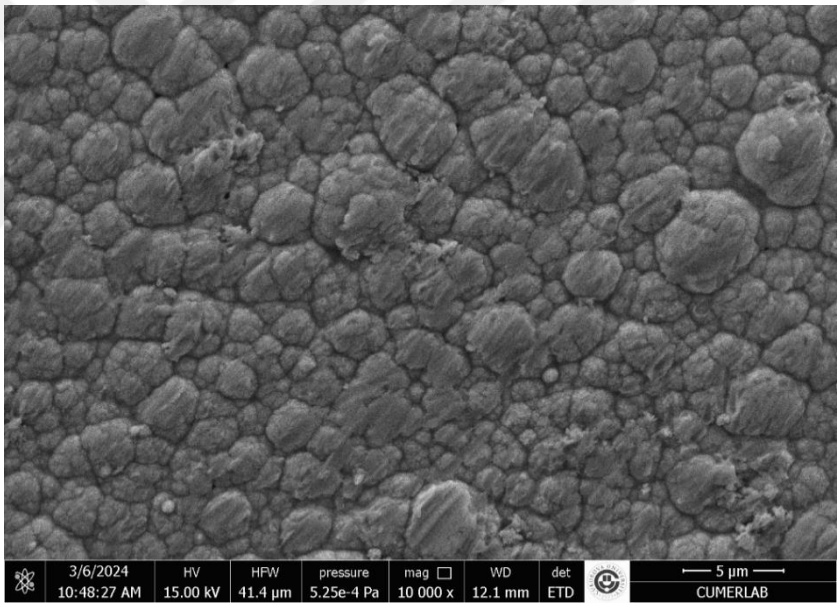

Figure 4.11. Surface morphology of Ni-B/ZrC composite coatings received with 6 g/L TMAB and 4 g/L ZrC bath concentration (6T4Z)

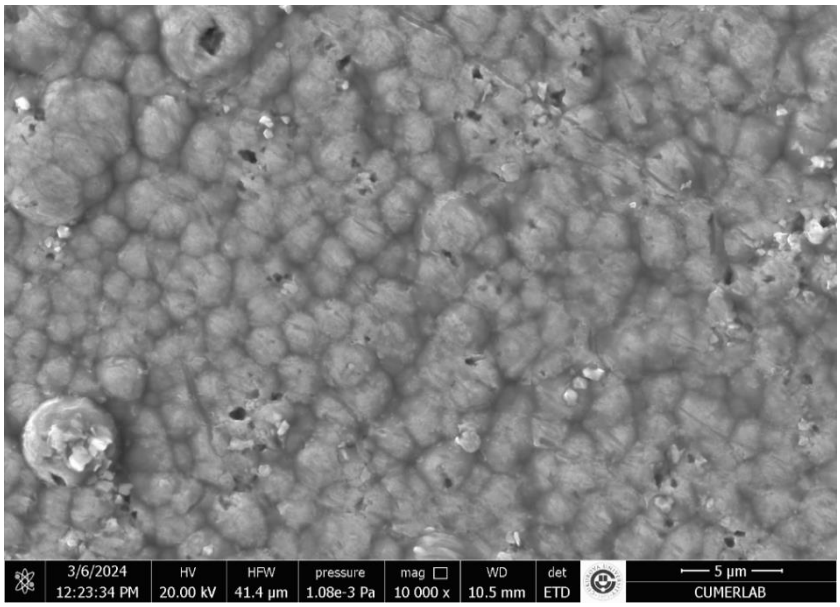

Figure 4.12. Surface morphology of Ni-B/ZrC composite coatings received with 6 g/L TMAB and 6 g/L ZrC bath concentration (6T6Z)

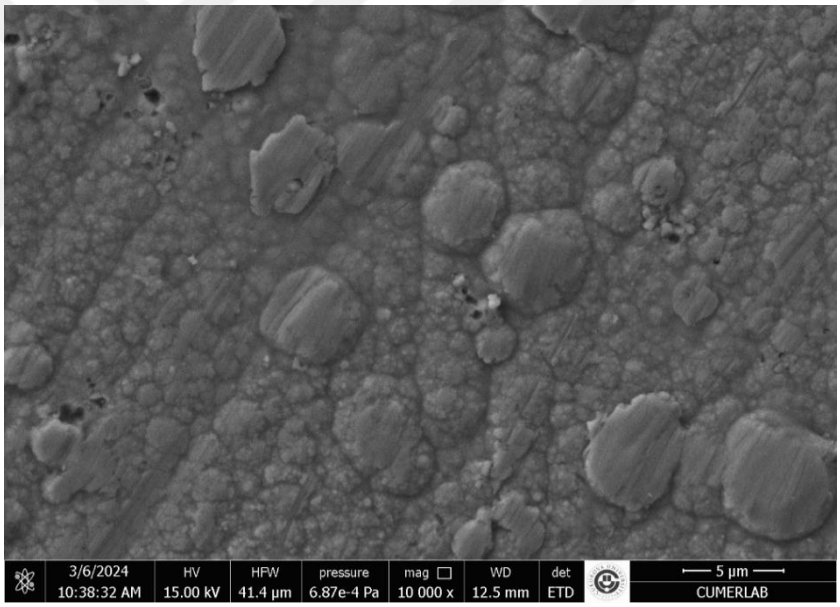

Figure 4.13. Surface morphology of Ni-B/ZrC composite coatings received with 9 g/L TMAB and 2 g/L ZrC bath concentration (9T2Z)

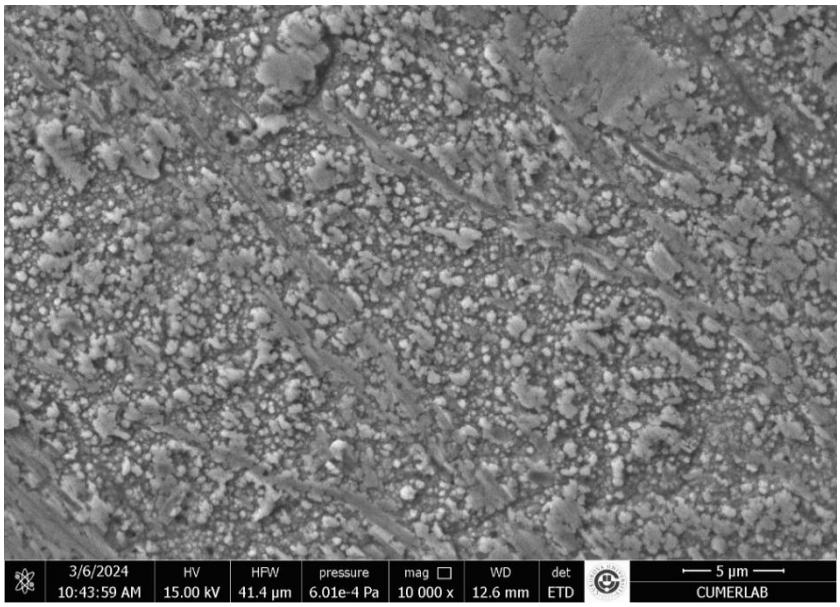

Figure 4.14. Surface morphology of Ni-B/ZrC composite coatings received with 9 g/L TMAB and 4 g/L ZrC bath concentration (9T4Z)

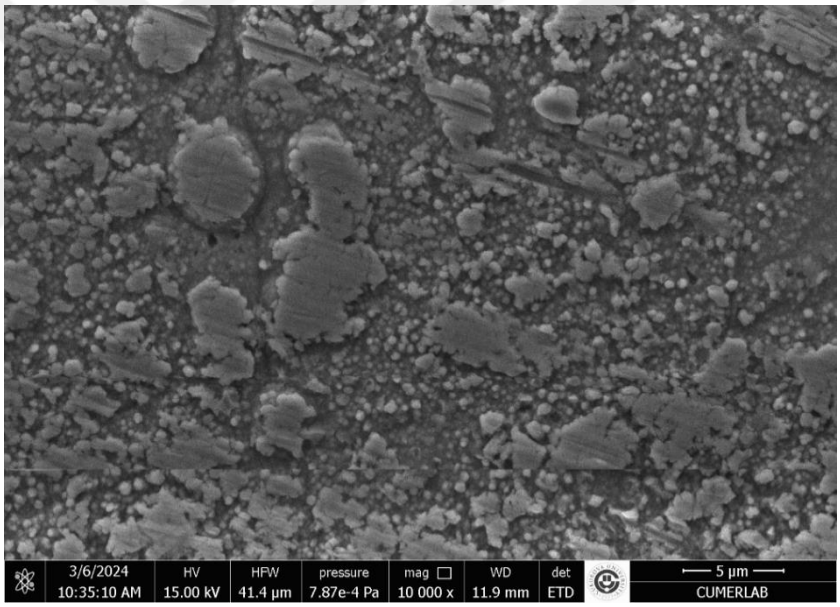

Figure 4.15. Surface morphology of Ni-B/ZrC composite coatings received with 9 g/L TMAB and 6 g/L ZrC bath concentration (9T6Z)

When the effects of changes in the TMAB and ZrC concentrations in the bath on the surface morphology of the coating were examined, it was observed that these changes had only minimal effects on the morphology. However, it was found that with the increase in TMAB and ZrC concentrations, the diameters of the circular structures formed on the surface slightly increased and were more sparsely distributed. Especially in Figure 4.13, it is seen that TMAB and ZrC formed sparse circular peaks on the surface. When the ZrC bath concentration reached the saturation level, deposits formed on the surface during coating due to the inability of the ultrasonic process to completely disperse the ZrC particles (He et al., 2018). Zhang and Li, (2018) investigated how

varying amounts of TMAB in the bath affected the surface quality and morphology of Ni-B/SiC composite coatings. Their findings revealed that higher TMAB concentrations resulted in smoother and rounder surface structures, indicating improved coating uniformity and quality. Similarly, Song et al., (2022) explored Ni-B/ZrC nanocomposite coatings produced via the pulsed current method. They reported that increasing ZrC doping led to larger unit cells on the coating surface, suggesting a direct influence of ZrC content on surface morphology.

SEM and EDS analyses revealed that the dark gray spots observed in the images were primarily attributed to carbon contamination. It is believed that these carbon traces originated during the reaction and degradation of organic compounds, such as SDS (sodium dodecyl sulfate) and saccharin, which were present in the electrolyte bath. During the electroplating process, these compounds can accumulate on the coating surface and subsequently decompose, leading to the formation of carbon-based residues. This observation highlights the potential impact of organic additives in the bath on the final surface characteristics of the coatings, emphasizing the need for careful control of bath composition to minimize unwanted contamination (Li et al., 2019).

Compared to other coatings, the 6T4Z nanocomposite coating exhibited a surface morphology free from defects such as pores and cracks. When looking at the SEM images, it is seen that the regular cauliflower structures formed on the surface in this combination are more pronounced compared to other structures and that these regular structures contribute to the development of optimal coating. These morphological features have produced extremely positive results in terms of preventing corrosion. The structure of the coating plays a crucial role in preventing water and other solvents from reaching the underlying surface. As shown in Figure 4.7 (3T2Z), the coating surface exhibits irregular, densely distributed structures. Within these structures, hill sizes are distributed heterogeneously, with smaller clusters visible between larger ones. This variation in morphology suggests a complex surface structure, where the distribution of material is not uniform. In Figure 4.11, it is evident that as the TMAB and ZrC bath concentrations increase, the hill sizes become larger, and more distinct circular structures begin to form on the surface. This phenomenon is attributed to the smooth growth of the crystal structure, which accumulates in a more organized manner on the surface. The larger clusters and the more defined circular features reflect improved crystalline formation and coating quality. However, for the samples with the highest TMAB concentrations (9T2Z, 9T4Z, 9T6Z), as seen in Figures 4.7 – 4.15, the surface morphology appears disrupted. This disruption suggests that while rising the TMAB concent from 3 $g \cdot L^{-1}$ to 6 $g \cdot L^{-1}$ results in an improvement in surface morphology, further increasing the concentration to 9 $g \cdot L^{-1}$ leads to a deterioration of the coating structure. This highlights the importance of finding an optimal TMAB concentration to achieve a well-formed, uniform surface morphology.

The EDS content analyses of the Ni-B/ZrC composite coatings, obtained with varying TMAB and ZrC bath concentrations, are presented in Figure 4.16. These analyses offer valuable insights into the elemental composition and distribution of TMAB and ZrC within the coating. By

examining the data, it is possible to assess how the concentrations of TMAB and ZrC influence the surface properties, particularly the uniformity of the coating, the distribution of nanoparticles, and the overall elemental balance.

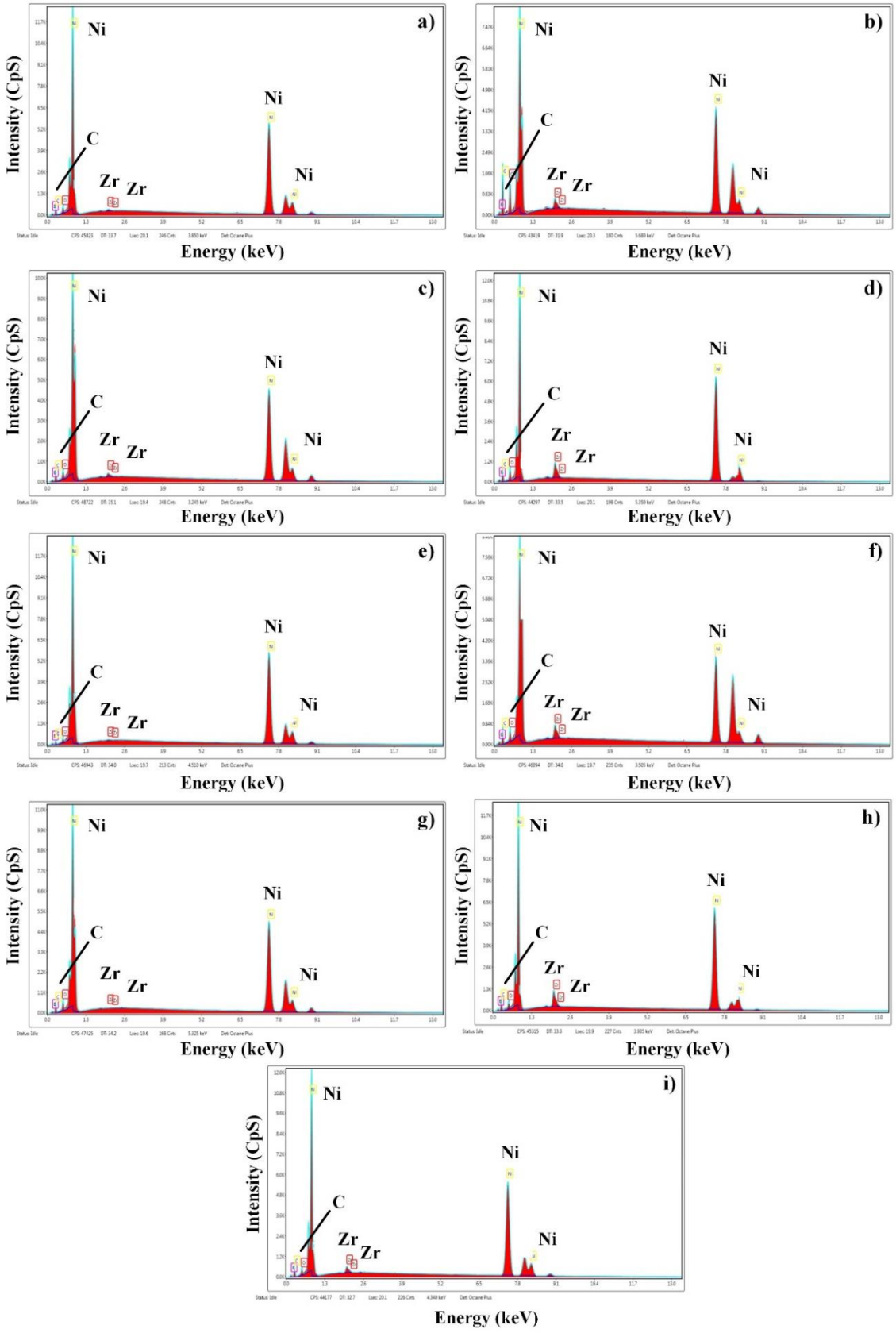

Figure 4.16. EDS analysis of Ni-B/ZrC composite coatings obtained at different bath concentrations. a) 3T2Z, b) 3T4Z, c) 3T6Z, d) 6T2Z, e) 6T4Z, f) 6T6Z, g) 9T2Z, h) 9T4Z, i) 9T6Z TMAB - ZrC bath content

The observation of peaks corresponding to Ni, B, Zr, and C elements as a result of EDS tests of composite coatings indicate that the electrodeposited coatings reinforced with ZrC are successfully integrated. In the analysis, impurities such as oxygen on the coating surface and copper originating from the substrate material were not included in the content percentage calculations. These analyses were conducted on multiple areas that best represent the coatings, with the most significant results being selected for graphical representation. The results indicate that as the TMAB concentration in the bath increases, the concentration of boron (B) in the coating initially rises, followed by a subsequent decrease. Especially, despite the decrease in the amount of boron in the case where the TMAB concentration is 9 $g \cdot L^{-1}$, this value is still higher than the lowest TMAB concentration of 3 $g \cdot L^{-1}$. Normally, it is expected that the amount of B element bound to the surface increases with the increase in the amount of TMAB in the bath content. However, excessive increases in TMAB concentration in the bath can disrupt the chemical equilibrium and diminish the effectiveness of TMAB. This can hinder the proper incorporation of the boron element into the coating. Once a certain concentration threshold is surpassed, the precipitation kinetics of boron may change, leading to a reduction in its integration into the coating. The atomic concentration data for TMAB is provided separately for each coating in Figure 4.17. This data provides important information in terms of understanding the effects of TMAB content on the coating composition. It was concluded that the chemical structure of the coating improved in the optimal concentration range of TMAB and that compositional analyses could be optimized accordingly. These findings are guided in terms of developing coating processes and obtaining more homogeneous composite coatings.

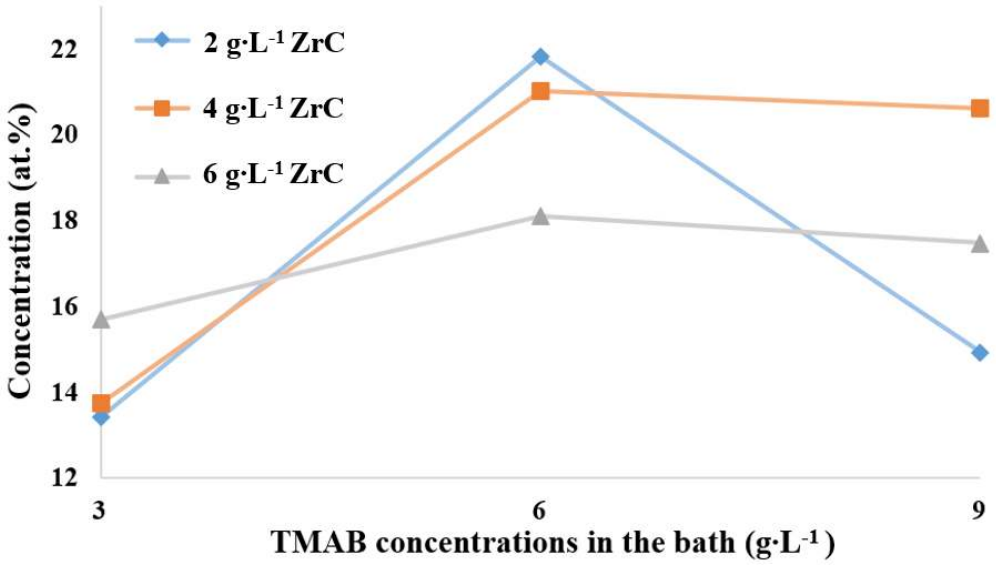

Figure 4.17. Atomic concentration of TMAB in the coating

As seen in Figure 4.17, it was observed that with the increase in TMAB bath concentration, the ZrC atom concentrations in the coating initially increased and then exhibited a decreasing trend.

The highest value of ZrC atom concentration was obtained with the combination of 6 $g \cdot L^{-1}$ TMAB and 2 $g \cdot L^{-1}$ ZrC, and this value was calculated as 21.82%. In contrast, the lowest ZrC atom concentration value was recorded as 13.43% in the coating obtained with 3 $g \cdot L^{-1}$ TMAB and 2 $g \cdot L^{-1}$ ZrC content. These results reveal that increasing the amount of TMAB in the bath content up to a certain level provides the successful integration of ZrC atoms into the coating structure, but beyond this level, changes in chemical equilibrium and deterioration in deposition kinetics negatively affect the integration. Ünal and Karahan (2018a) found in EDS analysis on Ni-B/hBN nanocomposite electrodeposition that there was a slight decrease in boron concentration when the TMAB concentration reached 9 $g \cdot L^{-1}$. This finding is consistent with the results obtained in this study and reveals how the bath concentration of TMAB can affect the elemental concentrations in the coating composition. In addition, to better understand the properties of the composite coating, an elemental mapping analysis of the coating called 6T4Z was performed and the results of this analysis are visualized in Figure 4.18. The elemental mapping results show that the ZrC particles exhibit a homogeneous distribution on the surface and this situation contributes positively to the general performance properties of the coating. Such analyses guide the optimization of coating properties and the development of coating processes.

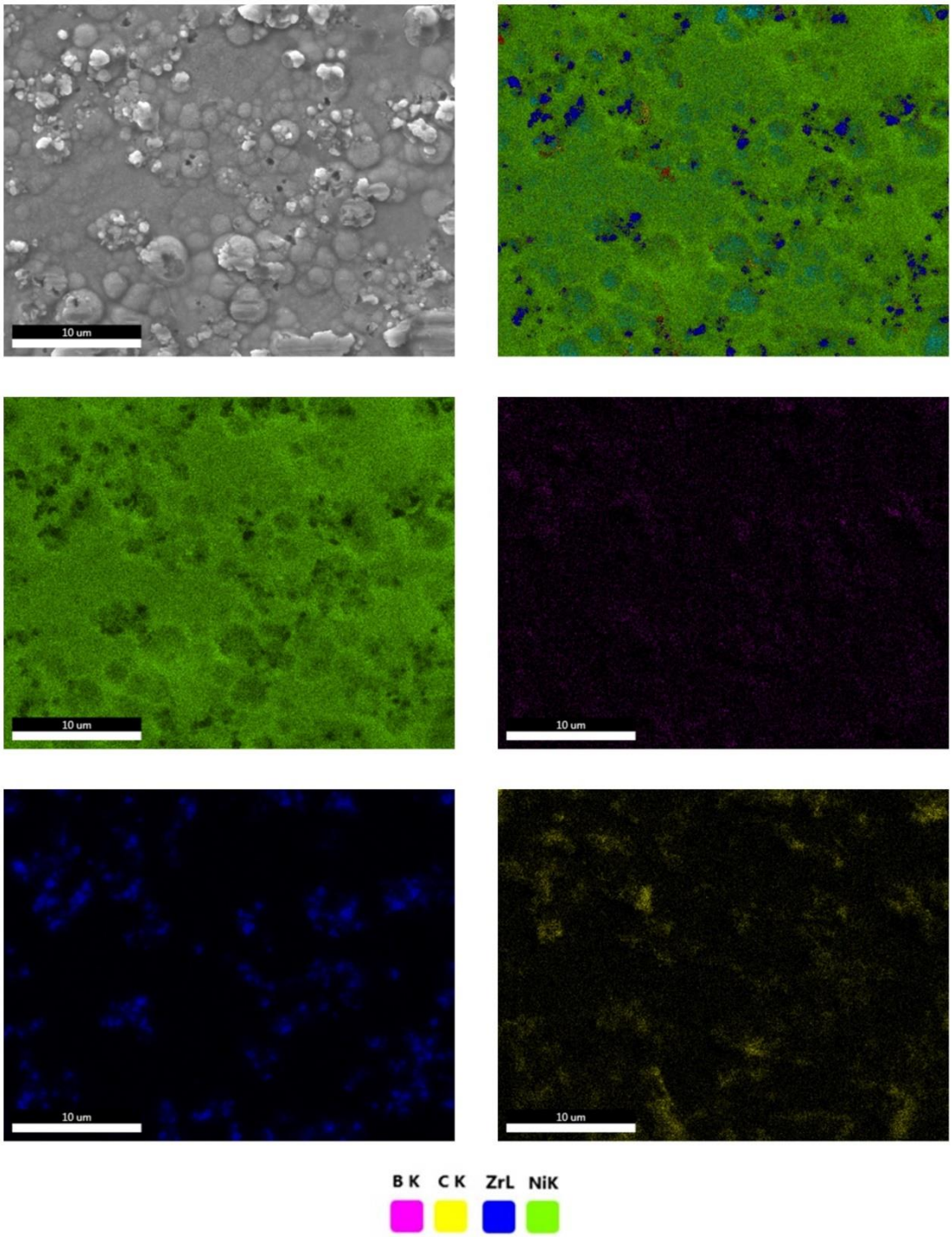

Figure 4.18. Elemental mapping analysis from the top surface of composite coatings obtained with 6 g/L TMAB and 4 g/L (6T4Z) bath concentration

The results obtained revealed that the ZrC nanoparticles and boron elements were distributed homogeneously throughout the coating surface. The zirconium (Zr) and carbon (C) elements forming the ZrC nanoparticles were integrated into the main structure together with the boron (B) elements in the alloy in a consistent manner. This confirms that ZrC is effectively included in the chemical content of the composite coating. The ZrC atom concentrations of each coating are shown in Figure 4.19. When the graph is examined, it is seen that the ZrC atom concentration in the coating increases

directly proportionally with the increase in the ZrC bath concentration. This finding shows that the ZrC nanoparticles have successfully settled into the coating structure and this situation is supported by the EDS analysis results. The homogeneous distribution of ZrC and its effective integration into the coating is a critical factor that improves the overall mechanical and chemical properties of the coating. This enables the coating to exhibit superior performance in application areas by increasing its properties such as corrosion resistance, hardness and wear resistance. Such results allow to better understand the role and potential of ZrC nanoparticles in coating technologies and provide important information for making coating processes more efficient.

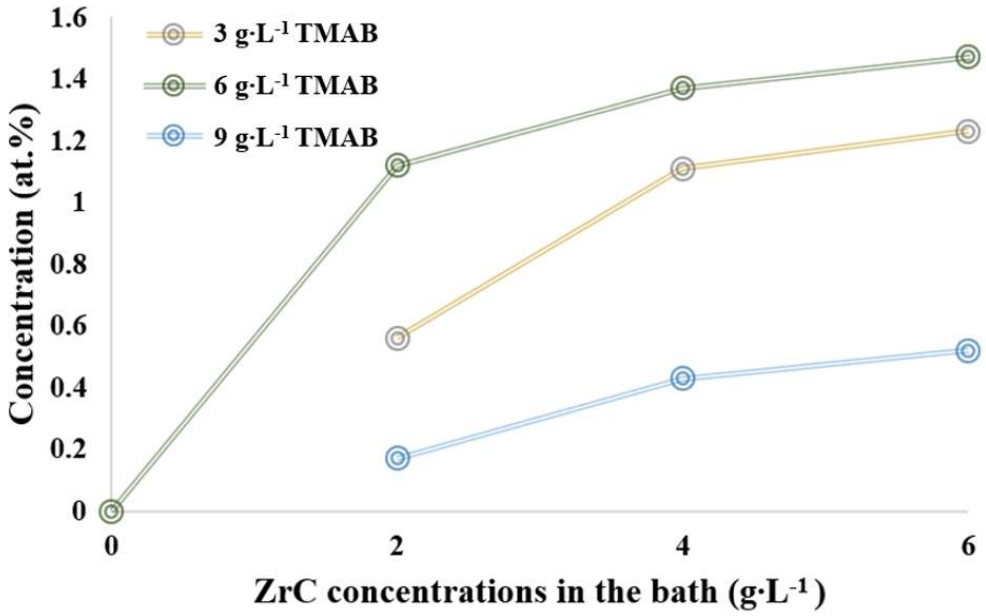

Figure 4.19. Atomic concentration of ZrC in the obtained coatings

According to the results, the highest TMAB atomic concentration was observed at 1.47% in the coating produced with 6 g·L⁻¹ TMAB and 6 g·L⁻¹ ZrC. In contrast, the lowest TMAB atomic concentration, 0.17%, was found in the coating obtained with 9 g·L⁻¹ TMAB and 2 g·L⁻¹ ZrC. These results clearly reveal the effects of changes in TMAB and ZrC concentrations on the coating composition. When the coating thicknesses were examined, it was observed that partial separations occurred in the coatings due to the forces applied during the sample-cutting process. However, this situation is not a factor affecting the general properties of the coating thicknesses. It was determined that the coating thicknesses varied throughout the measurements but were generally in the range of 10-20 µm. This thickness range shows that the coating was formed homogeneously and provided the desired mechanical properties. In addition, it was determined that the ZrC nanoparticles and boron elements used in the coatings were optimally distributed throughout the entire surface. These results confirm that the coating provides chemical and structural homogeneity and that the composite

coating targets were successfully achieved. In addition, the mapping analyses performed support that this composite coating structure was successfully achieved.

4.4. XRD Analysis of Ni-B/ZrC Nanocomposite Coatings

To examine the crystal structures of pure nickel, Ni-B, and Ni-B/ZrC coatings, X-ray diffraction (XRD) profiles of the coatings were received. During these analyses, information was obtained about the phase structures and atomic plane spacings of the crystal structures. XRD measurements were performed in the range of 2θ = 0-100°.

The device used to obtain patterns is an Empyrean model XRD device belonging to the PANalytical brand. This device produced CuKα radiation by operating at 40 kV voltage and 30 mA current values. The wavelength of the radiation used was determined as λ = 1.5418 Å. This high-precision device and parameters allowed the crystal structure analyses of the samples to be performed reliably and in detail.

$$D = \frac{0.94 \times \lambda}{\beta \times cos\theta} \tag{4.1}$$

The Debye-Scherrer equation (4.1) is a widely used equation to determine the average grain size of crystal structures. This equation is applied to estimate the crystallite sizes of nanomaterials based on X-ray diffraction data. The equation is expressed as follows:

The parameters for this equation are explained as follows:

- λ: X-ray wavelength (usually 1.5418 Å for CuKα).
- β: Full Width at Half Maximum (FWHM) of interest, expressed in radians.
- θ: Bragg reflection angle of interest.

$$\varepsilon = \beta \text{ x } 4 \tan\theta \tag{4.2}$$

Equation (4.2) was utilized to calculate the microstrain

$$\delta = \frac{1}{D^2} \tag{4.3}$$

Equation (4.3) is a fundamental equation used to calculate the dislocation density (δ) in materials. Dislocation density expresses the total length of dislocation lines in a unit volume or area of a material and is a critical parameter in evaluating microstructural properties. The equation is expressed as:

In this equation:

- δ: Dislocation density (dislocation line length per unit volume).
- D: Represents the average crystal grain size and is usually obtained from XRD analysis with the help of the Debye-Scherrer equation (Ünal, 2016).

XRD was utilized to examine the crystal structure of Ni-B/ZrC nanocomposite electrodeposition. The corresponding XRD patterns are displayed in Figure 20-22.

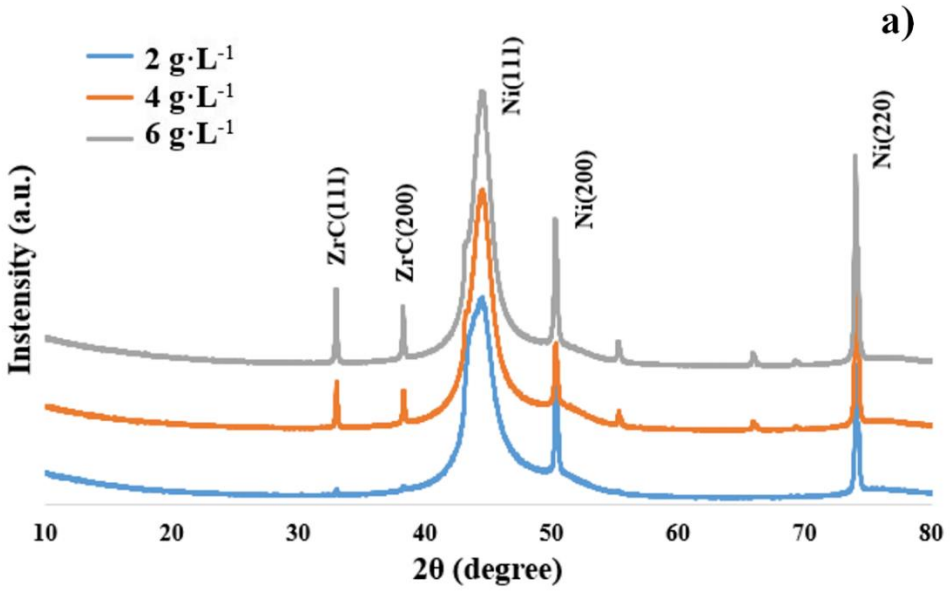

Figure 4.20. Crystal structure of Ni-B/ZrC composite coatings obtained at 3 g/L TMAB bath concentration

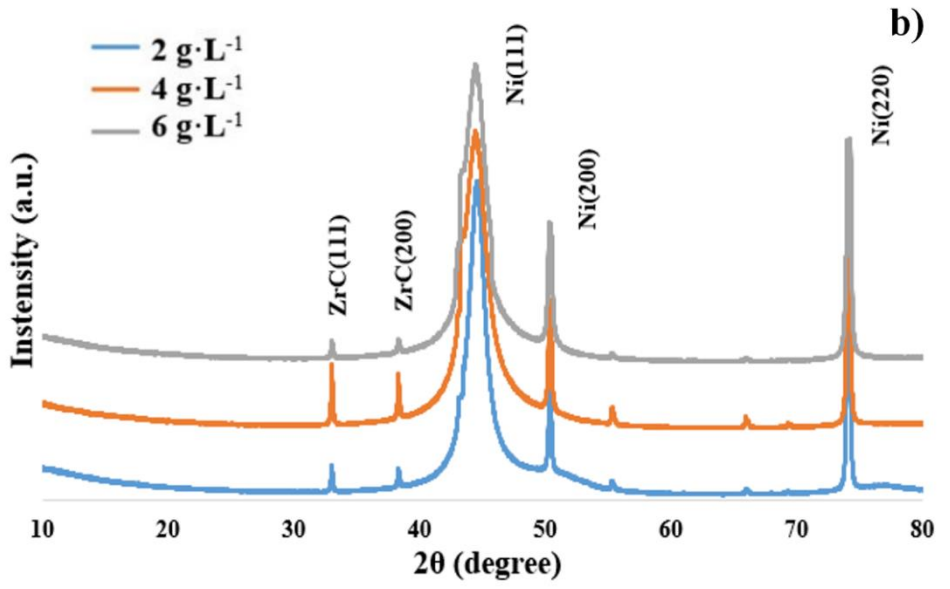

Figure 4.21. Crystal structure of Ni-B/ZrC composite coatings obtained at 6 g/L TMAB bath concentration

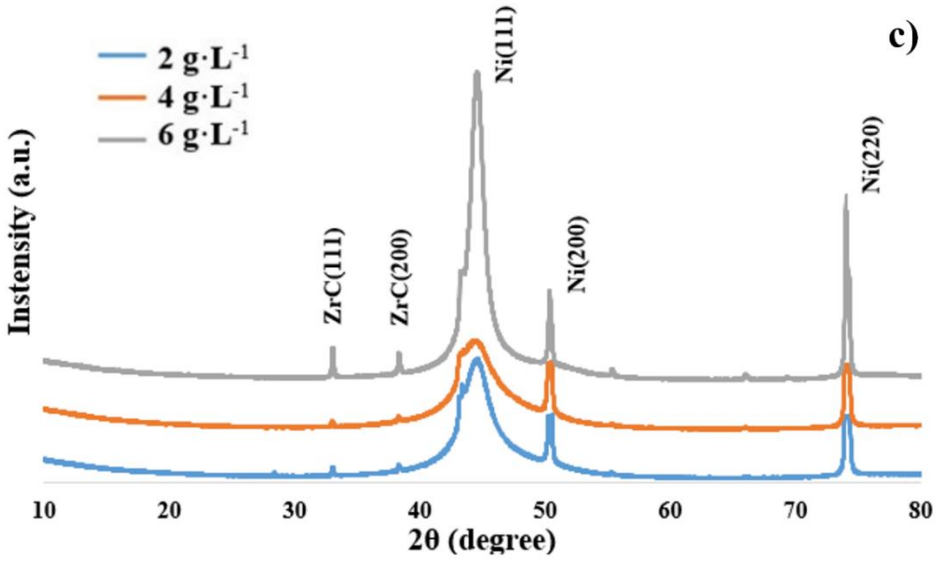

Figure 4.22. Crystal structure of Ni-B/ZrC composite coatings obtained at 9 g/L TMAB bath concentration

In accordance with the established literature, the characteristic peaks corresponding to the (111), (200), and (220) crystallographic planes of nickel (Ni) were observed at 44.441°, 51.784°, and 76.276°, respectively, in the X-ray diffraction (XRD) patterns. These peaks are well-known features of pure nickel, and they were evident in the XRD patterns of the Ni-B composite coatings produced by adding trimethylamine borane (TMAB) to the electrolyte used for depositing pure nickel. This finding supports the presence of pure nickel in the composite coating, consistent with reports in previous studies (Shakoor et al., 2014c; Ünal et al., 2019; Ünal and Karahan, 2018a, 2018b). In addition to these nickel peaks, literature studies have consistently shown that when reinforcing particles are incorporated into the electrolyte along with TMAB, the characteristic nickel peaks reappear in the resulting composite coatings. To investigate how TMAB and ZrC additions affect the crystallographic structure of the nickel matrix, composite coatings were produced using various concentrations of TMAB (3, 6, and 9 $g{\cdot}L^{-1}$) and ZrC (2, 4, and 6 $g{\cdot}L^{-1}$) in the electrolyte bath. The XRD analysis of the Ni-B/ZrC composite coatings revealed not only the expected peaks for nickel but also the (111) and (200) characteristic peaks of ZrC, indicating that the ZrC particles were successfully integrated into the nickel matrix. Detailed examination of the XRD data revealed interesting variations in the intensity and position of the peaks with changes in TMAB and ZrC concentrations. At a TMAB concentration of 3 $g{\cdot}L^{-1}$, the nickel peaks corresponding to the (111) and (200) planes initially diminished in intensity as the ZrC ratio increased. However, these peaks gradually escalated in intensity as the ZrC content further increased. This observation suggests that ZrC particles initially interfere with the crystallization of nickel, causing a reduction in peak intensity. As the ZrC concentration continued to increase, however, the peaks of nickel began to recover, indicating a possible reorganization or enhancement of the nickel crystal structure. At a higher TMAB concentration of 6 $g{\cdot}L^{-1}$, increasing the ZrC concentrations led to a broader and weaker

nickel peak intensity. This broadening and reduction in peak intensity suggests that the presence of ZrC particles at this TMAB concentration may cause a shift in the crystal growth mechanism, leading to the formation of a more disordered or amorphous nickel structure. The broadening of the peaks is often associated with a decrease in crystallite size and an increase in structural defects, which could be due to the high TMAB concentration inhibiting proper crystal growth by increasing the nucleation rate. At the highest TMAB concentration of 9 $g \cdot L^{-1}$, a similar trend was observed, with the nickel peaks initially decreasing in intensity and then increasing with further additions of ZrC. This behavior suggests that at higher TMAB concentrations, the effect of ZrC may promote nickel crystallization once a certain concentration sill of TMAB and ZrC is exceeded. Specifically, the initial decrease in nickel peak intensity could be attributed to the disruption of the crystallization process due to the high concentration of TMAB. As the ZrC concentration increases, it appears that the ZrC particles contribute to the stabilization of the crystal structure, leading to a recovery of the nickel peaks. Interestingly, the intensity of the nickel peaks at the 9 $g \cdot L^{-1}$ TMAB concentration was lower compared to the other bath concentrations, which can be associated to the more dominant effect of TMAB at higher concentrations. TMAB, being a complexing agent, may interfere with the formation of large nickel crystals, and this interference appears to be more pronounced at higher TMAB bath concentrations, thereby reducing the intensity of the nickel peaks (Ünal et al., 2019). As shown in Table 4.3, this reduction in the intensity of the nickel peaks and the change in peak broadening have significant implications for the crystal size and microstrain. The observed changes in peak intensity and broadening correlate with the crystallite size and microstrain values calculated from the XRD data. These findings suggest that both TMAB and ZrC have distinct roles at different bath concentrations. TMAB, which is known to promote a passing from crystalline to amorphous structures, has a significant impact on the nickel matrix. At lower ZrC concentrations (2, 4, and 6 $g \cdot L^{-1}$), the effect of TMAB is observed to initially decrease and then increase, which indicates a complex interaction between TMAB and ZrC in controlling the crystallization of the nickel matrix. This phenomenon suggests that ZrC particles are monotonously scattered within the coating solution when included in the bath, and that they play a key role in modulating the crystallization process of the nickel matrix. Furthermore, the presence of ZrC particles may inhibit the growth of larger crystallites by increasing the number of active nucleation sites, leading to a finer microstructure. This mechanism is consistent with the findings in the literature, where the addition of reinforcing particles in composite coatings often results in finer crystallites due to the increased nucleation rate (Aspillaga et al., 2023). These changes in microstructure are also reflected in the microhardness results, which show a correlation with the crystallite size and the degree of structural disorder observed in the XRD patterns.

Based on the results, it can be inferred that ZrC particles are monotonously scattered in the coating solution when introduced into the bath. This dispersion is believed to play a crucial role in modifying the crystallization process of the nickel matrix. Specifically, the presence of ZrC particles

is thought to prevent the growth of larger crystallites by increasing the number of active nucleation sites. This results in smaller crystallites and a finer microstructure in the resulting composite coatings, where microhardness results were found to align closely with the XRD findings, further supporting the theory that the presence of ZrC influences the crystallization dynamics. Interestingly, no previous research was identified in the literature that specifically examines the effects of TMAB and ZrC bath concentrations on the electrodeposition of Ni-B nanocomposite coatings. However, research on the impact of TMAB on Ni-B matrix has been conducted. Karahan et al., (2022) investigated the influence of TMAB content on the structural characterization of Ni-B alloy electroplating. Their results showed that as the TMAB bath concentration increased, the intensity of nickel peaks in the XRD profiles decreased, and the width of the peaks expanded. This phenomenon was explained by the smaller and more disordered crystal structure that resulted from the high TMAB concentration, which impeded the growth of larger nickel crystals. The reduced intensity and broadening of the peaks in the XRD profiles were indicative of the formation of smaller, more finely grained nickel crystals. This can be attributed to the fact that TMAB accelerates the precipitation rate of nickel ions, thereby limiting the time available for proper crystal growth and promoting the formation of smaller crystals with a higher number of nucleation sites. Mirak et al., (2018) also investigated the effects of TMAB on Ni-B coatings, producing modified coatings with varying TMAB concentrations. The XRD patterns from their study demonstrated where the peaks of nickel broadened, and the intensity decreased as the TMAB concentration increased. They also observed a significant reduction in the grain size of the crystal phase, which dropped from 13 nm to 2.3 nm for pure nickel. This reduction in grain size is a direct result of the increased number of nucleation sites caused by the higher concentration of TMAB in the electrolyte, which prevents proper crystal growth. As a consequence, smaller crystals form, leading to a more disordered and finer microstructure. This finding is consistent with the notion that TMAB, by accelerating nickel ion precipitation, disrupts the growth of large crystals, leading to a finer surface morphology. Table 4.3 presents the calculations for microstrain and crystal grain size, derived from the XRD patterns of Ni-B/ZrC composite coatings electrodeposited at different TMAB and ZrC concentrations. The crystal grain sizes and microstrain values were determined from the intensity peaks seen in the XRD patterns. These calculations offer valuable insights into how varying concentrations of TMAB and ZrC affect the structural characteristics of the coatings, particularly in terms of grain size and strain within the crystal lattice. This information helps to understand the impact of bath composition on the overall quality and performance of the coatings. In conclusion, the presence of TMAB and ZrC in the electrodeposition bath has a important impact on the crystallization and microstructure of Ni-B composite coatings. TMAB accelerates the precipitation of nickel, resulting in smaller crystal grains and a more disordered structure, while ZrC particles hinder the growth of larger crystallites by increasing nucleation sites, resulting in a finer grain size and improved surface morphology. These findings, combined with the XRD and microhardness data, provide a comprehensive understanding of how

bath concentration influences the properties of Ni-B/ZrC composite coatings, offering potential avenues for optimizing these coatings for various applications.

Table 4.3. Values obtained from XRD profiles of Ni-B/ZrC composite electroplatings deposited with different TMAB and ZrC bath concentrations

Coatings	**2θ (deg)**			**Crystal grain size (nm)**			**Microstrain**		
	2 g/L ZrC	4 g/L ZrC	6 g/L ZrC	2 g/L ZrC	4 g/L ZrC	6 g/L ZrC	2 g/L ZrC	4 g/L ZrC	6 g/L ZrC
3 g/L TMAB	44.44	44.48	44.28	15.2	12.9	13.5	12.7 x 10-3	15.8 x 10-3	14.3 x 10-3
6 g/L TMAB	44.58	44.44	43.94	10.2	8.3	8.2	17.9 x 10-3	23.5 x 10-3	23.6 x 10-3
9 g/L TMAB	44.28	44.56	44.50	17.3	11.7	18.7	11.1 x 10-3	16.7 x 10-3	10.3 x 10-3

When reviewing Table 4.3, it is evident that varying bath concentrations of TMAB and ZrC had a significant impact on the average crystal grain size of the composite coatings. As the ZrC concentration rised, the average crystal grain size initially decreased. However, the crystal grain size began to increase beyond a certain point, specifically at 3 $g \cdot L^{-1}$ and 9 $g \cdot L^{-1}$ TMAB concent. The initial reduction in crystal grain size can be attributed to the ZrC particles, which serve as nucleation sites, promoting the formation and growth of the nickel phase. This phenomenon highlights the role of ZrC in refining the microstructure of the coating during electrodeposition. These particles limit the growth of the nickel crystals, preventing them from forming larger, more regular grains, and as a result, the average crystal size becomes smaller. However, as the concentration of ZrC rises, the residual ceramic particles can become incorporated into the growing crystal structure, potentially causing agglomeration. This agglomeration reduces the number of nucleation sites available and allows the crystals to grow more freely, leading to an increase in the average crystal size. At a 3 g/L TMAB bath concent, the smallest crystal grain size (12.9 nm) was obtained at a 4 g/L ZrC bath concent, while the largest crystal grain size (15.2 nm) was observed at a 2 g/L ZrC bath concent. Similarly, at a 9 g/L TMAB bath concent, the smallest crystal grain size (11.7 nm) was found at a 4 g/L ZrC bath concent, while the largest grain size (18.7 nm) occurred at a 2 g/L ZrC concent.

At a 6 g/L TMAB bath concent, the trend was different from the 3 g/L and 9 g/L bath concentrations. In this case, the average crystal grain size decreased as the ZrC concentration rised. The smallest crystal grain size (8.2 nm) was recorded at a 6 g/L ZrC concentration, while the largest (10.2 nm) was found at a 2 g/L ZrC concentration. This suggests that at the 6 g/L TMAB concent, the ZrC particles had a more pronounced effect in inhibiting crystal growth, leading to smaller crystal sizes. The incorporation of ZrC nanoparticles into the Ni-B metal matrix alloy bath also led to a slight

reduction in the average crystal grain size. This effect can be explained by the physical blockage of grain boundary movement by the ZrC nanoparticles. By acting as a barrier at the grain boundaries, ZrC nanoparticles restrict the ability of grains to grow larger, resulting in a finer crystal structure.

Interestingly, the microstrain values exhibited an opposite trend to the crystal grain size. As the concentration of ZrC rised, the microstrain results initially increased and then decreased at both 3 g/L and 9 g/L TMAB bath concentrations. In contrast, at the 6 g/L TMAB bath concent, microstrain values increased with increasing ZrC concentrations. This indicates that the structural changes in the coatings, or the homogeneity of the ZrC distribution in the bath, influenced the microstrain. Specifically, at the 6 g/L TMAB concent, the ZrC particles seemed to contribute to a more homogeneous distribution within the coating, which positively affected the microstrain properties of the coating.

The inverse relationship between microstrain and crystal grain size, as observed in these results, further supports the notion that the structural properties of the composite coatings are interrelated. As the crystal grain size decreases, the microstrain leans to increase, and vice versa. The inverse changes observed in the microstrain and crystal grain size values indicate a consistent and complementary effect, highlighting the complex interaction between the ZrC nanoparticles, TMAB concentration, and the crystallization conduct of the Ni-B nanocomposite coatings. These findings underscore the importance of optimizing bath concentrations for tailoring the structural properties of the coatings, which can have significant implications for their performance in various applications

4.5. AFM Analysis of Ni-B/ZrC Nanocomposite Coatings

AFM (Atomic Force Microscopy) analysis was conducted to examine the surface morphology of the Ni-B and Ni-B/ZrC composite coatings in greater elaboration. The AFM pictures and corresponding surface roughness profiles of Ni-B and Ni-B/ZrC nanocomposite coatings, which were produced with varying bath concents of TMAB and ZrC particles, are received in Figure 4.23-4.32. The surface of the Ni-B matrix showed relatively low roughness, ranging from approximately 0 to 30 nm, indicating that the Ni-B coatings have a plain surface compared to the Ni-B/ZrC composite coatings. In contrast, the Ni-B/ZrC composite coatings exhibited a rougher surface for the inclusion of ZrC particles within the matrix. These ZrC particles caused the formation of surface features such as pits and peaks, contributing to the increased roughness. The increase in surface roughness with the addition of ceramic particles such as ZrC has been documented in other studies as well. For instance, Shakoor et al., (2014c) demonstrated that the addition of Al_2O_3 particles to the Ni-B metal matrix led to an increase in surface roughness due to the insolubility of Al_2O_3 particles, which disrupted the uniformity of the coating surface. Similarly, Shakoor et al., (2014b) deposited Ni-B alloy and Ni-B/Zn composite coatings using electroplating and found that the surface of the Ni-B alloy coatings was relatively smooth, with surface roughness results ranging from 0 to 40 nm. But, the Ni-B/Zn alloy coatings had a much rougher surface, with roughness values ranging from -30 nm to +30 nm, indicating that the presence of reinforcing particles increased the surface roughness. In this study, the variation in surface roughness can be explained by the addition of ZrC particles into the Ni-B matrix. While the base Ni-B matrix exhibits minimal variation in surface roughness, the addition of ZrC reinforcement received in a more complex surface texture (Shakoor et al., 2014c, 2014a, 2017). As indicated in Table 4.4, the surface roughness of the coatings increased with the addition of ZrC particles, with the highest average surface roughness (Ra) value recorded as 128.80 nm for the 6T4Z sample. The lowest Ra result was observed for the 6T0Z sample, which had a Ra of 31.68 nm. The trend showed that the average surface roughness (Ra) increased with the addition of ZrC particles up to a certain concentration, after which it began to decrease. This decrease in roughness at higher ZrC concentrations can be attributed to the formation of a supersaturated structure, which reduces the accumulation of ZrC particles on the surface, thus limiting further roughening. Additionally, the Rq value, which represents the geometric mean of deviations from the center mean line, followed a parallel trend to that of the average surface roughness (Ra) values. The increase in surface roughness with increasing ZrC content is consistent with the findings of previous studies, where the addition of reinforcing particles altered the surface morphology and roughness of composite coatings. The overall findings suggest that ZrC particles play a significant role in modifying the surface texture of Ni-B coatings, making the surface rougher, with the roughness level peaking at an optimal ZrC concentration before decreasing as the ZrC concentration exceeds a certain threshold.

Table 4.4. Surface roughness values of Ni-B/ZrC nanocomposite coatings deposited at different bath concentrations

Sample	Ra (nm)	Rq (nm)
3T0Z	30.66	41.98
3T2Z	51.63	58.99
3T4Z	58.03	65.74
3T6Z	65.28	70.23
6T0Z	31.68	42.65
6T2Z	108.46	123.94
6T4Z	128.80	153.33
6T6Z	89.15	106.75
9T0Z	35.87	58.02
9T2Z	49.88	61.99
9T4Z	68.15	80.75
9T6Z	58.72	67.41

The three-dimensional AFM images shown in Figure 4.23-4.32 further support the previous observations regarding the surface morphology of Ni-B and Ni-B/ZrC composite coatings. The Ni-B coating, due to its inherent characteristics, tends to promote hydrogen evolution, which in turn leads to the development of significant surface porosity. This porosity obstructs the normal formation of crystallites, preventing a well-defined crystalline structure from developing on the coating surface. In conclusion, the surface of the Ni-B coating remains relatively smooth but exhibits a porous texture that can influence its performance in certain applications.

In addition, the incorporation of ZrC nanoparticles into the Ni-B matrix brings about notable changes in the coating's behavior. ZrC particles act as nucleation sites, accelerating the nucleation rate during the electrodeposition process. This results in a more controlled and directional growth of the coating, where the crystalline structure becomes more organized and well-defined. The increased nucleation rate not only helps to promote better crystal formation but also reduces the overall density of the crystal structure, allowing for the growth of larger unit cells on the surface. These larger unit cells contribute to the roughening of the surface, enhancing the overall surface roughness. The rise in surface roughness due to the addition of ZrC nanoparticles can have a significant impact on how the coating interacts with external environmental factors (Aspillaga et al., 2023). A rougher surface can potentially improve the coating's adhesion properties and may influence its behavior in corrosive environments, wear resistance, or other surface-related interactions. Thus, the structural changes induced by the inclusion of ZrC nanoparticles may provide additional functional benefits to the Ni-B coatings, improving their overall performance in various applications where surface characteristics play a crucial role.

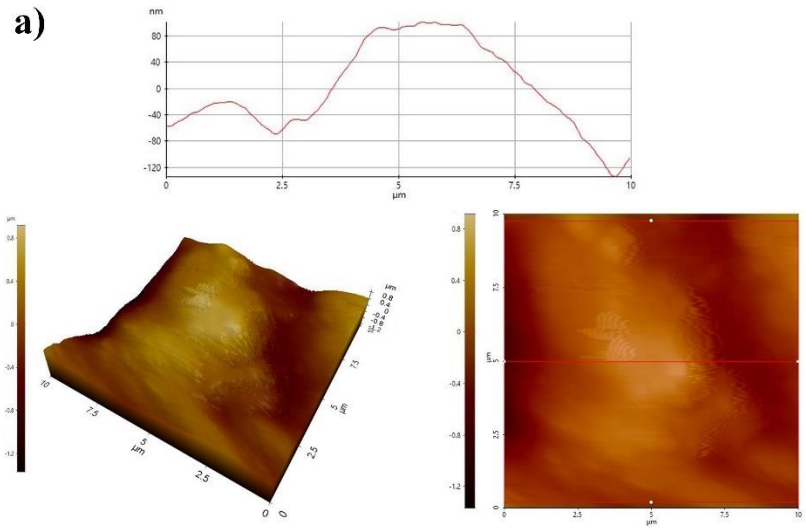

Figure 4.23. Three-dimensional AFM pictures and surface roughness profiles of the coating received at 6 g/L TMAB and 0 g/L ZrC bath concentrations

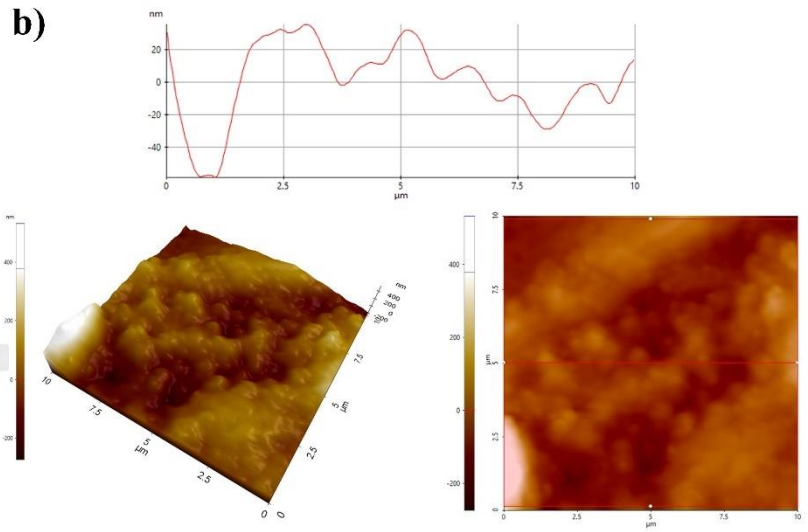

Figure 4.24. Three-dimensional AFM pictures and surface roughness profiles of the coating received at 3 g/L TMAB and 2 g/L ZrC bath concentrations

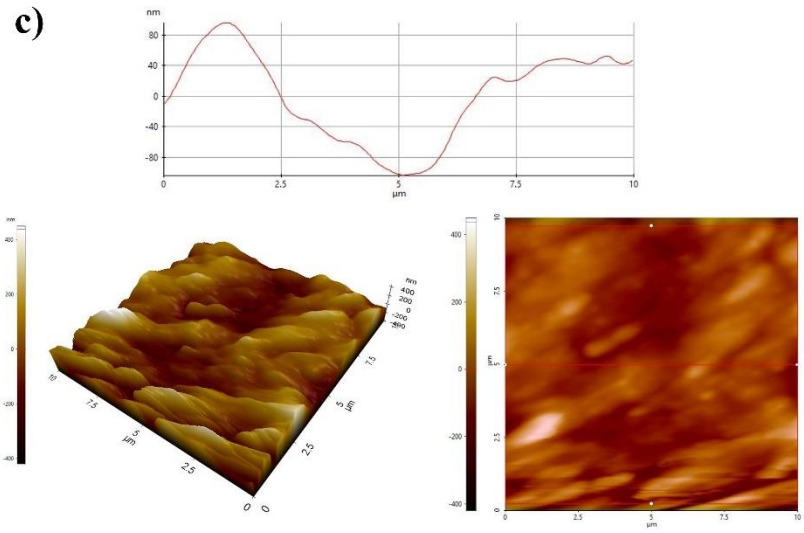

Figure 4.25. Three-dimensional AFM pictures and surface roughness profiles of the coating received at 3 g/L TMAB and 4 g/L ZrC bath concentrations

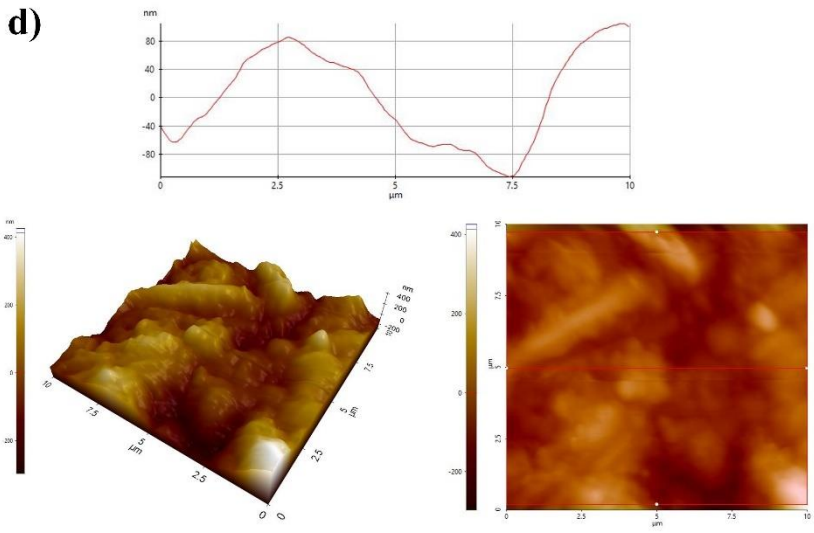

Figure 4.26. Three-dimensional AFM pictures and surface roughness profiles of the coating received at 3 g/L TMAB and 6 g/L ZrC bath concentrations

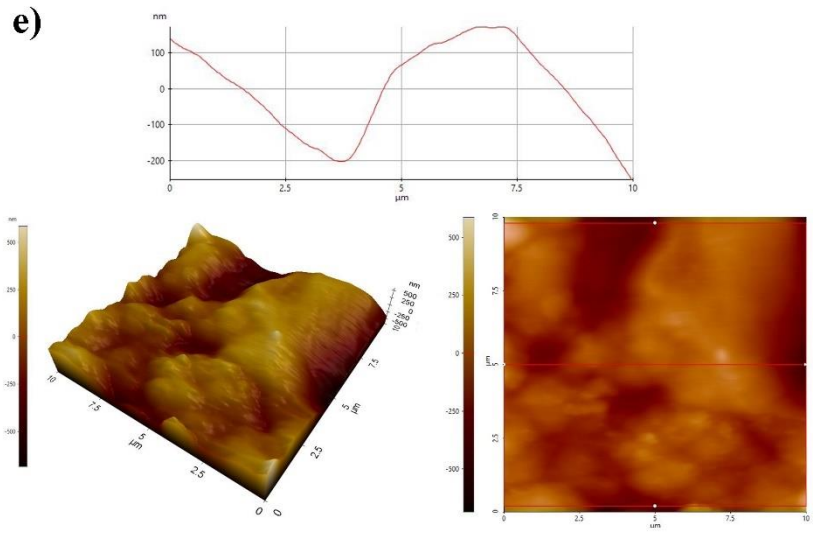

Figure 4.27. Three-dimensional AFM pictures and surface roughness profiles of the coating received at 6 g/L TMAB and 2 g/L ZrC bath concentrations

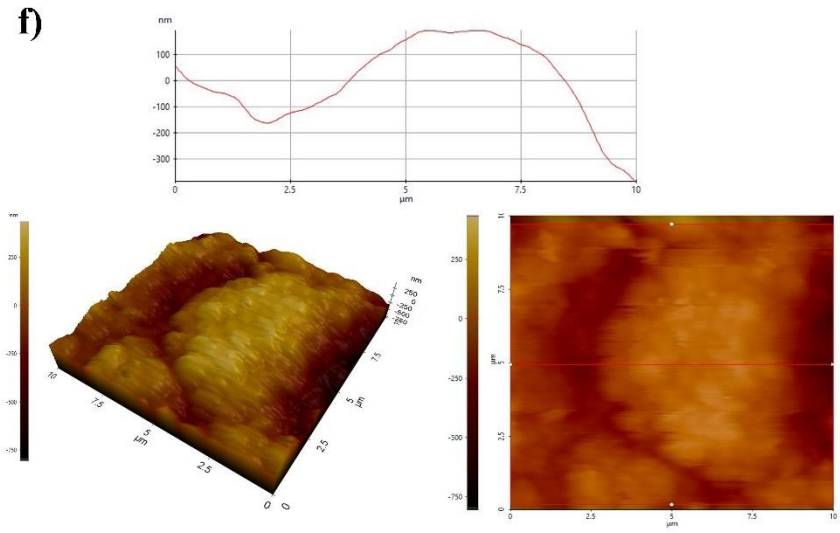

Figure 4.28. Three-dimensional AFM pictures and surface roughness profiles of the coating received at 6 g/L TMAB and 4 g/L ZrC bath concentrations

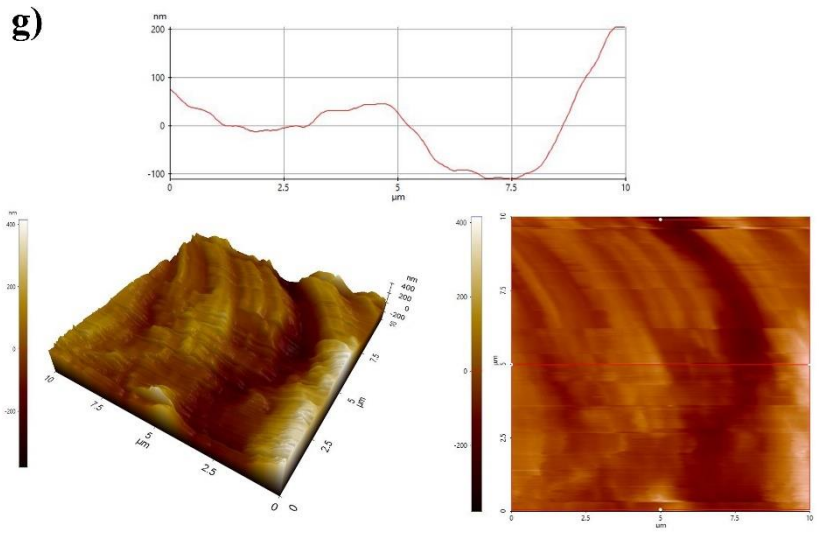

Figure 4.29. Three-dimensional AFM pictures and surface roughness profiles of the coating received at 6 g/L TMAB and 6 g/L ZrC bath concentrations

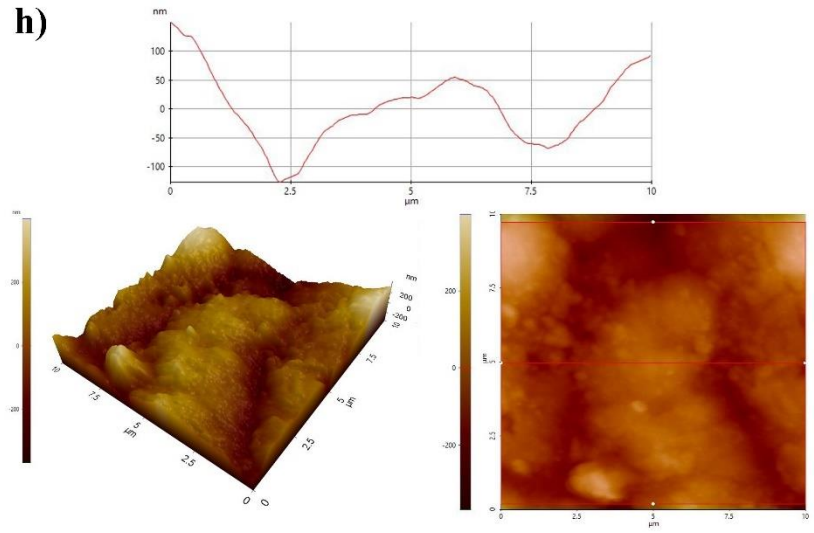

Figure 4.30. Three-dimensional AFM pictures and surface roughness profiles of the coating received at 9 g/L TMAB and 2 g/L ZrC bath concentrations

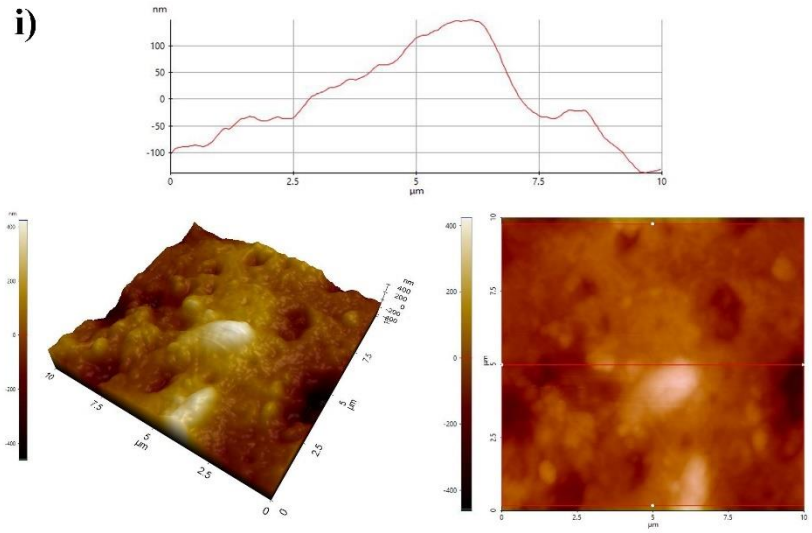

Figure 4.31. Three-dimensional AFM pictures and surface roughness profiles of the coating received at 9 g/L TMAB and 4 g/L ZrC bath concentrations

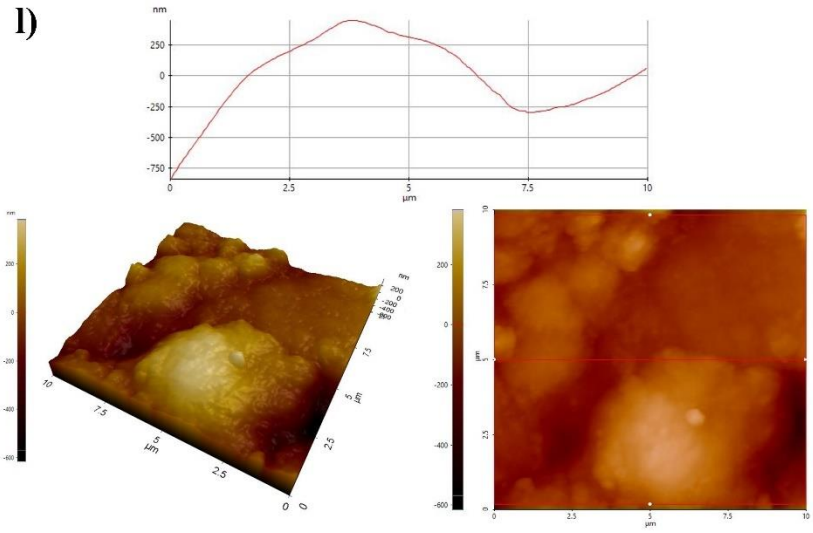

Figure 4.32. Three-dimensional AFM pictures and surface roughness profiles of the coating received at 9 g/L TMAB and 6 g/L ZrC bath concentrations

4.6. Corrosion Performances of Ni-B/ZrC Nanocomposite Coatings

The corrosion performance of the produced Ni-B/ZrC nanocomposite coatings was evaluated using two methods: open circuit potential measurement and potentiodynamic polarization curve techniques. Both tests were carried out in 3.5% NaCl solvent. The corrosion performances of Ni-B/ZrC nanocomposite coatings were investigated at 2, 4, 6 g/l ZrC and 3, 6, 9 g/l bath concentrations. In addition, the corrosion performances of copper and Ni-B alloy were also investigated for comparison.

4.6.1. Open Circuit Potential Analysis of Ni-B/ZrC Nanocomposite Coatings

To compare the open circuit potential curves of Ni-B/ZrC nanocomposite coatings with the anodic dissolution potential (ADP) curves of copper and Ni-B alloy coatings, Figure 4.33 presents the results. The ADP curves were recorded for 3600 seconds to ensure the establishment of a stable potential value in a 3.5% NaCl solution by mass. This experimental setup allowed for a direct comparison of the corrosion performance of the Ni-B/ZrC nanocomposite with that of copper and Ni-B alloy coatings under similar conditions, offering valuable insights into their relative corrosion resistance. The ADP potential recorded in an ionic solution represents the equilibrium potential between cathodic and anodic reactions. In addition, it reflects the balance between oxidation and reduction processes occurring in the solution medium. If the solution medium is corrosive, we can accept this recorded ADP potential as corrosion potential. We can say that the coatings compared with each other are more resistant to corrosion than those on the more negative side in terms of open circuit potentials (Trentin et al., 2022). Figure 4.33 illustrates the variation in Open Circuit Potential (OCP) overtime, which serves as an electrochemical corrosion analysis for the Ni-B/ZrC nanocomposite coatings. The OCP potential is defined as the equilibrium potential between cathodic and anodic reactions, representing the balance of oxidation and reduction processes in the electrolyte environment. In the context of corrosion, the OCP value can be considered as the corrosion potential, providing crucial insights into the tendency of a material to corrode in a given electrolyte. The OCP data, measured before conducting other corrosion tests, offers initial information regarding the corrosion resistance of the Ni-B/ZrC nanocomposite coatings. By comparing the open circuit potentials, it becomes evident that coatings exhibiting more positive OCP values show better corrosion resistance. On the contrary, those with more negative potentials are more prone to corrosion. The Ni-B/ZrC nanocomposite coatings, produced at varying TMAB and ZrC bath concents, exhibit significantly improved corrosion resistance compared to both the copper plate and pure Ni-B alloy coatings. As shown in Figure 4.33, the average corrosion potential of the Ni-B alloy coatings is approximately -0.23 V. In contrast, the 6T4Z coating, which demonstrates the most positive corrosion potential between the Ni-B/ZrC nanocomposite coatings, shows an average open circuit potential (OCP) value of approximately -0.15 V. This indicates that the inclusion of ZrC nanoparticles and optimal TMAB concentration enhances the corrosion performance of the Ni-B/ZrC nanocomposite coatings, making them more durable in corrosive environments. This indicates that the addition of TMAB and ZrC reinforcements into the Ni-B coating significantly improves its corrosion potential, shifting it towards more positive values. This shift in potential suggests that the ZrC particles act as an effective corrosion preventive, enhancing the resistance of the coating to corrosive environments.

These findings align with studies by Waware, et al., (2018c) who demonstrated that the incorporation of AlN (aluminum nitride) second-phase particles into Ni-B/AlN composite coatings led to a notable enhancement in corrosion resistance. Similar to the present study, their research

emphasized the role of secondary phases, like AlN, in reinforcing the corrosion protection characterization of Ni-B-based coatings. This supports the idea that the addition of reinforcing nanoparticles, such as ZrC in this study, can significantly develop the corrosion resistance of composite coatings, thereby enhancing their performance in aggressive environments. Their research demonstrated that the corrosion performance of Ni-B/AIN coatings increased threefold compared to pure Ni-B coatings. Similarly, other studies have shown that adding reinforcement particles such as Al_2O_3, V_2O_5/ZrO_2, and Tl_2O_3 to Ni-B alloys improves the corrosion resistance of the composite coating (Li, et al., 2018a; Li, et al., 2018b; Waware et al., 2018a, 2018b). For this reason, the incorporation of ZrC particles in Ni-B coatings follows a similar trend, improving the overall corrosion resistance by mitigating the effects of the corrosive environment.

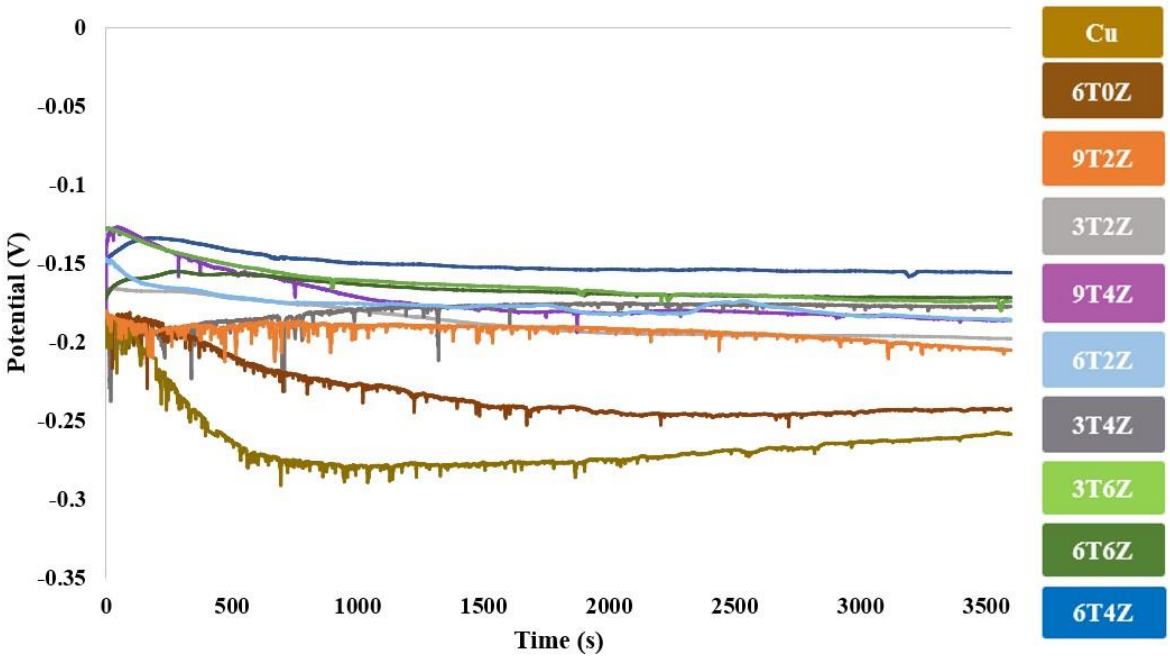

Figure 4.33. Open Circuit Potential Analysis of Ni-B/ZrC electroplatings prepared at different bath concentrations

4.6.2. Potentiodynamic Polarization Analysis of Ni-B/ZrC Nanocomposite Coatings

Potentiodynamic polarization tests were conducted to assess the corrosion attitude of the Ni-B/ZrC composite coatings in a 3.5% NaCl solution. The potential range for the tests spanned from 250 mV below the open circuit potential (OCP) to 250 mV above the OCP, and the scanning speed was set at 0.166 mV/s. These conditions allow for the evaluation of both anodic and cathodic polarization curves, providing valuable insights into the material's resistance to corrosion under controlled conditions. Corrosion parameters such as corrosion potential (E_{cor}), corrosion current (I_{cor}), and corrosion rate were determined using the Tafel extrapolation method. This method involves extrapolating the anodic and cathodic polarization curves to calculate the corrosion current (I_{cor}), which is directly related to the corrosion rate of the material. A lower corrosion current indicates a

more corrosion-resistant material, as it signifies a slower rate of electrochemical reactions at the surface. The corrosion potential (E_{cor}), which indicates the equilibrium between anodic and cathodic reactions, is another key parameter. More positive corrosion potentials are generally indicative of better corrosion resistance, as they suggest that the material is less prone to oxidation in a corrosive environment. By analyzing these corrosion parameters, the potentiodynamic polarization tests provide critical data on the performance of Ni-B/ZrC composite coatings in comparison to the pure Ni-B alloy and the copper substrate. The use of Tafel extrapolation allows for a precise quantification of corrosion resistance, helping to evaluate the effectiveness of the ZrC particles and TMAB bath concents in enhancing the corrosion properties of the Ni-B alloy matrix.

Figure 4.34 presents Tafel curves that illustrate the influence of varying TMAB and ZrC bath concents on the corrosion performance of Ni-B/ZrC composite electrodepositions. These curves provide insights into the anodic and cathodic behaviors of the coatings, which are crucial for understanding their corrosion resistance. The Tafel curves help to identify the corrosion current (I_{cor}), corrosion rate and corrosion potential (E_{cor}) of the samples, allowing for a detailed analysis of the electrochemical performance of the coatings. The results derived from these Tafel curves are summarized in Table 4.5, which includes corrosion parameters such as the corrosion potential (E_{cor}) and corrosion current (I_{cor}) for each sample. Additionally, the corrosion rates of the Ni-B/ZrC composite coatings are calculated based on the Tafel extrapolation process. For comparison, the corrosion performance of the copper plate and Ni-B matrix coatings is also included in Table 4.5 and Figure 4.34, enabling a clear understanding of the improvements in corrosion resistance achieved by the addition of ZrC particles and TMAB to the coatings.

By analyzing the Tafel curves, it is possible to observe the effects of TMAB and ZrC concentrations on the overall corrosion resistance of the coatings. Coatings with more positive corrosion potentials and lower corrosion currents demonstrate better corrosion resistance, as they are less susceptible to oxidation in the corrosive electrolyte. This comparative analysis helps highlight the enhanced corrosion protection provided by the Ni-B/ZrC composite coatings compared to the pure Ni-B matrix and the copper substrate.

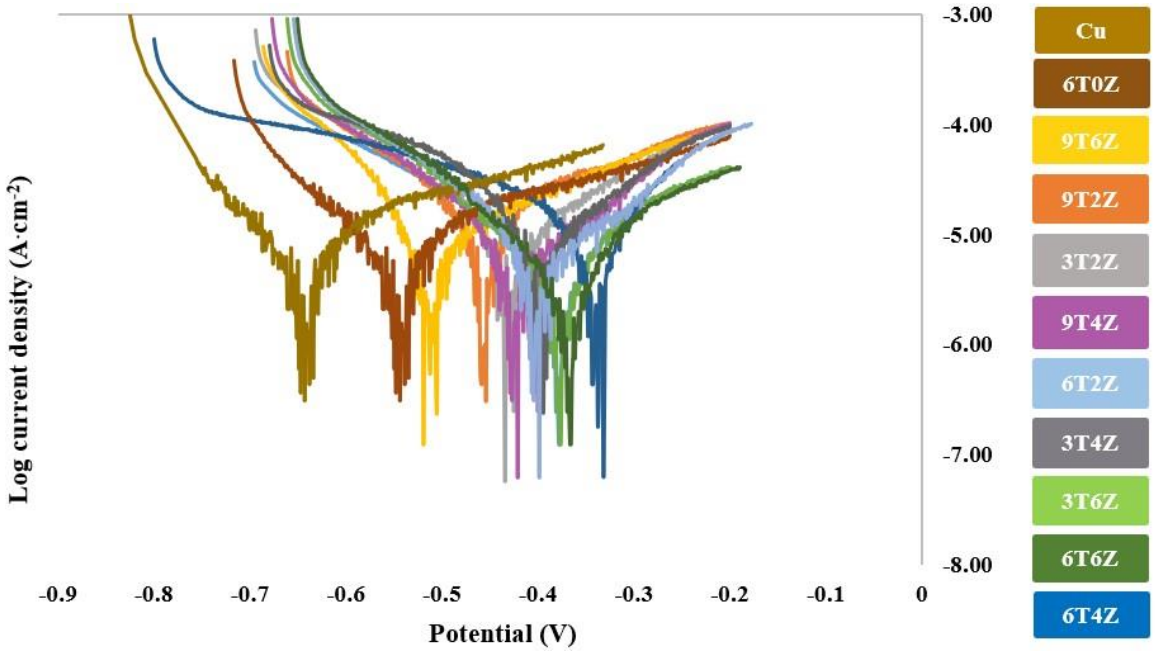

Figure 4.34. Potentiodynamic polarization analysis of Ni-B/ZrC nanocomposite electroplating with diverse TMAB and ZrC bath content

Table 4.5. Numerical results of potentiodynamic polarization analysis

Coatings	Ecor (V)	Icor (A)	Corrosion year (mm/year)
Copper	-0.643	11.42×10^{-5}	5.26
6T0Z	-0.544	4.90×10^{-5}	2.25
3T2Z	-0.430	4.01×10^{-5}	1.84
3T4Z	-0.399	3.75×10^{-5}	1.72
3T6Z	-0.378	3.47×10^{-5}	1.59
6T2Z	-0.407	3.75×10^{-5}	1.72
6T4Z	-0.333	1.48×10^{-5}	0.68
6T6Z	-0.366	2.65×10^{-5}	1.21
9T2Z	-0.454	4.06×10^{-5}	1.86
9T4Z	-0.421	3.93×10^{-5}	1.80
9T6Z	-0.519	4.12×10^{-5}	1.89

When the results were analyzed, the obtained Ni-B/ZrC nanocomposite coatings showed considerably superior corrosion resistance compared to both copper and Ni-B alloy coatings. An increase in TMAB concentration slightly diminishes corrosion resistance, as observed in the comparison of corrosion currents. Specifically, the sample with a TMAB and ZrC bath concentration coded 6T4Z displayed the lowest corrosion current, while the sample with the 6T0Z concentration exhibited the highest. When evaluating corrosion performance, it was found that composite coatings

with bath concentrations of 6T6Z, 3T6Z, 3T4Z, 6T4Z, 9T4Z, and 3T2Z exhibited similar potential values. In contrast, the 9T6Z coating was an outlier, with a more negative corrosion potential. This deviation can be attributed to the altered microstructure or phase formation caused by the combination of 9 g/L TMAB and 6 g/L ZrC bath concentrations, leading to a heterogeneous coating surface and potentially more active corrosion sites. The highest corrosion resistance was achieved with the 6T4Z nanocomposite coating, while the 9T6Z coating demonstrated the lowest. These findings highlight the influence of both TMAB and ZrC grains on the corrosion characteristics of the coatings, where the inclusion of ZrC nanoparticles contributed positively to the corrosion resistance. In contrast, higher TMAB concentrations, especially at 9 $g \cdot L^{-1}$, may have compromised corrosion resistance due to internal stresses leading to the formation of cracks in the coating.

Upon reviewing the literature, it has been noticed that the addition of TMAB to the bath concentration tends to reduce corrosion performance (Chang et al., 2017; Colli et al., 2024; Ünal and Karahan, 2018b). This is primarily due to the internal tensions created within the coating, which lead to the formation of both large and small cracks. These cracks can provide pathways for corrosion, undermining the protective properties of the coating. In contrast, fine-grained materials, such as those produced with ZrC nanoparticles, are generally more resistant to corrosion due to their denser and more compact structure. This indicates that ZrC nanoparticles have a positive influence on enhancing the coating's corrosion performance. Upon closer examination of the results, it have apparent that each particle incorporated into the bath concent plays a distinct role in shaping the coating's final structure. This complexity highlights the intricacy of the production bath preparation process, where the precise control of particle concentrations and bath conditions is crucial in determining the properties and performance of the resultant coatings. Therefore, while TMAB concentrations can lead to a decrease in corrosion resistance, ZrC nanoparticles contribute positively by improving the coating's structural integrity and enhancing its overall corrosion resistance.

5. CONCLUSIONS

In this research, Ni-B/ZrC composite coatings were successfully electrodeposited onto copper plate using the DC electrodeposition method. The study aimed to find the influence of varying TMAB and ZrC bath concentrations on the coatings' properties, with a focus on their crystal structure, mechanical properties, surface morphology, and corrosion resistance. The key findings from the study are as follows:

- The addition of ZrC reinforcement particles significantly impacted the crystal structure of the electrodeposits, particularly at 3 g/L and 6 g/L TMAB bath concentrations. At a 9 g/L TMAB bath concent, TMAB exhibited a more pronounced effect on the crystal structure.
- The crystal size first decreased and then slightly increased as the ZrC content varied between 2-4-6 g/L. These findings are consistent with the literature, indicating the complex role of ZrC in the crystal growth process.
- The addition of ZrC nanoparticles contributed to the enhancement of the coating's mechanical properties, particularly in terms of hardness. The highest hardness value (HV = 1020.4) was achieved with 4 g/L ZrC and 6 g/L TMAB bath concentrations, marking an improvement of almost 2.2 times higher than that of pure Ni-B alloy. This increase in hardness is attributed to the crystal thinning effect reason by the ZrC reinforcement particle, which refines the grain structure and develops the overall mechanical characterization of the coating.
- The surface morphology of the composite coatings resembled a cauliflower-like structure. As the amount of ZrC nanoparticles rised, the circular peaks created on the surface happened less frequently and moved further apart. This trend suggests that ZrC nanoparticles influence the surface texture, leading to the formation of a more rugged and heterogeneous surface as the concentration of ZrC increases.
- The Ni-B/ZrC composite coatings demonstrated important improvements in corrosion resistance compared to both the copper plate and pure Ni-B alloy coatings. The corrosion current for copper was found to be 11.42 x 10^{-5}, while the lowest corrosion current value (1.48 x 10^{-5}) was obtained with the 6T4Z coded TMAB and ZrC bath concentration. This result highlights the beneficial role of ZrC nanoparticles in enhancing the corrosion resistance of the coatings by acting as an inhibitor against corrosive environments.
- The Ni-B/ZrC composite coatings exhibited superior mechanical and corrosion resistance properties, making them an excellent choice for applications requiring enhanced durability. The study demonstrated that by adjusting the TMAB and ZrC concent, it is possible to tailor the coatings' properties for optimal performance in specific environments.

In conclusion, the research expands our understanding of the potential of Ni-B/ZrC composite deposited via the DC electrodeposition method. These coatings show great promise in applications where both mechanical strength and corrosion resistance are critical, and further exploration of the bath concentrations could lead to even more refined and optimized coatings.

REFERENCES

Ahmadiyeh, S., Rasooli, A., and Hosseini, M. G., 2019. Ni–B/SiC nanocomposite coating obtained by pulse plating and evaluation of its electrochemistry and mechanical properties. Surface Engineering, 35(10): 861–872.

Alavi, M. A., and Morsali, A., 2010. Syntheses and characterization of Mg(OH)2 and MgO nanostructures by ultrasonic method. Ultrasonics Sonochemistry, 17(2): 441–446.

Ali, A., Zhang, N., and Santos, R. M., 2023. Mineral Characterization Using Scanning Electron Microscopy (SEM): A Review of the Fundamentals, Advancements, and Research Directions. Applied Sciences, 13(23).

Arai, S., Kasai, S., and Shohji, I., 2010. Boron Particle Composite Plating with Ni–B Alloy Matrix. Journal of The Electrochemical Society, 157(2).

Aslan, S., and Duru, E., 2022. Microstructure and Wear Properties of Electrodeposited Ni-B-Al2O3 Composite Coating on Low Carbon Steel at Elevated Temperature. Journal of Materials Engineering and Performance, 31(2): 1693–1704.

Aspillaga, L., Jan Bautista, D., Daluz, S. N., Hernandez, K., Renta, J. A., and Lopez, E. C. R., 2023. Nucleation and Crystal Growth: Recent Advances and Future Trends. Engineering Proceedings, 56(1).

Bahrami Mousavi, A., Baghery, P., Peikari, M., and Rashed, G., 2012. Preparation and Characterization of Ni-Cr Nanocomposite Coatings Containing TiO2 Nanoparticles for Corrosion Protection. Anti-Corrosion Methods and Materials, 59(6): 279–284.

Bakan, E., 2011. Elektrolitik Parlak Gümüş Kaplama Banyolarinin Geliştirilmesi, MSc Thesis, İstanbul Teknik University, İstanbul, p. 151.

Beattie, S. D., and Dahn, J. R., 2003. Single Bath, Pulsed Electrodeposition of Copper-Tin Alloy Negative Electrodes for Lithium-ion Batteries. Journal of The Electrochemical Society, 150(7).

Bekish, Y. N., Poznyak, S. K., Tsybulskaya, L. S., and Gaevskaya, T. V., 2010. Electrodeposited Ni-B alloy coatings: Structure, corrosion resistance and mechanical properties. Electrochimica Acta, 55(7): 2223–2231.

Brenner, A., 1963. Electrodeposition of Alloys: Principles and practice. Electrodeposition of Alloys, United States: Academic Press.

Buelens, C., Cells, J. P., & Roos, J. R., 1983. Electrochemical aspects of the codeposition of gold and copper with inert particles. Journal of Applied Electrocemistry, 13: 541-548.

Chandrasekar, M. S., and Pushpavanam, M., 2008. Pulse and Pulse Reverse Plating-Conceptual, Advantages and Applications. Electrochimica Acta, 53(8): 3313–3322.

Chang, C. R., Hou, K. H., Ger, M. Der, and Wang, J. R., 2017. Characteristics of Nickel Boron Coatings Prepared by Direct Current Electrodeposition Technique. International Journal of Electrochemical Science, 12(3): 2055–2069.

Chen, X.-B., Birbilis, N., Abbott, T. B., Chen, X. B., Birbilis, N., and Abbott, T. B., 2011. Review of Corrosion-Resistant Conversion Coatings for Magnesium and Its Alloys. In Advanced Magnesium Technologies, 67(3).

Cheng, Y. S., and Yeung, K. L., 2001. Effects of electroless plating chemistry on the synthesis of palladium membranes. Journal of Membrane Science, 182(1-2): 195-203.

Choudhary, S., Garg, A., and Mondal, K., 2016. Relation Between Open Circuit Potential and Polarization Resistance with Rust and Corrosion Monitoring of Mild Steel. Journal of Materials Engineering and Performance, 25(7): 2969–2976.

Colli, A. N., Dominguez-Benetton, X., and Fransaer, J., 2024. Modeling Electrode Shape Changes in Electrodeposition and Electrochemical Dissolution. Journal of The Electrochemical Society, *171*(7): 73501.

Cui, X. J., Lin, X. Z., Liu, C. H., Yang, R. S., Zheng, X. W., and Gong, M., 2015. Fabrication and corrosion resistance of a hydrophobic micro-arc oxidation coating on AZ31 Mg alloy. Corrosion Science, 90: 402–412.

Das, S., Banthia, S., Patra, A., Sengupta, S., and Singh, S. B., 2018. Novel bilayer Zn–Ni/Ni–Co–SiC nanocomposite coating with exceptional corrosion and wear properties by pulse electrodeposition. Journal of Alloys and Compounds, 738: 394–404.

Davis, J. R., 2001. Surface engineering for corrosion and wear resistance. ASM International: Institute of Materials.

Demir, M., 2021. Yeni Tip Ni-Cr/hBN Fonksiyonel Kompozit Kaplamaların Elektrodepolama Yöntemi Ile Üretilmesi, Mekanik ve Korozyon Özelliklerinin Incelenmesi. PhD Thesis, İskenderun Teknik University, Hatay, p. 191.

Dilsizoğlu, T., Karahan, İ. H., and Tozar, A., 2023. Farklı Moleküler Ağırlıklı Kitosan Katkılı Hidroksiapatit/Kitosan Biyokompozit Kaplamaların Araştırılması. Iğdır Üniversitesi Fen Bilimleri Enstitüsü Dergisi, 13(3): 1703–1712.

Dini, J. W., 1994. Electrodeposition: The Materials Science of Coatings and Substrates. Noyes Publications, Park Ridge, 367pp.

Doğan, F., Duru, E., Uysal, M., Akbulut, H., and Aslan, S., 2022. Tribology Study of Pulse Electrodeposited Ni-B-SWCNT Composite Coating. JOM, 74(2) : 574–583.

Doğan, F., Uysal, M., Duru, E., Akbulut, H., and Aslan, S., 2020. Pulsed electrodeposition of Ni-B/TiN composites: effect of current density on the structure, mechanical, tribological, and corrosion properties. Journal of Asian Ceramic Societies, 8(4): 1271–1284.

Dong, L., Li, Y., Huang, M., Hu, X., Qu, Z., and Lu, Y., 2022. Effect of Anodizing Surface Morphology on the Adhesion Performance of 6061 Aluminum Alloy. International Journal of Adhesion and Adhesives, 113.

Duru, E., Doğan, F., Uysal, M., Akbulut, H., and Aslan, S., 2021. Optimization of Ni-B coating bath and effect of DMAB concentration on hardness and wear. Surfaces and Interfaces, 22.

Ehl, R. G., and Ihde, A. J., 1954. Faraday's Electrochemical Laws and The Determination Of Equivalent Weights. Journal of Chemical Education, 31(5): 226.

Eom, H., Kang, J., Jang, S., Kwon, O., Choi, S., Shin, J., and Nam, I., 2022. Evaluating the Electrochemical Properties of Supercapacitors using the Three-Electrode System. Journal of Visualized Experiments, 179.

Erbil, M., 2012. Korozyon: İlkeler-Önlemler. Korozyon Derneği Yayını, Ankara.

Fayyaz, O., Bahgat Radwan, A., Sliem, M. H., Abdullah, A. M., Hasan, A., and Shakoor, R. A., 2021. Investigating the Properties of Electrodeposited of Ni-P-ZrC Nanocomposite Coatings. ACS Omega, 6(49): 33310–33324.

García-Lecina, E., García-Urrutia, I., Díez, J. A., Morgiel, J., and Indyka, P., 2012. A Comparative Study of The Effect of Mechanical and Ultrasound Agitation on The Properties Of Electrodeposited Ni/Al2O3 Nanocomposite Coatings. Surface and Coatings Technology, 206(11–12): 2998–3005.

García-Lecina, E., García-Urrutia, I., Díez, J. A., Salvo, M., Smeacetto, F., Gautier, G., Seddon, R., and Martin, R., 2009. Electrochemical Preparation and Characterization of Ni/Sic Compositionally Graded Multilayered Coatings. Electrochimica Acta, 54(9): 2556–2562.

Genchi, G., Carocci, A., Lauria, G., Sinicropi, M. S., and Catalano, A., 2020. Nickel: Human health and environmental toxicology. In International Journal of Environmental Research and Public Health, 17(3).

Girão, A. V., Caputo, G., and Ferro, M. C., 2017. Application of Scanning Electron Microscopy–Energy Dispersive X-Ray Spectroscopy (SEM-EDS). Comprehensive Analytical Chemistry, 75: 153–168.

Harsimran, S., Santosh, K., and Rakesh, K., 2021. Overview Of Corrosion and Its Control: A Critical Review. In Proceedings on Engineering Sciences 3(1): 13–24.

He, T., He, Y., Li, H., Su, Z., Fan, Y., and He, Z., 2018. Fabrication of Ni-W-B4C Composite Coatings and Evaluation of Its Micro-Hardness and Corrosion Resistance Properties. Ceramics International, 44(8): 9188–9193.

Hosseini, M. G., Ahmadiyeh, S., and Rasooli, A., 2019. Pulse plating of Ni–B/WC nanocomposite coating and study of its corrosion and wear resistance. Materials Science and Technology, 35(10): 1248–1256.

Huang, X., Su, S., Xu, Z., Miao, Q., Li, W., and Wang, L., 2023. Advanced Composite Materials for Structure Strengthening and Resilience Improvement. Buildings, 13(10).

Joshua, A. M., Cheng, G., and Lau, E. V., 2023. Soft matter analysis via atomic force microscopy (AFM): A review. Applied Surface Science Advances, 17.

Kamnerdkhag, P., Free, M. L., Shah, A. A., and Rodchanarowan, A., 2017. The Effects of Duty Cycles on Pulsed Current Electrodeposition of Zn–Ni–Al2O3 Composite on Steel Substrate:

Microstructures, Hardness and Corrosion Resistance. International Journal of Hydrogen Energy, 42(32): 20783–20790.

Karabulut, A., Durmaz, M., Kilinc, B., Sen, U., and Sen, S., 2017. Effect of H3BO3 on the corrosion properties of Ni-B based electroplating coatings. Acta Physica Polonica A, 131(1): 147–149.

Karahan, İ. H., Aminifazl, A., and Golden, T. D., (2022). Effect of TMAB Concentration on Structural, Mechanical and Corrosion Properties of Electrodeposited Ni–B Alloys. Journal of the Indian Chemical Society, 99(6).

Karami, H., and Babaei, H., 2012. Electroplating Nanostructured Hard Gold through the Pulse Galvanostatic Method. International Journal Electrochemical Science, 7: 601-614.

Karslioglu, R., and Akbulut, H., 2015. Comparison Microstructure and Sliding Wear Properties of Nickel-Cobalt/CNT Composite Coatings By DC, PC and PRC Current Electrodeposition. Applied Surface Science, 353: 615–627.

Kollia, C., Spyrellis, N., Amblard, J., Froment, M., and Maurin, G., 1990. Nickel Plating by Pulse Electrolysis: Textural and Microstructural Modifications Due to Adsorption/Desorption Phenomena. Journal of Applied Electrochemistry, 20.

Krishnaveni, K., Narayanan, T. S. N. S., and Seshadri, S. K., 2009. Corrosion resistance of electrodeposited Ni-B and Ni-B-Si3N4 composite coatings. Journal of Alloys and Compounds, 480(2): 765–770.

Lapinski, J., Pletcher, D., and Walsh, F. C., 2011. The Electrodeposition of Nickel-Graphite Composite Layers. Surface and Coatings Technology, 205(21–22): 5205–5209.

Lee, K. H., Chang, D., and Kwon, S. C., 2005. Properties of Electrodeposited Nanocrystalline Ni-B Alloy Films. Electrochimica Acta, 50(23): 4538–4543.

Lelevic, A., and Walsh, F. C., 2019. Electrodeposition of Ni-P composite coatings: A review. Surface and Coatings Technology, 378: 124803.

Li, B., Li, X., Huan, Y., Xia, W., and Zhang, W., 2018a. Influence of Alumina Nanoparticles on Microstructure and Properties Of Ni-B Composite Coating. Journal of Alloys and Compounds, 762: 133–142.

Li, B., Zhang, W., Huan, Y., and Dong, J., 2018b. Synthesis and Characterization of Ni-B/Al2O3 Nanocomposite Coating by Electrodeposition Using Trimethylamine Borane as Boron Precursor. Surface and Coatings Technology, 337: 186–197.

Li, B., Zhang, W., and Li, D., 2020. Synthesis and properties of a novel Ni–Co and Ni–Co/ZrO2 composite coating by DC electrodeposition. Journal of Alloys and Compounds, 821.

Li, D., Li, B., Du, S., and Zhang, W., 2019. Synthesis of a novel Ni–B/YSZ metal-ceramic composite coating via single-step electrodeposition at different current density. Ceramics International, 45(18): 24884–24893.

Li, H., He, Y., Luo, P., Fan, Y., He, T., Zhang, Y. H., Xiang, Y., He, Y., and Song, R., 2021. Fabrication of the ZrC reinforced Ni–W composite coating and exploration of its mechanical properties and corrosion resistance. Surface and Coatings Technology, 421.

Güney İ., Y., 2020. Elektrokaplama Yöntemi ile 316L Paslanmaz Çelik Üzerine Rh ve Ag Film Kaplamaların Korozyon Özelliklerinin Araştırılması, MSc Thesis, Atatürk University, Erzurum, p.117.

Liu, H., Wang, H., Yu, W., He, Y., Xia, F., Ma, C., and Shakoor, A., 2021. Effect of Tin Concentration on Microstructure and Properties of Ni/W–Tin Composites Obtained by Pulse Current Electrodeposition. Ceramics International, 47(17): 24331–24339.

Low, C. T. J., Wills, R. G. A., and Walsh, F. C., (2006). Electrodeposition of composite coatings containing nanoparticles in a metal deposit. Surface and Coatings Technology, 201(1–2): 371–383.

Lu, H., Zheng, F., Zhang, M., and Guo, M., 2014. Effects of preparing conditions on controllable one-step electrodeposition of ZnO nanotube arrays. Electrochimica Acta, 132: 370–376.

Mao, Q., Liu, Y., and Zhao, Y., 2024. A review on copper alloys with high strength and high electrical conductivity. Journal of Alloys and Compounds, 990.

Marrese, M., Guarino, V., and Ambrosio, L., 2017. Atomic Force Microscopy: A Powerful Tool to Address Scaffold Design in Tissue Engineering. Journal of Functional Biomaterials, 8(1): 7.

Mirak, M., and Akbari, A., 2018. Microstructural Characterization of Electrodeposited and Heat-Treated Ni-B Coatings. Surface and Coatings Technology, 349: 442–451.

Mohamed, A. M. A. and Golden, T. D., 2016. Electrodeposition of Composite Materials, United States.

Morana, R., 2006. The Influence of Particle Type and Process Conditions on Electrodeposited Composite Coatings. Institute of Polymer Technology and Materials Engineering, Loughborough University.

Gezerman, A. O., 2007. Nikel Kaplama Banyolarının Karakteristiklerinin İncelenmesi. MSc Thesis, Yıldız Teknik University, İstanbul, p. 50.

Musbah, A., Eljaafari, W., Fessatwi, E., Elsahli, Y., and Com, W., 2022. Comparison Between Chemical Vapor Deposition CVD and Physical Vapor Deposition PVD Coating Techniques: A Review Paper. Scientific Research Journal for Metal Engineering and Technologies, 2(1): 79-90.

Nasirpouri, F., 2017. Electrodeposition of Nanostructured Materials. Springer Series in Surface Sciences, Springer Series in Surface Sciences, Tabriz, 333s.

Ogihara, H., Miyamoto, K., Udagawa, K., and Saji, T., 2011. Electrodeposition of super hard Ni-B/diamond composite coatings. Chemistry Letters, 40(10): 1072–1073.

Ogihara, H., Udagawa, K., and Saji, T., 2012. Effect of Boron Content and Crystalline Structure on Hardness in Electrodeposited Ni-B Alloy Films. Surface and Coatings Technology, 206(11–12): 2933–2940.

Ogihara, H., Wang, H., and Saji, T., 2014. Electrodeposition of Ni-B/SiC composite films with high hardness and wear resistance. Applied Surface Science, 296: 108–113.

Omar, A., Mubaraki, M., Abdullah, N. H., Alsabaeei, A., Hend, M., Al-Sabaeei, A., Memon, A. M., Khan, M. I., Sutanto, H., Izzi, N., and Yusoff, M., 2021. Determining the Effect of Ageing of Nano-Clay Modified Bitumen Using Atomic Force Microscopy. Transactions on Civil Engineering, 28(5): 2543-2545.

Oriňáková, R., Turoňová, A., Kladeková, D., Gálová, M., and Smith, R. M., 2006. Recent Developments In The Electrodeposition Of Nickel and Some Nickel-Based Alloys. Journal of Applied Electrochemistry, 36(9): 957–972.

Özdemir, R., 2010. Elektrodepolama Yöntemi ile Elde Edilen Znfe İnce Filmlerinin Elektriksel Özdirenç Özelliklerinin Sezgisel Yöntemler Yardımıyla İncelenmesi. MSc Thesis, Kilis 7 Aralık Üniversitesi, Kilis, p. 139.

Özdemir, R., 2019. The Effect of Additives on Structural and Magnetic Properties of CoNi Alloy Thin Film Coatings Produced by Electrodeposition. Gazi University Fen Bilimleri Dergisi, 7(3): 661-675.

Öztekin, K., 2014. Çinko Kaplanmış Karbon Çeliğinin Na-Okzalat ve Na-Tartarat Ortamlarında Polianilin ve Poli O-Anisidin ile Kaplanarak Korozyon Direncinin Geliştirilmesi. MSc Thesis, Mustafa Kemal University, Hatay, p. 143.

Ramezani, M., Mohd Ripin, Z., Pasang, T., and Jiang, C. P., 2023. Surface Engineering of Metals: Techniques, Characterizations and Applications. In Metals, 13(7).

Rezende, T. G. L., Cesar, D. V., do Lago, D. C. B., and Senna, L. F., 2016. A review of Corrosion Resistance Nanocomposite Coatings. Electrodeposition of Composite Materials.

Saini, A., Singh, G., Mehta, S., Singh, H., and Dixit, S., 2023. A Review on Mechanical Behaviour of Electrodeposited Ni-Composite Coatings. International Journal on Interactive Design and Manufacturing, 17(5): 2247–2258.

Schlesinger, M. and Paunovic, M., 2010. Modern electroplating. United States: John Wiley ve Sons, Inc.

Shah, A. R., Shutt, R. R. C., Smith, K., Hack, J., Neville, T. P., Headen, T. F., Brett, D. J. L., Howard, C. A., Miller, T. S., and Cullen, P. L., 2021. Neutron studies of Na-ion battery materials. Journal of Physics: Materials, 4(4).

Shahzad, K., Radwan, A. B., Fayyaz, O., Shakoor, R. A., Uzma, M., Umer, M. A., Baig, M. N., and Raza, A., 2021. Effect of Concentration of TiC on The Properties of Pulse Electrodeposited Ni–P–TiC Nanocomposite Coatings. Ceramics International, 47(13): 19123–19133.

Shakoor, R. A., Kahraman, R., Waware, U. S., Wang, Y., and Gao, W., 2014a. Synthesis and properties of electrodeposited Ni-B-CeO2 composite coatings. Materials and Design, 59: 421–429.

Shakoor, R. A., Kahraman, R., Waware, U. S., Wang, Y., and Gao, W., 2014b. Synthesis and Properties of Electrodeposited Ni-B-Zn Ternary Alloy Coatings. International Journal of Electrochemical Science, 9(10).

Shakoor, R. A., Kahraman, R., Waware, U. S., Wang, Y., & Gao, W., 2015. Properties of Electrodeposited Ni-B-ZrO2 Composite Coatings. International Journal of Electrochemical Science, 10(3): 2110-2119.

Shakoor, R. A., Kahraman, R., Waware, U., Wang, Y., and Gao, W., 2014c. Properties of Electrodeposited Ni-B-Al2O3 Composite Coatings. Materials and Design, 64: 127–135.

Shakoor, R. A., Waware, U. S., Ali, K., Kahraman, R., Popelka, A., Yusuf, M. M., and Hasan, A., 2017. Novel Electrodeposited Ni-B/Y2O3 Composite Coatings with Improved Properties. Coatings, 7(10).

Sheu, H. H., Tzeng, Y. C., and Syu, J. H., 2019. Study of the strengthening mechanism of electrodeposited Ni-B thin films with ultra-low boron content. Materials Letters, 238: 275–277.

Singh, R., Noor, I. M., Singh, P. K., Bhattacharya, B., and Arof, A. K., 2018. Synthesis of active absorber layer by dip-coating method for perovskite solar cell. Journal of Molecular Structure, 1158: 229–233.

Song, J., He, Y., Li, H., Zhang, Y., Liu, B., Song, R., Zhang, Z., and He, Y., 2022. Preparation of pulse electrodeposited Ni-B/ZrC composite coatings and investigation of their mechanical properties and corrosion resistance. Surface and Coatings Technology, *447*.

Song, J., Huang, H., Wang, X., and Shi, W., 2023. Status and Prospects of Surface Texturing: Design, Manufacturing and Applications. Surface Science and Technology, 1(1).

Stoljarova, A., Regenspurg, S., Bäßler, R., Mathiesen, T., and Nielsen, J. B., 2021. Effect of Lead and Copper Containing Brine on Steel Materials for Geothermal Applications – A Corrosion Study. Geothermics, 91.

Torabinejad, V., Aliofkhazraei, M., Assareh, S., Allahyarzadeh, M. H., and Rouhaghdam, A. S., 2017. Electrodeposition of Ni-Fe alloys, composites, and nano coatings–A review. Journal of Alloys and Compounds, 691: 841–859.

Trentin, A., Pakseresht, A., Duran, A., Castro, Y., and Galusek, D., 2022. Electrochemical Characterization of Polymeric Coatings for Corrosion Protection: A Review of Advances and Perspectives. Polymers, 14(12).

Uluisik, I., Karakaya, H. C., and Koc, A., 2018. The importance of boron in biological systems. Journal of Trace Elements in Medicine and Biology, 45: 156–162).

Ünal, E., and Karahan, H., 2018a. Effects of ultrasonic agitation prior to deposition and additives in the bath on electrodeposited Ni-B/hBN composite coatings. Journal of Alloys and Compounds, 763: 329–341.

Ünal, E., and Karahan, H., 2018b. Production and characterization of electrodeposited Ni-B/hBN composite coatings. Surface and Coatings Technology, 333: 125–137.

Ünal, E., Yasar, A., and Karahan, I. H., 2019. A review of electrodeposited composite coatings with Ni-B alloy matrix. Materials Research Express 6(9).

Ünal, E., Yaşar, A., and Karahan, İ. H., 2023. Effect of trimethylamine borane (TMAB) bath concentration on electrodeposited Ni–B/TiC nanocomposite coatings. Ceramics International, *49*(15): 25516–25529.

Ünal E., 2016. Ni-B/hBN Kompozit Kaplamaların Elektrodepolama Yoluyla Üretilmesi ve Özelliklerinin İncelenmesi. MSc Thesis, İskenderun Teknik University, Hatay, p. 187.

Wang, M., Xue, Z., Yan, S., He, J., Shao, Q., Ge, W., and Lu, B., 2022. Pulse Electrodeposited Super-Hydrophobic Ni-Co/WS2 Nanocomposite Coatings with Enhanced Corrosion-Resistance. Coatings, 12(12).

Wang, Y., Wang, S. J., Shu, X., Gao, W., Lu, W., and Yan, B., 2014. Preparation and property of sol-enhanced Ni-B-TiO2 nano-composite coatings. Journal of Alloys and Compounds, 617: 472–478.

Wahab, M.A., 2024. Mirror Combination Scheme in Reciprocal Lattice. In: Mirror Symmetry. Springer Series in Solid-State Sciences, Springer, Singapore.

Waware, U. S., Hamouda, A. M. S., Bajaj, B., Borkar, T., and Pradhan, A. K., 2018a. Synthesis and characterization of electrodeposited Ni-B-Tl2O3 composite coatings. Journal of Alloys and Compounds, 769: 353–359.

Waware, U. S., Hamouda, A. M. S., & Pradhan, A. K., 2018b. Effect of codeposition of mixed nanoparticles (V2O5 and ZrO2) on the structure and properties of Ni-B nanocomposite coating. Journal of Alloys and Compounds, 752: 253–259.

Waware, U. S., Hamouda, A. M. S., and Wasekar, N. P., 2018c. Mechanical properties, thermal stability and corrosion behavior of electrodeposited Ni-B/AlN nanocomposite coating. Surface and Coatings Technology, 337: 335–341.

Younus, S., and Arshad, M., 2019. Thermal Spray Coating: A Brief Understanding. International Journal of Advanced Research, *7*(10): 919–928.

Zech, N., Podlaha, E. J., and Landolt, D., 1999. Anomalous Codeposition of Iron Group Metals: II. Mathematical Model. Journal of The Electrochemical Society, 146(8).

Zhang, D., Cui, X., Jin, G., Cai, Z., & Dong, M., 2018. Thermal stability of Ni-B/La2O3 coatings by electro-brush plating technique. Surface and Coatings Technology, 349: 1042–1047.

Zhang, J., Dai, W., Wang, X., Wang, Y., Yue, H., Li, Q., Yang, X., Guo, C., and Li, C., 2023. Micro-arc oxidation of Al alloys: mechanism, microstructure, surface properties, and fatigue damage behavior. Journal of Materials Research and Technology, 23: 4307–4333.

Zhang, W., and Li, B. (2018). Electrochemical Properties and XPS Analysis of Ni-B/SiC Nanocomposite Coatings. International Journal of Electrochemical Science, 13(4): 3516–3526.

Zhang, Y., Zhang, S., He, Y., Li, H., He, T., Fan, Y., and Zhang, H., 2021. Mechanical properties and corrosion resistance of pulse electrodeposited Ni-B/B4C composite coatings. Surface and Coatings Technology, 421.

Zhang, Z., Jiang, C., Liao, Z., and Wei, G., 2021. Effect of electrodeposition parameters on the evolution of crystallographic texture and internal stress of Ni/ZrC composite coatings. Materials Today Communications, 27.

CURRICULUM VITAE

Ömer Hükümdar graduated from Yavuzlar Primary School in 2010 and Danişment Gazi Anatolian High School in 2014. Then, he started his undergraduate education at Çukurova University, Department of Automotive Engineering in 2015. He started his master's degree in the same department of Çukurova University in 2022. He works as a Research Assistant at Çukurova University, Department of Automotive Engineering.